Thermal Structure of Mid-Crustal Shear Zones

Sarah Elizabeth Mazza

Thesis submitted to the faculty of the Virginia Polytechnic Institute and State University in partial fulfillment of the requirements for the degree of

Master of Science
In
Geosciences

Richard D. Law
Mark J. Caddick
James A. Spotila

May 1st, 2013
Blacksburg, VA

Keywords: quartz fabric, deformation temperature, dynamic recrystallization, P-T conditions, Main Central Thrust, Sgurr Beag Thrust

Thermal Structure of Mid-Crustal Shear Zones

Sarah Elizabeth Mazza

Abstract

Analysis of quartz c-axis fabrics and microstructures from ductily deformed rocks allows for the examination of the kinematics associated with crustal deformation. This thesis expands on the current knowledge of the kinematic evolution of the Himalayas and Scottish Caledonides, by examining samples from the Main Central Thrust (MCT) (Himalayas) and the Sgurr Beag Thrust (SBT) (Scottish Caledonides). Metamorphic temperatures (Tm) associated above the MCT are inverted; chapter one attempts to test if deformation temperatures (Td) correlate to Tm, indicating that ductile shearing occurred during peak Tm. In the Scottish Caledonides, Td and Tm increase from foreland to hinterland, potentially indicating a right way up thermal structure; chapter two presents Td and Tm associated with the region around the SBT.

Above the MCT, quartz c-axis fabrics yield Td ranging between 500-650 °C, corresponding to the temperatures of dynamic recrystallization for subgrain rotation (SGR) and grain boundary migration (GBM). Up to 1000m above the MCT, Td and Tm are within error of each other, suggesting that shearing occurred during peak Tm; while further away from the MCT Tm is significantly hotter than Td, suggesting that shearing continued past Tm.

Deformation associated with the upper part of the Moine thrust sheet and the SBT yields quartz c-axis fabrics with Td ranging between 395-583 °C, corresponding to the regional dynamic recrystallization. Tm calculations original to this study yield pressure-temperature constraints of 4.8-5.8 kbar and 586-625 °C. Tm is within error of Td, suggesting that deformation and metamorphism were synchronous.

Acknowledgments

First and foremost my parents, Ralph and Kate Mazza, deserve much credit and thanks for all they have done for me. They raised me to peruse my dreams and allowed me to develop into the woman I am today. They encouraged constant discovery through multiple life enhancing experiences. Without their constant support I would not be where I am today.

Anne Mazza, my little sister who always has (and always will) inspired me to be the best person I can be.

Drew Coleman and Allen Glazner, my undergraduate professors and mentors who sparked my curiosity for geological sciences.

Rick Law, my Masters advisor, who provided the ideal amount wisdom and support. He has allowed me to develop this thesis around ideas and concepts I found interesting, all the while encouraging me to further grow as a geologist. I have valued the time we have worked together, both in the lab and in the field, and look forward to future years as colleagues and friends. And to his wife, Clare, who provided good laughs and times both in Ullapool and at the pub in town.

Mark Caddick and Jim Spotila, mentors and committee members who provided discussion that enhanced my learning and geologic discovery.

Don Stahr, Matt Francsis, Kyle Ashley, and Nick Heaverlo, who kept ideas flowing in the office, and served as much needed sounding boards.

Lastly, my amazing boyfriend, James Dale, who has always shown support of my academic development. I have learned so much about life with him, and have cherished all of our adventures.

Attributions

Chapter two may be submitted for publication to the *Journal of Structural Geology* in the future.

Chapter three will be submitted for publication to the *Journal of Structural Geology* as "Mazza, S.E., Law, R.D., Caddick, M.J., Krabbendam, M. Thermal Structure of the Moine and Sgurr Beag Thrust Sheets, NW Scotland." S.E. Mazza was responsible for the quartz c-axis fabrics and P-T constraints. R.D. Law aided in field collection of all samples, as well as valued discussion and interpretation the results. M.J. Caddick aided in the construction of P-T modeling and interpretation. M. Krabbendam drafted two of the cross sections. S.E. Mazza wrote the manuscript and drafted most of the figures.

List of Figures

CHAPTER 2

CHAPTER 3

List of Tables

CHAPTER 3

CHAPTER 1

Introduction to Mid-Crustal Shear Zones

Sarah E. Mazza

1.1 Introduction to Mid-crustal Shear Zones

With increasing depth in the earths crust a transition occurs in the mechanisms by which rocks deform, with brittle fracture being the dominant process at relatively shallow depths and crystal plastic flow being dominant at deeper, hotter depths. The depth at which this transition occurs (referred to as the brittle-ductile transition zone) is controlled by a number of extrinsic and intrinsic factors such as local geothermal gradient and rocks type. For normal geothermal gradients of 20-30 °C per km and rock types in which quartz is the load-bearing mineral phase, plastic deformation starts at ~ 300 °C (depths of 10-15 km). Traced from shallow to deep crustal levels through the brittle-ductile transition zone, individual faults progressively change in character from isolated fractures to zones of distributed fracturing to wide anastomosing shear zones in which pervasive shearing is associated with crystal plastic deformation and dynamic recrystallization. Within these mid- to deep-crustal shear zones grain scale microstructures and crystal fabrics provide information on the kinematics of flow (e.g. shear senses and 3D strain types), while their metamorphic mineral assemblages provide information on the temperatures and pressures under which mineral growth occurred. Metamorphic mineral growth may either pre-date, be synchronous with, or post-date pervasive deformation in these shear zones. In contrast, temperatures at which plastic deformation and dynamic recrystallization occurred may be estimated using the opening angles of quartz c-axis fabrics (thermometer of Kruhl, 1998) and microstructures associated with different quartz recrystallization regimes (Stipp et al. 2002a, b). In cases where metamorphic mineral growth occurred during pervasive shearing temperatures indicated by metamorphic mineral assemblages should be similar to deformation temperatures indicated by microstructures and crystal fabrics.

In this thesis two orogen-scale mid-crustal shear zones are examined: a) the Main Central thrust, eastern Nepalese Himalaya and, b) the Sgurr Beag thrust, NW Scottish Caledonides. In these case studies, the primary aim is to quantify temperatures of deformation, and specifically how deformation temperatures change traced both across individual shear zones (footwall to hanging wall) and from shallower (more foreland positioned) to deeper (hinterland position) crustal levels. Where pelites containing suitable metamorphic mineral assemblages are present, temperatures and pressures of metamorphism have also been estimated using microprobe-based thermobarometry techniques. Comparison of the two data sets suggests that pervasive deformation in both shear zones occurred at close to peak metamorphic conditions (lower to mid-amphibolite facies), with deformation temperatures increasing from footwall to hanging wall.

CHAPTER 2

Thermal Structure of the Main Central Thrust, Mount Everest Region, Nepalese Himalaya

Sarah E. Mazza

2.1. Abstract

Inversion of metamorphic isograds is a common phenomena in large scale mid-crustal thrust zones, with metamorphic grade increasing up structural section. The Main Central Thrust (MCT) of the Himalaya is a high strain shear zone with well documented telescoping of inverted metamorphic isograds. Deformation temperature data from the hanging wall to the MCT is limited, but temperatures from studies along strike generally increase up structural section from ~500 ˚C to ~650 ˚C in sympathy with both metamorphic isograds and quartz recrystallization regimes.

Using optically-measured quartz c-axis fabrics and the Kruhl (1998) fabric opening angle thermometer we have attempted to quantify deformation temperatures associated with penetrative shearing along the MCT 'zone' in the Mount Everest region of eastern Nepal. Our samples were collected by M. Hubbard and M. Streule from both Lesser Himalayan Series rocks in the footwall to the MCT and Greater Himalayan Series rocks in the hanging wall to the MCT. Compared with previously published studies of fabrics from similar structural positions along strike in other parts of the Himalaya, the c-axis fabrics from these samples are unusually diffuse but, in agreement with along-strike studies, combined fabric and quartz recrystallization regime data generally indicate structurally upwards increasing deformation temperatures.

2.2. Introduction

South of Mount Everest in the Nepalese Himalayas a classic example of inverted metamorphic isograds is exposed above the Main Central thrust (MCT) (Figs. 2.1 and 2.2) (Gansser, 1964; Hodges et al., 1988; Hubbard, 1989, 1996). Here the MCT is marked by a broad (km-scale) shear zone that locally dips 30-40° to the north, placing rocks of the Greater Himalayan Series (GHS) over Lesser Himalayan Series (LHS) rocks. The GHS in the Everest region consists of a 30 km thick slab of amphibolite facies metamorphic rocks (Jessup et al., 2006; Searle et al., 2006), bounded to the north by the South Tibetan Detachment System (STDS), and progressively deformed under mid-crustal conditions. The LHS consists of unmetamorphosed to relatively low-grade metamorphic rocks, that also dip 30-60° to the north, northeast. Thrusting and normal faulting associated with southward-directed extrusion and exhumation of the GHS are generally regarded as being synchronous, based on structural and geochronological studies (see review by Godin et al., 2006). Thrusting along the MCT in eastern Nepal was originally suggested to have occurred at ~20-22 Ma, based on Ar^{40}/Ar^{39} and U-Pb ages of monazite (Hodges et al., 1996; Hubbard and Harrison, 1989; Johnson et al., 2001). However, recent studies based on melt crystallization suggest movement along the MCT may

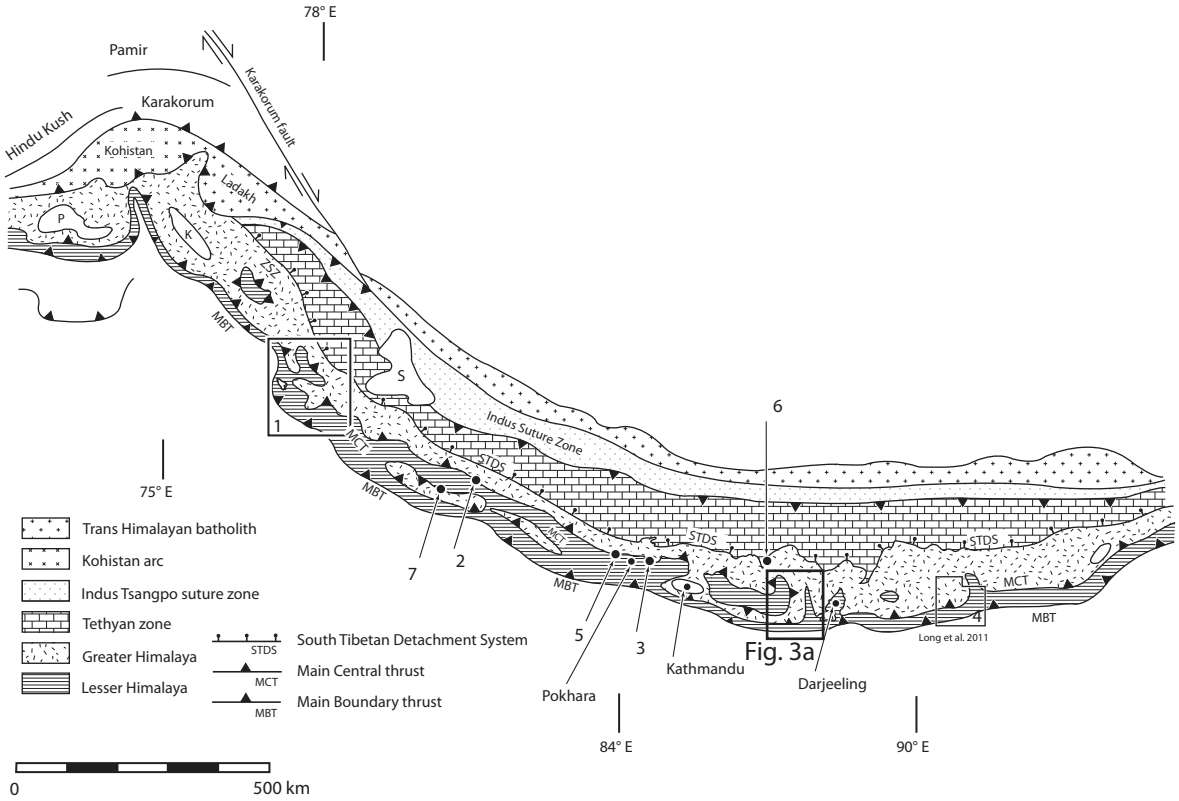

Figure 2.1
General geologic map of the Himalaya; adapted from Burchfiel et al. (1992); Célérier et al. (2009); Larson et al. (2010); Law et al. (in press); Long et al. (2011); Searle et al. (2003). Sections across the Main Central Thrust, discussed in text include: 1) Law et al. (in press) 2) Yakymchuk et al. (2012) 3) Larson et al. (2010) 4) Long and McQuarrie (2010) 5) Larson and Godin (2009), 7) Srivastava and Mitra (1996). Section across the STDS (Law et al. 2004, 2011) discussed in text is indicated by location 6. Location of the main study area (Dudh Kosi to Arun River valleys) south of Mt. Everest (Fig. 2.3a) is indicated.

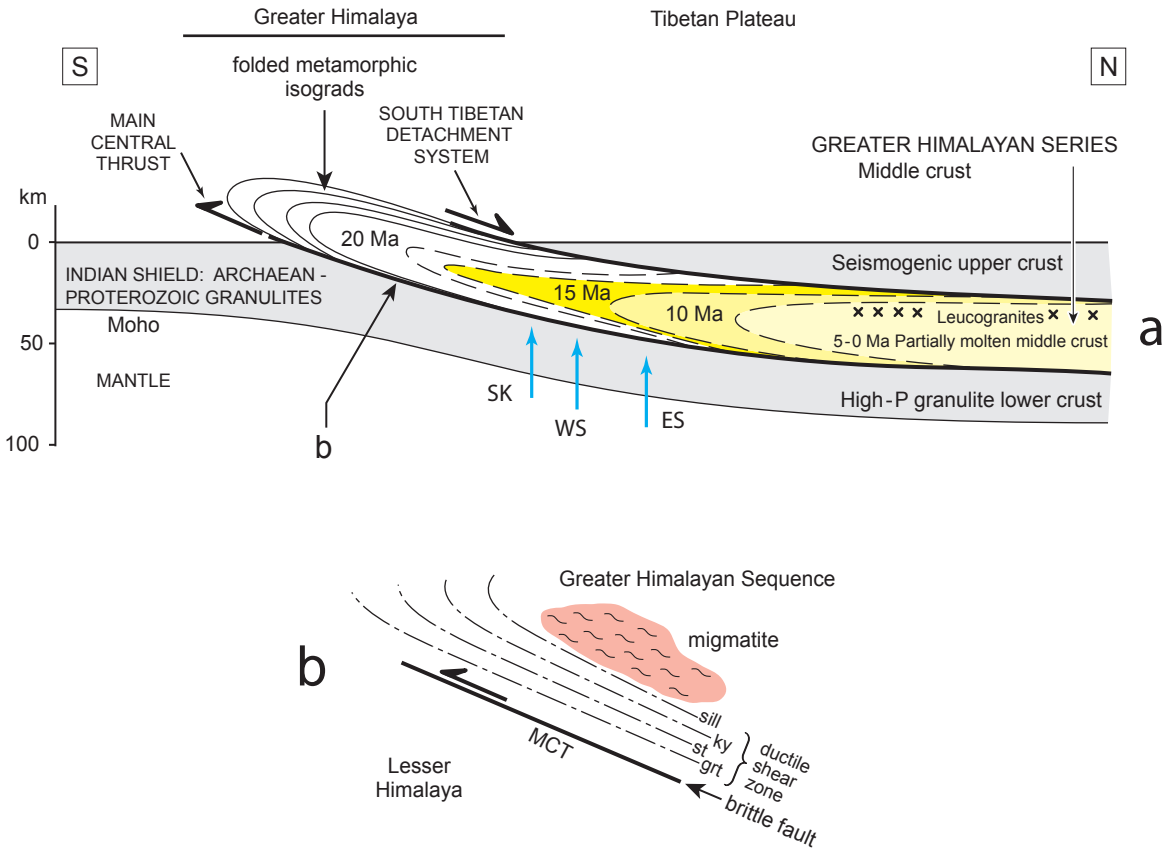

Figure 2.2
Diagram for channel flow model. (a) Schematic cross section diagram for channel flow model showing extrusion of a partially molten mid-crustal slab (Greater Himalayan Series), bound to the south by a south vergent ductile thrust zone (Main Central Thrust) and to the north by a north vergent low-angle normal shear zone (South Tibetan Detachment System). Folding of metamorphic isograds occurs as a result of channel flow; adapted from Searle et al. (2006); Searle et al. (2007). (b) telescoping of inverted metamorphic isograds above the MCT.

have been still active at ~16 Ma (Daniel et al., 2003; Kohn et al., 2004; Kohn et al., 2005). Minimum displacement along the MCT in the western Himalayas is estimated at approximately 125 km (DeCelles et al., 2001, 2002; Robinson et al., 2003, 2006; Kohn et al. 2004). A total of 210-280 km of horizontal shortening produced by thrust faulting is estimated for eastern Nepal, with 140-210 km of this displacement accommodated by the MCT (Schelling, 1992).

Numerous models have been proposed to explain inversion of metamorphic isograds in the hanging wall to the MCT. These include: **1)** ductile shearing along the MCT (Hubbard, 1996); **2)** the "hot iron" model in which hotter rocks are placed over cooler rocks by either thrusting (LeFort 1975) or intrusion of High-Himalayan leucogranites (Hodges et al., 1988); **3)** folding (Fig. 2.2a; Searle and Rex, 1989) or imbrication (Harrison et al., 1997) of originally right-way up isograds; **4)** heat 'focusing' (Jaupart and Provost, 1985) or frictional heating (Molnar and England, 1990; England and Molnar, 1993) along the MCT; **5)** southward-directed channel flow within the GHS (Fig. 2.2a) (Beaumont et al., 2001; Beaumont et al., 2004; Searle et al., 2006; Searle et al., 2007). It is important to note, that while inversion of isograds along the base of the GHS is generally accepted with metamorphic grade increasing up section towards the north (Fig. 2.2b), there is a tacit assumption that isograds are either hinterland (northward) dipping - or if locally foreland dipping, dip less steeply south than the local ground surface. If isograds at least locally dip more steeply to the south than the ground surface then they would be right way up.

Temperatures of metamorphism (and P-T histories) in the GHS have been well documented along the length of the Himalaya, but less is known about deformation temperatures associated with thrusting along the MCT. In the Sutlej Valley of NW India, (Fig. 2.1) Law et al. (in press) using quartz c-axis fabric opening angles have demonstrated that deformation temperatures increase up section in the GHS from ~ 540-600 °C in the immediate hanging wall to the MCT to ~ 620-670 °C in the core of the GHS. In the hanging wall to the Almore Thrust of NW India, Srivastava and Mitra (1996) show that deformation temperatures based on quartz and feldspar microstructures increase up section from 400 to 600 °C. In western and central Nepal,

Figure 2.3

Next page. Geologic map and cross sections of area between the Dudh Kosi and Arun river valleys. (a) Geologic map between Dudh Kosi and Arun river vallery; location of samples reported in this study are indicated by black squares. Samples were collected in four main units: 1) Chlorite grade metaquartzites and schists from the Lesser Himalayan Series (LHS); 2) Garnet-biotite schists from the LHS; 3) Num and Paphlu gneisses of the Greater Himalayan Series (GHS); 4) Para-, ortho-, and calc-silicate gneisses of the GHS. Positioning of the MCT is based on Searle et al. (2008) and unpublished field maps in PhD theses of Hubbard (1988) and Streule (2009). Two of the main sampling transects are indicated by lines A-A' (Hinku River Valley) and B-B' Dudh Kosi River Valley). (b) Geologic cross-section for the Hinku River Valley; sample locations are indicated with circles. (c) Geologic cross-section for the Dudh Kosi River Valley; sample locations are indicated with circles. Vertical and horizontal scales are equal in both cross sections.

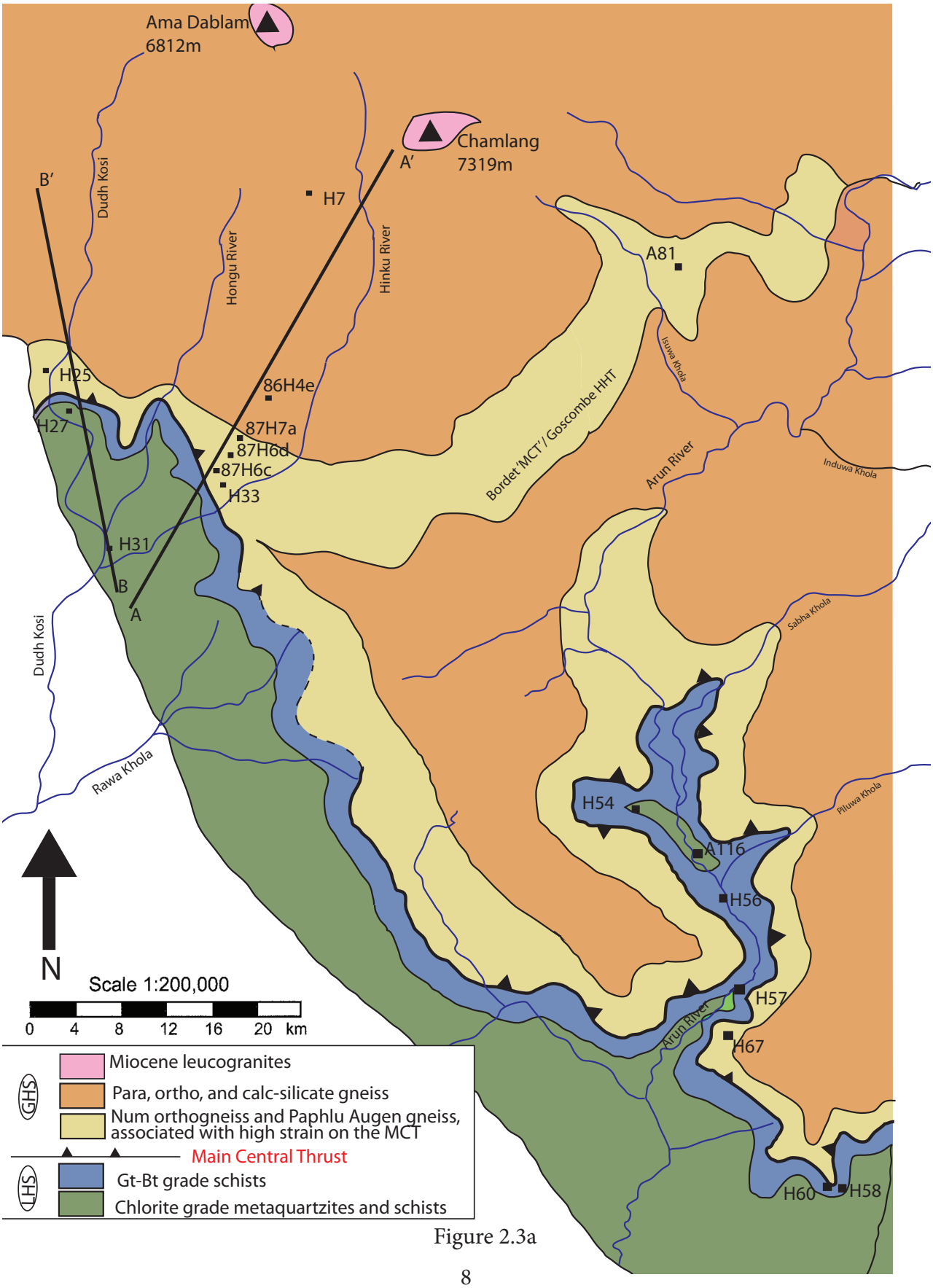
Ama Dablam
6812m
Chamlang
7319m
A'
B'
Dudh Kosi
Hongu River
Hinku River
H7
A81
Isuwa Khola
Bordet'MCT'/ Goscombe HHT
Arun River
Induwa Khola
H25
H27
86H4e
87H7a
87H6d
87H6c
H33
H31
B
A
Dudh Kosi
Sabha Khola
Rawa Khola
H54
Piluwa Khola
A116
H56
H57
Arun River
H67
H60
H58
N
Scale 1:200,000
0 4 8 12 16 20 km
Miocene leucogranites
GHS
Para, ortho, and calc-silicate gneiss
Num orthogneiss and Paphlu Augen gneiss, associated with high strain on the MCT
Main Central Thrust
LHS
Gt-Bt grade schists
Chlorite grade metaquartzites and schists

Figure 2.3a

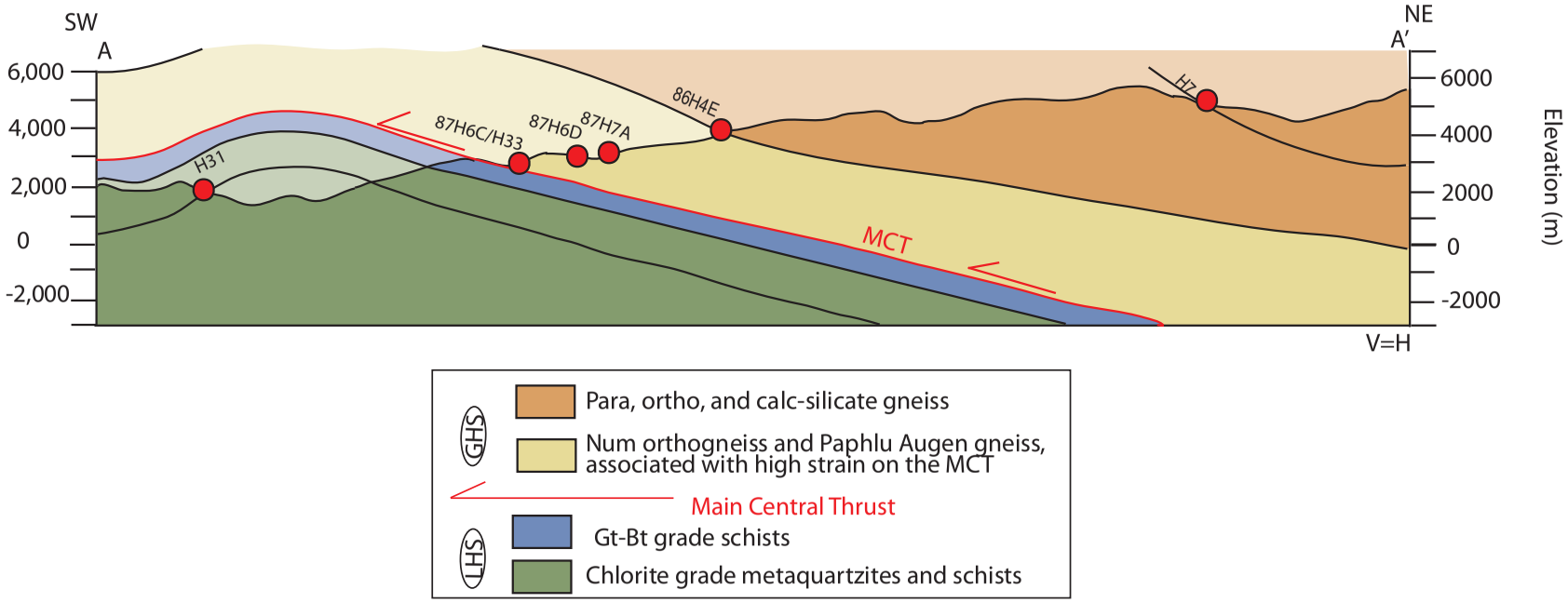
SW
A
NE
A'
6,000
4,000
2,000
0
-2,000
6000
4000
2000
0
-2000
Elevation (m)
V=H
H31
87H6C/H33
87H6D
87H7A
86H4E
H7
MCT
GHS
LHT
Para, ortho, and calc-silicate gneiss
Num orthogneiss and Paphlu Augen gneiss, associated with high strain on the MCT
Main Central Thrust
Gt-Bt grade schists
Chlorite grade metaquartzites and schists

Figure 2.3b

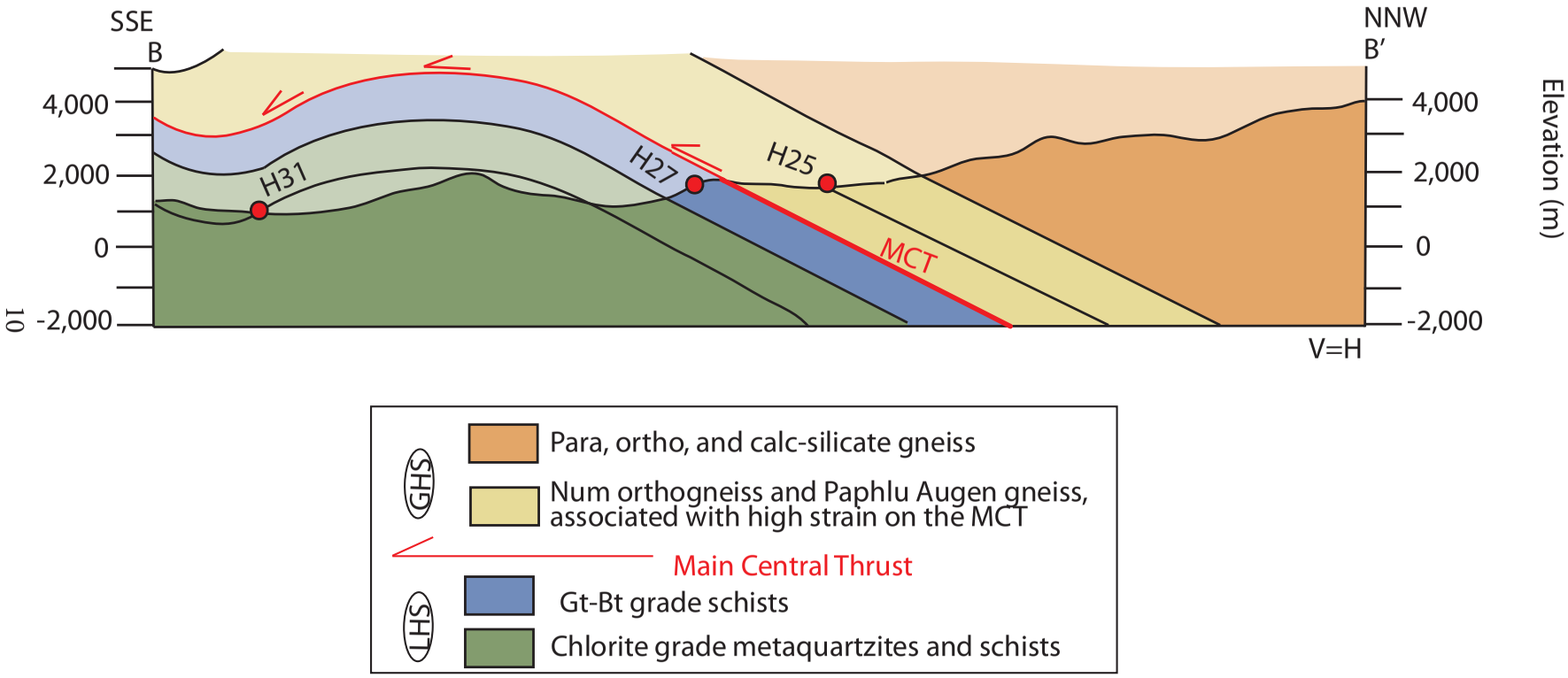
SSE
B
NNW
B′
4,000
2,000
0
-2,000
H31
H27
H25
MCT
Elevation (m)
V=H
GHS
Para, ortho, and calc-silicate gneiss
Num orthogneiss and Paphlu Augen gneiss, associated with high strain on the MCT
Main Central Thrust
LHS
Gt-Bt grade schists
Chlorite grade metaquartzites and schists

Figure 2.3c

Yakymchuk et al. (2012), Larson and Godin (2009), and Larson et al. (2010) have estimated deformation temperatures of ~500 °C in the immediate hanging wall to the MCT, increasing up section within the GHS to ~ 650 °C . In the eastern Himalaya of Bhutan, Long and McQuarie and Long et al. (2010; 2011) have estimated deformation temperatures ranging from 500°C to 670°C based on quartz recrystallization regimes (Stipp et al. 2002). Locations for these study areas are also shown in Fig. 2.1.

Using samples collected by Mary Hubbard and Mike Streule for their respective Ph.D. dissertations (Hubbard, 1988; Streule, 2009), we attempt to estimate deformation temperatures associated with shearing along the MCT in the Mount Everest region of eastern Nepal (Figs. 2.1 and 2.3) using the quartz c-axis opening angle thermometer developed by Kruhl (1998) (Fig. 2.4) in combination with the quartz recrystallization regime thermometer discussed by Stipp et al. (2002).

2.3. Geological Background

The Himalayan orogenic belt has formed in response to north-south shortening driven by collision of the Indian and Asian continents that commenced at ~45-55 Ma. Shortening has resulted in formation of tectonic features such as the Main Boundary thrust (MBT), the Main Central thrust (MCT), and the South Tibetan Detachment System (STDS). The MBT is often regarded as marking the Himalayan 'metamorphic front', and places unmetamorphosed to low grade metamorphics of the LHS over Siwalik sediments of the Indian plains (e.g. Goscombe et al., 2003). South of Mount Everest in the Arun Valley of eastern Nepal (Fig. 2.3), the GHS is composed of migmatitic upper amphibolite facies and metasedimentary rocks. At the base of the GHS is the MCT ductile shear zone (MCTZ) (Searle et al., 2008), which contains inverted kyanite to biotite metamorphic isograds. The MCTZ is marked by highly strained Phaplu augen gneiss, Num Orthogneiss, and Ulleri Formation rocks (Goscombe et al., 2006; Searle et al., 2008). The MCT as originally defined by Bordet (1961) in this area, and later referred to by Goscombe et al. (2006) as the High Himal Thrust (HHT) is a 100-400m, thick zone of intensely sheared rocks that marks a jump in metamorphic grade, and represents an Upper-Plate/Lower-Plate boundary of primary structural importance (Goscombe et al., 2006). Above the HHT are amphibolite facies Barun gneiss, Black gneisses, and Jannu-Kangchenjunga gneisses intruded by Miocene age leucogranites (Goscombe et al., 2006; Searle et al., 2008). The LHS in this area is composed of greenschist and amphibolite facies pelitic schists, quartzites, marbles and calc-silicates (Corrie et al., 2010). The LHS also includes the Seti Formation schists and calc-silicates

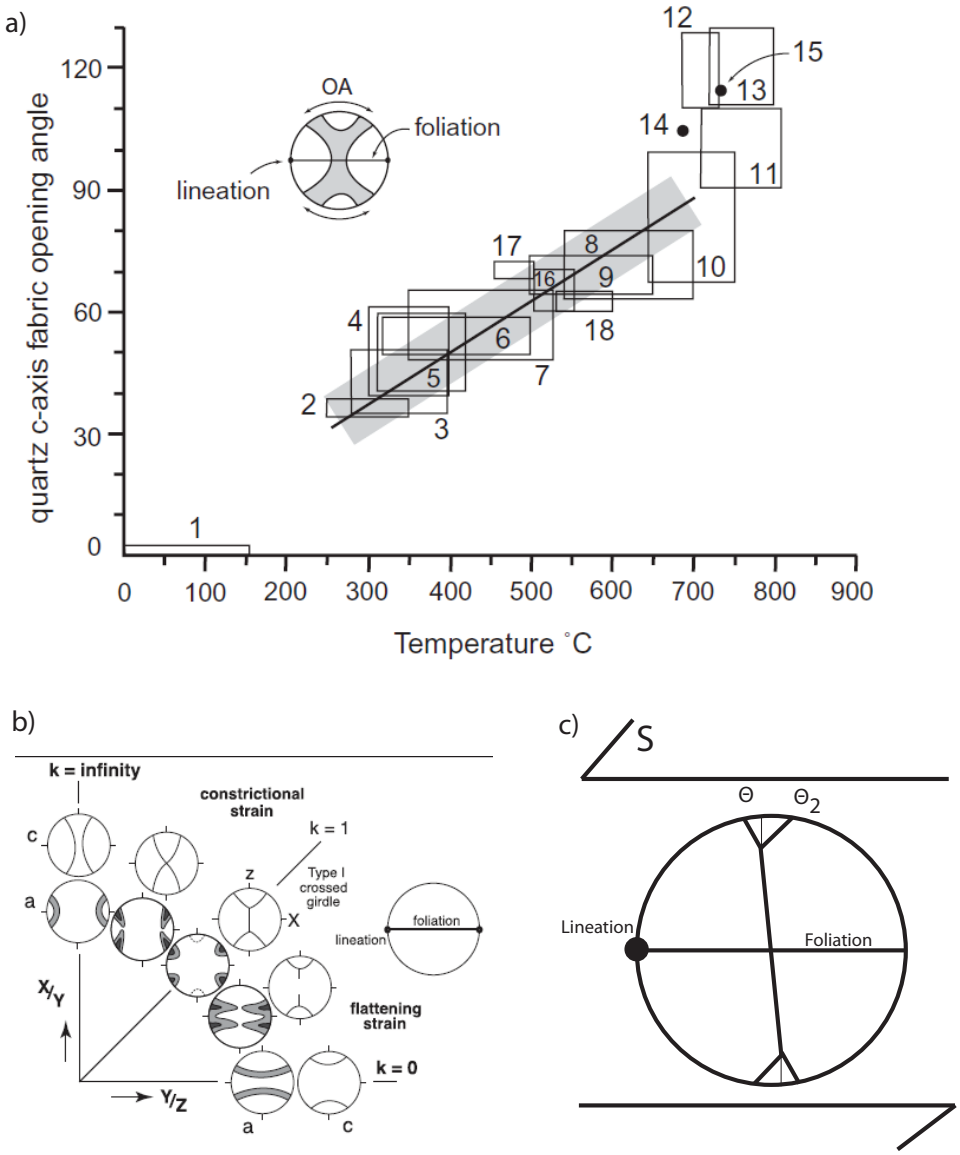

Figure 2.4
Quartz c-axis fabric applications. (a) Quartz c-axis fabric opening angle thermometer of Kruhl (1998); boxes indicate studies used to construct best-fit linear relationship between opening angles and deformation temperatures up to 650 °C. (b) Range of quartz c-axis fabrics associated with flattening to constrictional strains; modified from Schmid and Casey (1986). (c) Explanation of shear sense indicated by quartz c-axis fabric asymmetry, where fabric opening angle is defined by $\theta + \theta 2$ and $\theta < \theta 2$ for sinistral shear sense shown.

and the Kathmandu Group schists (Goscombe et al., 2006). Brunel (1986) and Brunel and Kienast (1986) have noted that in the Arun Valley zones of high strain are characterize by a top-to-the-south shear sense.

The structural framework and positioning of the MCT is the subject of on-going debate due to lack of generally accepted criteria for its positioning and frequently poor exposure at lower elevations on the southern flank of the Himalaya. To date, there have been six different definitions of the MCT. First described by Heim and Gansser (1939) and again by Gansser (1964), the MCT was regarded as placing high grade GHS rocks over low grade LHS. This definition of lithological contrasts was further supported by noting the thrusting of orthogneisses over quartzites (Daniel et al., 2003; Gansser, 1983). The structural position of the kyanite isograd was another criterion used until the 1980's to define the MCT (Bordet, 1961; Colchen et al., 1986; LeFort, 1975). Isotopic data such as U-Pb dates from detrital zircon (Parrish and Hodges, 1996), Nd isotopes (Robinson et al., 2001; Martin et al., 2005), and the location of young U-Pb/Th-Pb ages from monazites (Harrison et al., 1997) have also been used to define the MCT.

However, Searle et al. (2008) argued that these methods define either stratigraphy or metamorphic conditions, and do not use structural indicators. Goscombe et al. (2006) also noted that the MCT has been incorrectly referred to as a stratigraphic boundary, and instead suggest the concept of the *Himalayan Unconformity* to account for Nd values that differ between the LHS and the GHS. The Phaplu augen gneiss was formerly part of the LHS, but is now generally associated with the GHS based on the definitions of the MCT adopted by Goscombe et al. (2006) and Searle et al. (2008).

For this study, the Searle et al. (2008) definition of the MCT is used, namely: *"the base of the large-scale zone of high strain and ductile deformation, commonly coinciding with the base of the zone of inverted metamorphic isograds, which places Tertiary metamorphic rocks of the GHS over unmetamorphosed or low-grade rocks of the LHS."*

2.4. Microstructures and quartz c-axis fabrics

Microstructures and crystallographic fabrics (primarily optically measured quartz c-axis fabrics with more limited X-ray derived a-axis fabrics) have previously been used to characterize penetrative shearing along the MCT (e.g. NW Himalaya - Grasemann et al. 1999, Bhattacharya and Weber, 2004, Law et al. in press; Central Himalaya - Bouchez and Pêcher, 1976, Larson and Godin 2009, Larson et al. 2010; eastern Himalaya - Grujic et al. 1996). Samples described in this study were collect in the Mt. Everest region of Nepal by Mary Hubbard and Mike Streule as part of their PhD research at MIT and Oxford, respectively (Hubbard, 1988; Streule, 2009). Thin sections were cut parallel to lineation and perpendicular to foliation, and examined using

an optical petrographic microscope and Leitz universal stage. In all samples quartz has been dynamically recrystallized, and in some samples exhibits microstructural evidence for grain boundary adjustments possibly associated with annealing. Quartz c-axis fabrics were measured optically on recrystallized grains, a minimum of 600 grains (maximum of 1000 grains) being measured in each sample using an Excel macro developed by S. Mulcahy at University of California, Davis. Fabrics were plotted and contoured on a lower hemisphere stereonet using the *Stereoplot* software package developed by N. Mancktelow at ETH, Zurich.

We classify quartz microfabrics associated with dynamic recrystallization using the terminology proposed by Stipp et al. (2002). Stipp et al. (2002) proposed that the three main types of recrystallization mechanism in quartz (grain boundary bulging, subgrain rotation and grain boundary migration) may be used to infer broad ranges of likely deformation temperature, assuming 'average' geologic strain rates. Here we use the term *bulging* (BLG) to describe recrystallized quartz grains that are small (~10μm), with all recrystallized grains located adjacent to parent grain boundaries, and indicating inferred deformation temperatures of ~280 °C to ~400 °C. Starting at approximately 400 °C subgrain rotation (SGR) becomes the dominant recrystallization mechanism, and is indicated by an increase in recrystallized grain size (15-30 μm), a higher percentage of recrystallized grains and a *"core and mantle"* type microstructure. SGR is the dominant recrystallization mechanism up to deformation temperatures of ~500 °C, above which grain boundary migration (GBM) recrystallization becomes dominant. GBM is indicated by large recrystallized grains (>30μm) with lobate grain boundaries. BLG, SGR, and GBM correlate to the experimentally produced regime 1, regime 2, and regime 3 microstructures, respectively, described by Hirth and Tullis (1992).

2.4.1 Hinku River

The structurally lowest sample, H31(Fig. 2.3a), collected from the LHS near the fork of the Dudh Kosi and Hinku Rivers at ~ 1830 m beneath the MCT (Fig. 2.3b), is a quartz + muscovite + chlorite + plagioclase metapelite from the LHS (Fig. 2.5a). Muscovite and chlorite define the macroscopic foliation, with top to the south shear indicators preserved in the phyllosilicates. Quartz is fine grained (35-65 μm) suggesting subgrain rotation recrystallization has occurred, while rare larger quartz grains have lobate boundaries, suggesting GBM. Phyllosilicate rich bands effectively "pin" quartz grain boundaries. Plagioclase in this sample behaves rigidly with no microstructural evidence that it underwent dynamic recrystallization. The quartz c-axes fabric in H31 defines an asymmetric Type 1 (Lister, 1977) cross-girdle fabric,

with a top-to-the-south shear sense (Fig. 2.6). The cross girdle fabric is diffuse with a maximum density of 3 times uniform.

Approximately 500 m above the MCT (as mapped by Streule, 2009) following the Hinku River, sample H33 is a quartz + muscovite + biotite + plagioclase + garnet + K-feldspar mylonitized gneiss (Fig. 2.5b) from the GHS
(Fig. 2.3a, b). Large grains of plagioclase show perthitic texture, while smaller plagioclase grains show sericitic alteration. Muscovite, biotite, and quartz mark the macroscopic foliation, with plagioclase tails and micas indicating a top-to-the-south shear sense. Quartz grains are slightly annealed, approaching equilibrium grain boundaries with 120° intersections. GBM dominates the preserved dynamic recrystallization microstructures, and is best preserved in the largest grains. The quartz c-axis fabric from H33 is an asymmetric Type 1 cross girdle, with a top-to-the-south shear sense (Fig. 2.6). Compared with H31, the fabric is more clearly defined with a maximum density of 3.5 times uniform.

Sample 87H-6c is a metapelite from approximately the same structural position as H33 (Fig. 2.3a, c), with a mineral assemblage of muscovite + chlorite + quartz + plagioclase + garnet (Fig. 2.5c). Foliation is strongly developed within the muscovite and secondary chlorite domains. Quartz grains are dominantly annealed, with several lobate relict grain boundaries, indicating the local operation of GBM. Within the phyllosilicate-rich domains, quartz grain boundaries are dominantly “pinned”, while in the quartz-rich domains recrystallization is dominated by GBM and annealed grain boundaries are able to sweep over small mica grains. Garnets in the mica-rich domains are euhedral. Hubbard (1989) estimated a temperature of 520 °C for this sample based on garnet-biotite thermometry.

Sample 87H-6d is a quartz + muscovite + biotite + plagioclase metapelite (Fig. 2.5d) collected at ~ 1000 m above the MCT in the Hinku River Valley (Fig. 2.3a, b). Foliation is defined by muscovite, biotite, and quartz domains. Quartz grains are heavily annealed, but when dynamic recrystallization is preserved, GBM is dominant. Pinning of quartz grain boundaries occurs near large phyllosilicates, while the quartz grain boundaries are able to sweep over smaller phyllosilicates. The quartz c-axis fabric is a diffuse (maximum of 3 times

---

Figure 2.5
Next page. Microstructures associated with samples along the Hinku River Valley transect (see Figs. 2.3a, b for locations). (a) H31 with lobate quartz grain boundaries (L) and mica pinning (P); (b) H33 with annealing in quartz grains (A) and lobate quartz grain boundaries (L); (c) 87H-6c with annealing of quartz grains (A) and lobate quartz grain boundaries (L); (d) 87H-6d with annealing in quartz grains (A) and quartz grain boundaries 'sweeping' over mica grains (S); (e) 86H-4e with chess-board extinction (x) and blocky grain boundary bulging (B); (f) H7. All scale bars are 500 μm in length.

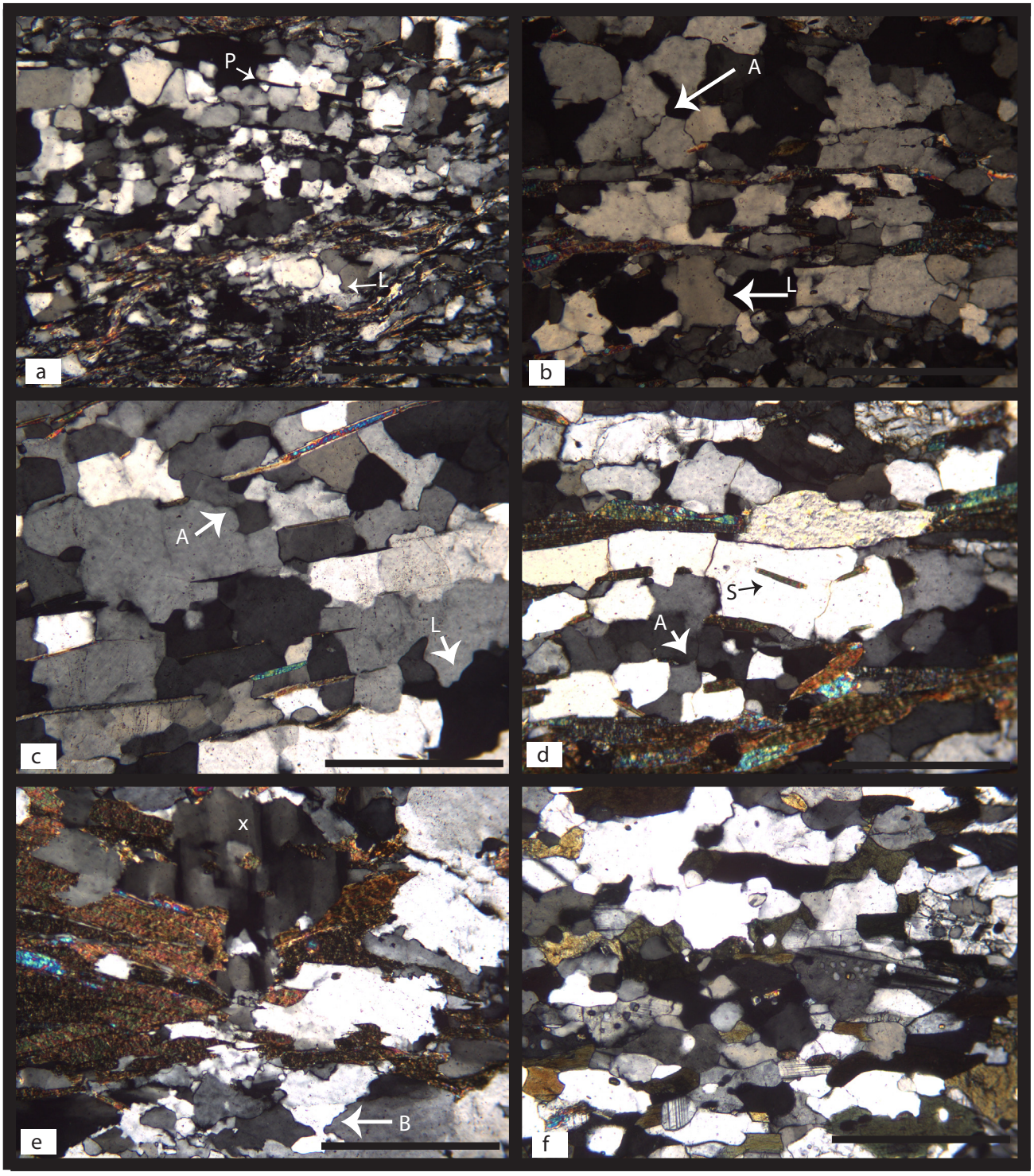

Figure 2.5

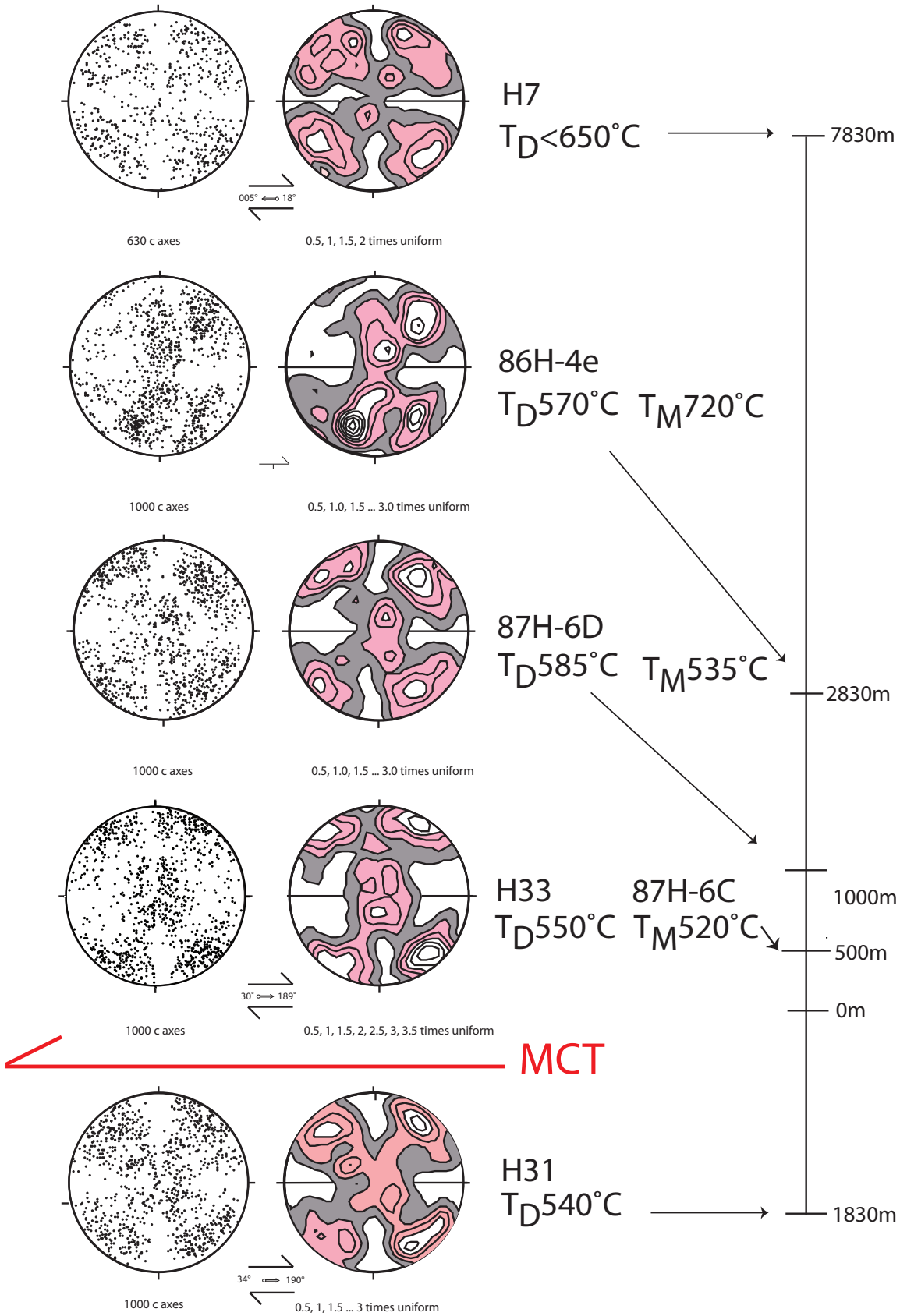
H7
T_D<650˚C
7830m
005° ⟸ 18°
630 c axes
0.5, 1, 1.5, 2 times uniform
86H-4e
T_D570˚C T_M720˚C
1000 c axes
0.5, 1.0, 1.5 ... 3.0 times uniform
87H-6D
T_D585˚C T_M535˚C
2830m
1000 c axes
0.5, 1.0, 1.5 ... 3.0 times uniform
H33
T_D550˚C
87H-6C
T_M520˚C
1000m
500m
0m
30° ⟹ 189°
1000 c axes
0.5, 1, 1.5, 2, 2.5, 3, 3.5 times uniform
MCT
H31
T_D540˚C
1830m
34° ⟹ 190°
1000 c axes
0.5, 1, 1.5 ... 3 times uniform

Figure 2.6

uniform density) asymmetric Type 1 cross girdle (Fig. 2.6) but, as this sample does not have an orientation marker, it is not possible to determine a shear sense with respect to geographic coordinates. Hubbard (1989) published a garnet-biotite thermometry temperature of 535 °C for this sample.

Approximately 2830 m structurally above the MCT is sample 86H-4e (Fig. 2.3a, b), a quartz + biotite + muscovite + feldspar + garnet gneiss (Fig. 2.5e). A weak foliation is defined by biotite-rich domains. Quartz grains are generally large, with checkerboard extinction patterns. Grain boundaries are marked by blocky bulging-type dynamic recrystallization microstructures. The quartz c-axis fabric from this sample defines a diffuse (maximum of 3 times uniform) asymmetric Type 1 cross girdle (Fig. 2.6). Hubbard (1989) published a garnet-biotite thermometry temperature of 720 °C for this sample.

Furthest structurally above the MCT in the Hinku River transect is sample H7 (7830 m above the MCT) (Fig. 2.3a, b), a quartz + chlorite + epidote green quartzite (Fig. 2.5f). Foliation is preserved in quartz and chlorite domains, and chlorite grains indicate a weak top to the south shear sense. The larger quartz grains have undulose extinction, while GBM is the dominant dynamic recrystallization mechanism. Some of the quartz rich domains are annealed, with grain boundaries approaching 120° equilibrium orientations. The quartz c-axis fabric of H7 defines a diffuse (maximum of 2 times uniform) Type 1 cross girdle (Fig. 2.6).

2.4.2 Dudh Kosi River

Sample H31 is also shown in the Dudh Kosi River traverse, as its locations is useful for comparing MCT footwall rocks in both traverses. For descriptions of microstructures and quartz fabrics, see above section.

Figure 2.6
Previous page. Optically measure quartz c-axis fabrics for metapelites (H31, 87H-6D), mylonitized gneisses (H33, 86H-4e) and quartzite (H7) from the Hinku River transect (see Fig. 2.3a, 3b for locations). Asymmetric fabrics for H31, H33, and H7 indicate top-to-the-south shear sense. Fabrics for 87H-6D and 86H-4e are asymmetric, but lack structural orientation to indicate shear sense. Deformation temperatures (TD) estimated from fabric opening angles and temperatures of metamorphism (TM) estimated by garnet-biotite thermometry (Hubbard, 1989) in individual samples are shown. Note: samples H33 and 87H-6C are from the same structural position above the MCT. Structural position of samples above/below the MCT are indicated by scale bar. All lower hemisphere equal area projections; foliation oriented 'east-west' and vertical, mineral stretching lineation trends 'east-west'.

Sample H27 was collected at ~ 500 m structurally below the MCT along the Dudh Kosi River (Figs. 2.3a, c) and is a quartz + muscovite + plagioclase + chlorite metapelite (Fig. 2.7a) from the LHS. Foliation is marked by quartz and muscovite grains. Plagioclase grains have lobate grain boundaries. Quartz is generally fine grained (50-60 μm) with microstructures indicating operation of both SGR and GBM, with GBM being the dominant dynamic recrystallization mechanism. Minor annealing has occurred in this sample. The quartz c-axis fabric is a diffuse (maximum of 3 times uniform) asymmetric Type 1 cross girdle, but due to the lack of a sample orientation marker, no geographic shear sense can be derived (Fig. 2.8).

H25 was collected at ~ 1330 m above the MCT (Fig. 2.3a, c) and is a mylonitized quartz + plagioclase + muscovite + biotite gneiss (Fig. 2.7b). Foliation is defined by quartz and muscovite grains, with muscovite grains indicating top to the south shear sense. GBM is the dominant recrystallization in quartz, with an increase in grain size (120-170 μm) relative to sample H27 collected from the footwall of the MCT. Quartz grain boundaries are able to "sweep" over small phyllosilicates. Plagioclase shows both myrmekitic texture and some lobate grain boundaries, hinting of dynamic recrystallization. The quartz c-axis fabric from this sample is a strongly defined asymmetric Type 1 cross-girdle (maximum of 4 times uniform), indicating a top to the south shear sense (Fig. 2.8).

2.4.3 Arun River

Sample H54 is a muscovite bearing quartzite (95% quartz) (Fig. 2.9a) collected at 300 m below the MCT in the Arun River valley (Fig. 2.3a). Foliation is defined by small micas that give

---

Figure 2.7
Next page. Microstructures associated with samples from the Dudh Kosi River Valley transect (see Figs. 2.3a, c for locations). (a) H27 with lobate quartz grain boundaries indicated (L); (b) H25 with quartz grain boundaries 'sweeping' over mica grains (S) and lobate (L) grain boundaries. All scale bars are 500 μm in length.

Figure 2.8
Next page. Optically measured quartz c-axis fabrics for metapelites (H31, H27) and mylonitized gneiss (H25) from the Dudh Kosi River Valley transect (see Figs. 2.3a, c for locations). Asymmetric fabrics for H31 and H25 indicate top-to-the-south shear sense. H27 has no orientation marker and therefore shear sense cannot be determined in geographic coordinates. All lower hemisphere equal area projections; foliation oriented 'east-west' and vertical, mineral stretching lineation trends 'east-west'. Structural position of samples above/below the MCT are indicated by scale bar.

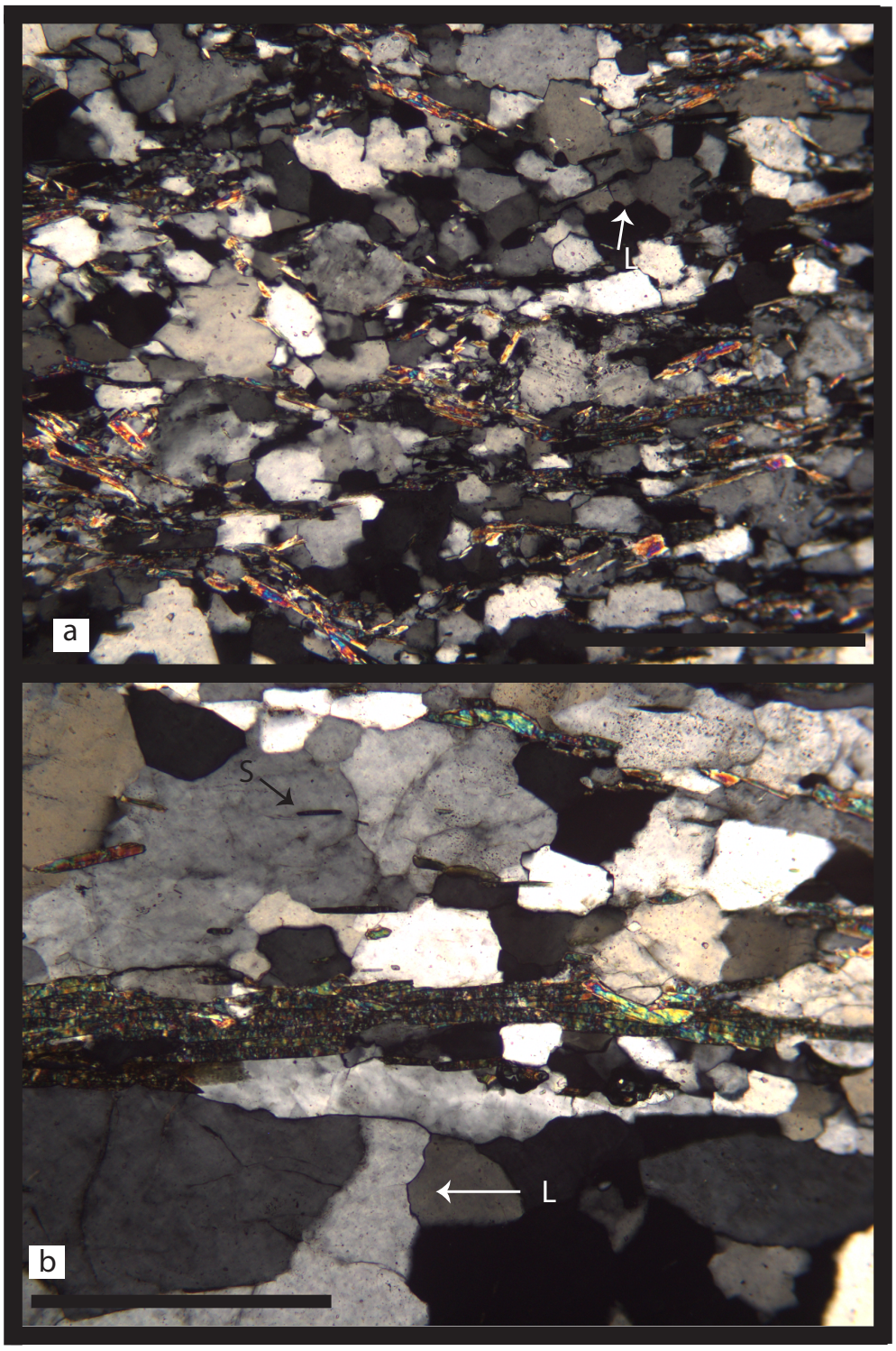

Figure 2.7

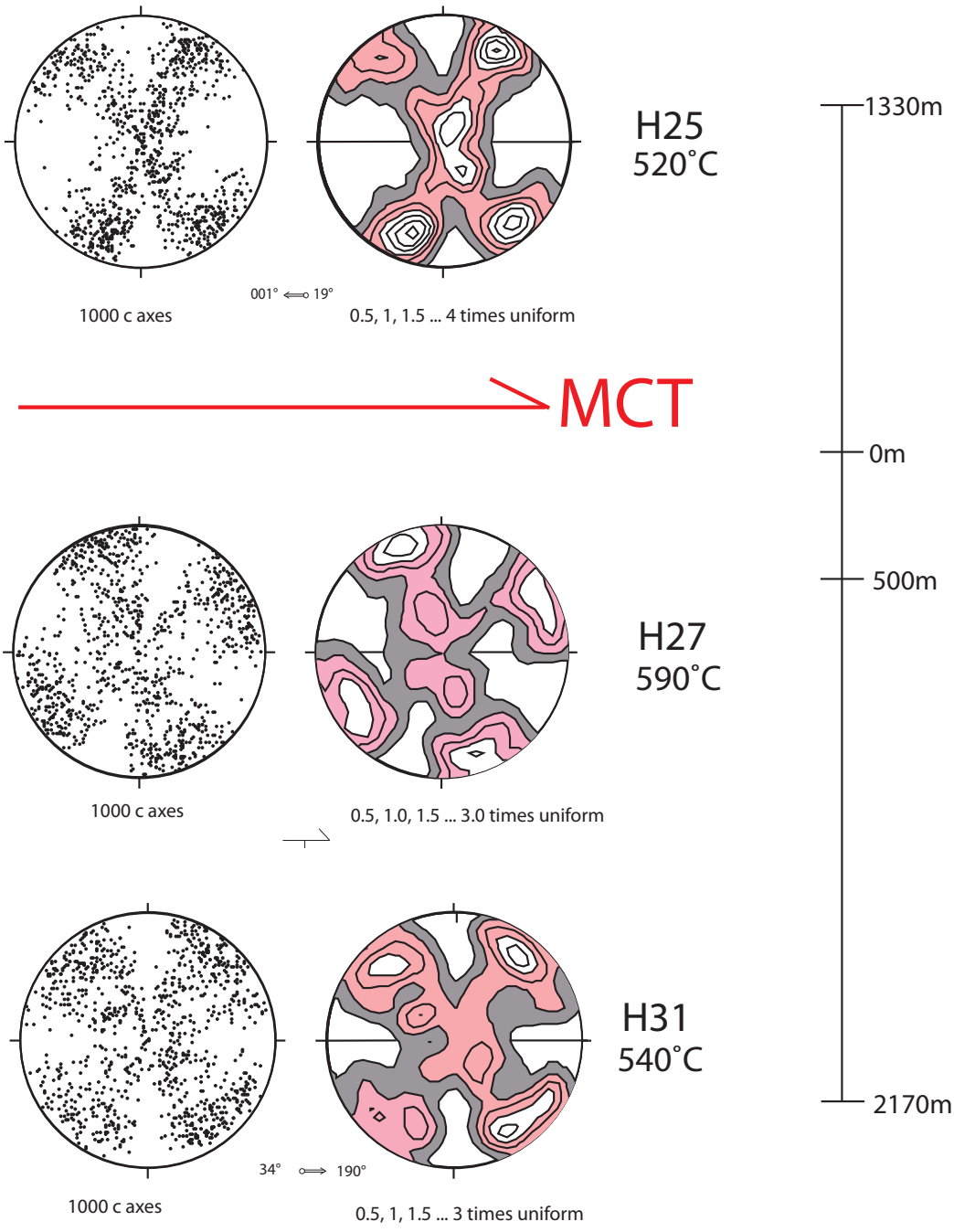
H25
520˚C
001° ⟸ 19°
1000 c axes
0.5, 1, 1.5 ... 4 times uniform
MCT
H27
590˚C
1000 c axes
0.5, 1.0, 1.5 ... 3.0 times uniform
H31
540˚C
34° ⟹ 190°
1000 c axes
0.5, 1, 1.5 ... 3 times uniform
1330m
0m
500m
2170m

Figure 2.8

quartz grains a tabular outline. No dynamic recrystallization microstructures have been preserved in this sample, as quartz grains are dominantly annealed. Trails of small mica grains within the larger quartz grains attest to the mobility of quartz grain boundaries. The quartz c-axis fabric is a "tightly-defined" (maximum of 4.5 times uniform density distribution) asymmetric Type 1 cross girdle, with a top to the NE shear sense (Fig. 2.10).

Sample A116 is another muscovite bearing quartzite (98% quartz) (Fig. 2.9b) collected at 8 km to the ESE from H54 at a structural distance of 3000 m below the MCT (Fig. 2.3a). A weak foliation is defined by quartz grains in this sample. Where quartz grains are not annealed, lobate boundaries are present indicating the local operation of low temperature and/or high strain rate grain boundary bulging. The quartz c-axis fabric from this sample defines a small circle girdle about the macroscopic stretching lineation (Fig. 2.10) indicating deformation in the constrictional strain field (Fig. 2.4b; Schmid and Casey, 1986).

Sample H58 was collected adjacent to the MCT (at approximately 300 m below the mapped position of the MCT) and to the southeast of samples H54 and A116 (Fig. 2.3a). This sample is a muscovite bearing quartzite (Fig. 2.9c) in which the mica grains define a weak foliation. GBM is dominant in the quartz grains, and trails of mica inclusions within the quartz grains indicate the widespread mobility of quartz grain boundaries. The quartz c-axis fabric from this sample defines an asymmetric Type 1 cross girdle (maximum of 3.5 times uniform) indicating a top to the southwest shear sense (Fig. 2.10).

2.5. Deformation Temperatures

Deformation temperatures associated with penetrative shearing in our samples may be estimated from the measured quartz c-axis fabrics from our samples using the fabric opening angle thermometer described by Kruhl (1998), who compiled multiple experimental and field-based studies correlating c-axis fabric opening angles with temperatures of deformation and/or metamorphism (Fig. 2.4b). The relationship between opening angle and deformation temperature is linear through greenschist to mid-upper amphibolite facies conditions (Kruhl, 1998; see discussion by Morgan and Law 2004) and is limited to deformation temperatures less than ~650-700 °C. Temperature estimates based on the Kruhl (1998) opening angle thermometer are usually quoted with an uncertainty of ± 50 °C and are dependent on critical resolved shear stresses for operative crystal glide systems being controlled by deformation temperature, rather than hydrolytic weakening or strain rate (cf. Tullis et al., 1973; Lister and Hobbs, 1980; Law et al., 2004; Morgan and Law, 2004).

Along the Hinku river (Fig. 2.3a) quartz c-axis fabric opening angles indicate deformation temperatures ranging from 540 °C to <650 °C (Fig. 2.6). From 3170 m below

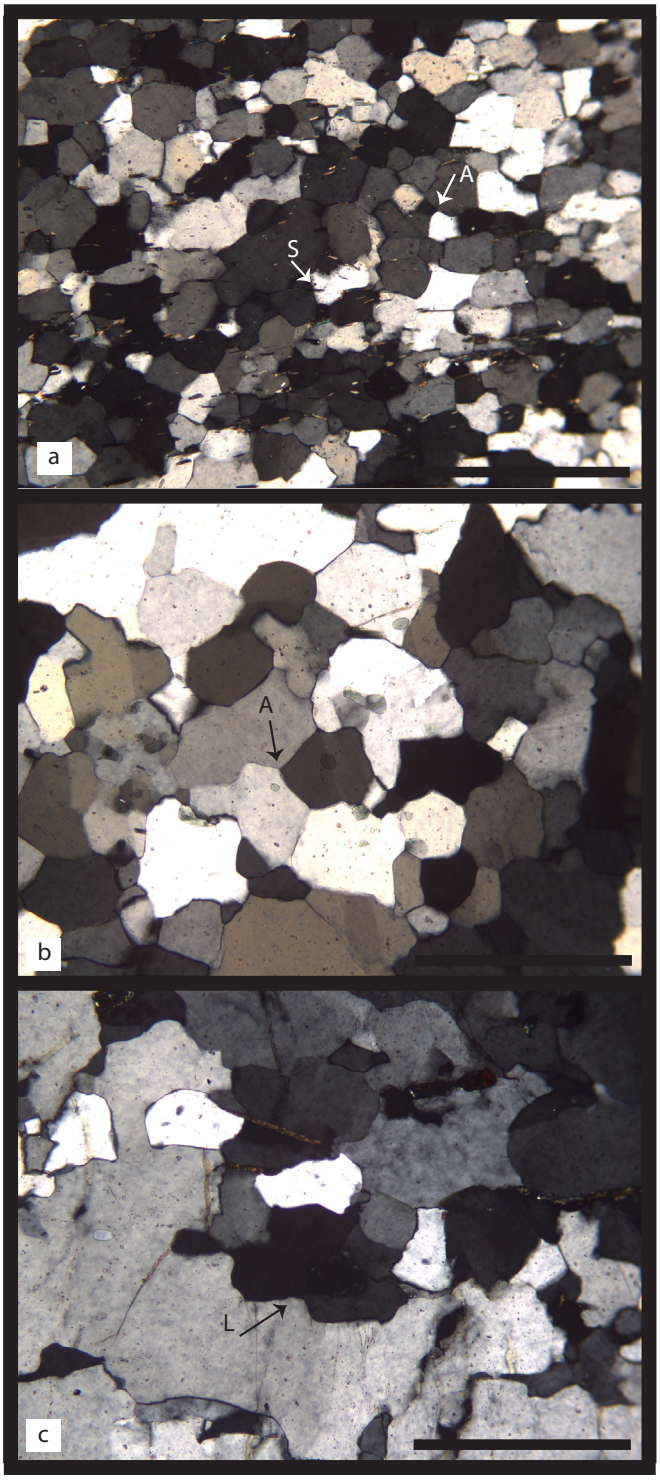

Figure 2.9
Microstructures associated with samples from the Arun River Valley transect (see Fig. 2.3a for locations). (a) Annealing (A) of quartz grains in sample H54 and quartz grain boundaries 'sweeping' over mica grains (S); (b) Annealing (A) of quartz grains in sample A116; (c) Lobate (L) quartz grain boundaries in sample H58. All scale bars are 500μm in length.

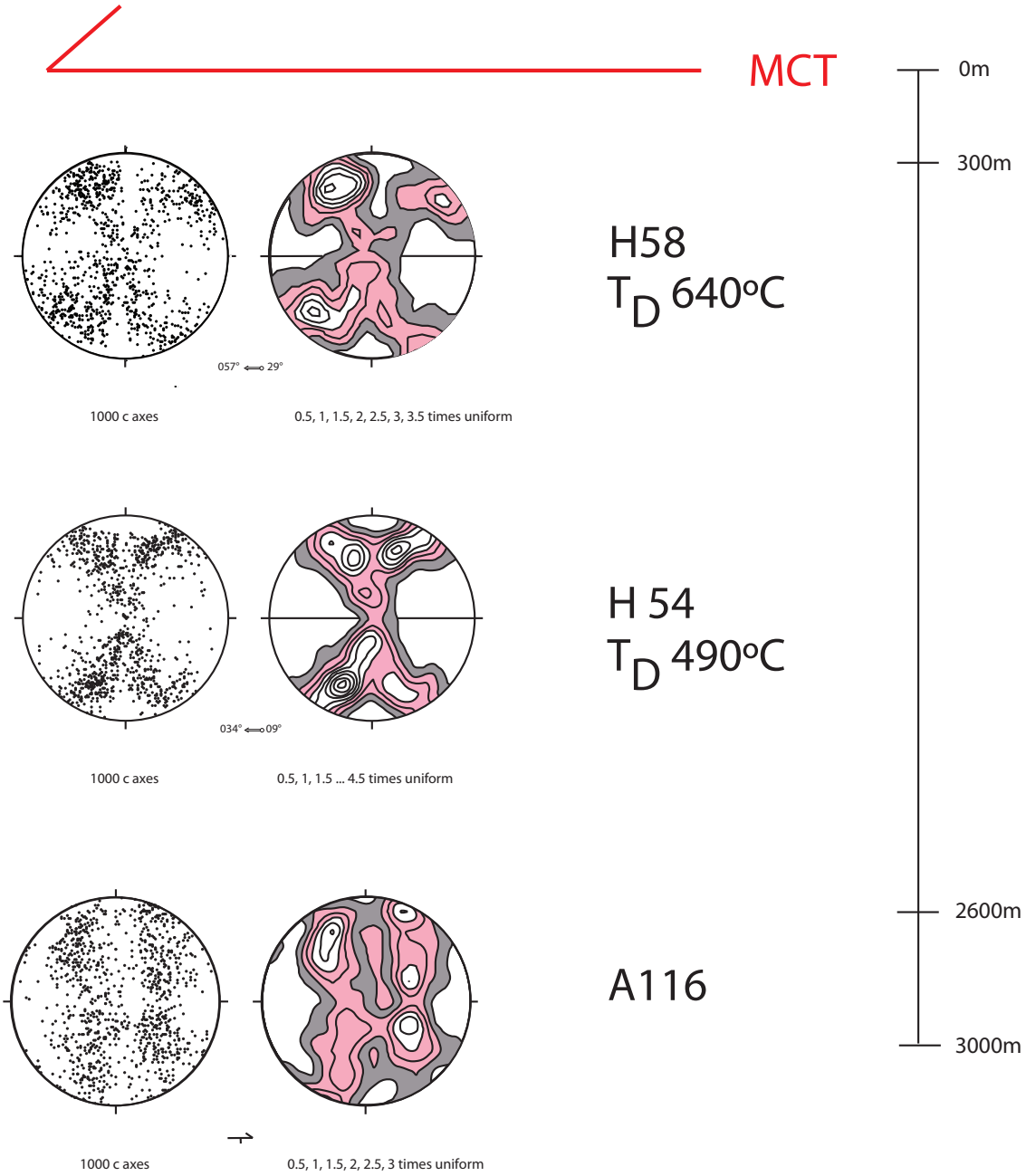

Figure 2.10
Optically measured quartz c-axis fabrics for quartzites (A116, H54, H58) from the Arun River Valley transect (see Fig. 2.3a for locations). The external fabric asymmetry in H58 indicates a top-to-the-northeast shear sense, while external asymmetry in H54 indicates a top-to-the-southwest shear sense. Small circle-girdle fabric centered about lineation in sample A116 indicates deformation within the constrictional strain field (Schmid and Casey, 1986); no orientation marker for this sample. All lower hemisphere equal area projections; foliation oriented 'east-west' and vertical, mineral stretching lineation trends 'east-west'; no macroscopic foliation (but strong linear grain shape fabric) present in A116.

the MCT (sample H31) to 2830 m above the MCT (sample 86H-4e) estimated deformation temperatures only vary within a 45 °C temperature range (samples H31, H33, 87H-6D, and 86H-4e). Along the Dudh Kosi river, quartz c-axis opening angles yield deformation temperatures from ranging from 520 to 590 °C (Fig. 2.8; samples H31, H27, and H25). The hottest of the samples is H27, found 330m below the MCT (Fig. 2.3a, c), with an estimated deformation temperature of 590 °C. In the Arun River Valley, quartz c-axis opening angles yield deformation temperatures ranging from 490 (H54) to 640 °C (H58) at 2600 m to 300 m below the MCT, respectively (Fig. 2.10).

2.6. Discussion

2.6.1 Deformation temperatures across the Main Central Thrust

Deformation temperatures indicated by fabric opening angles in both the hanging wall and footwall to the MCT in the Mount Everest region are generally above 500 °C (Figs. 2.6, 2.8 and 2.10). In the Hinku Valley deformation temperatures in the high 500 °C range are recorded up to 3 km above the MCT, increasing to 650 °C at 8 km above the MCT, near the migmatic core of the GHS (Fig. 2.6). Microstructures and fabric opening angles from the Dudh Kosi river valley indicate deformation temperatures greater than 500 °C in both the hanging wall and footwall to the MCT (Fig. 2.8). In the Arun Valley only the footwall to the MCT was sampled (Fig. 2.10). A strongly developed cross-girdle c-axis fabric in sample H54 located at 2600 m below the MCT indicates a deformation temperature of 490 °C, while a poorly defined opening angle in sample H58 (Fig. 2.10) at 300 m beneath the MCT could be indicate a deformation temperature of 640 °C. However, in comparison with other samples from this approximate structural position this temperature estimate seems implausibly high.

Deformation studies along strike in NW India, west-central Nepal and Bhutan all indicate deformation temperatures greater than 500 °C in the hanging wall to the MCT (Larson and Godin 2009; Larson et al. 2010, Long et al. 2011; Law et al. in press), while temperatures in the footwall to the MCT are generally lower. Observed microstructures (quartz recrystallization regime, brittle-plastic behavior of feldspar) generally agree with estimated temperatures based on fabric opening angles.

For example, to the east of the Mount Everest study area the immediate footwall to the MCT in Bhutan was penetratively sheared under at lower amphibolite facies conditions, with both SGR and GBM quartz microstructures developing (Long et al., 2011). Long et al. (2011) observed SGR as the dominant recrystallization regime in the footwall LHS rocks, corresponding to deformation temperatures of 400-500 °C. Adjacent to the MCT at the top of the LHS, GBM

is the dominant recrystallization regime, indicating deformation temperatures greater than 500 °C. In the hanging wall to the MCT in this region, Long and McQuarrie (2010) noted that GBM is the dominant quartz recrystallization mechanism, and that traced up section in to the core of the GHS the presence of quartz chessboard extinction patterns increases indicating deformation temperatures of 650 °C or higher.

To the west of the Everest region in central Nepal, Larson and Godin (2009) observed microstructural evidence for GBM in all their samples above the MCT. The quartz c-axis fabrics they observed indicated deformation temperatures ranging from 500 to 670 °C, with temperatures of ~ 500 °C at up to 7km above the MCT. Further to the west in the Sutlej Valley of NW India, Law et al. (in press) have documented deformation temperatures based on fabric opening angles that increase both with structural position above the MCT and relative foreland-hinterland position of individual sampling transects. In the more foreland transects deformation temperatures of ~ 530-550 °C were recorded adjacent to the MCT that then increase non-linearly with structural distance above the MCT to ~ 600 °C at ~ 1200 m above the thrust. In the more hinterland positioned transects temperatures of ~600 °C were estimated adjacent to the MCT that increase to ~ 670 °C at 2200 m above the thrust. The close correspondence between deformation temperatures and temperatures of metamorphism indicated by multiple mineral phase thermometry in these transects was interpreted as indicating that penetrative shearing associated with the preserved fabrics occurred at close to peak metamorphic temperatures.

In the Mount Everest study area temperatures of metamorphism are constrained for three samples in the Hinku River valley (Fig. 2.3a, b) based on garnet-biotite thermometry (Hubbard, 1989). At distances of 500 and 1000 m above the MCT temperatures indicated by fabric opening angles and garnet-biotite thermometry are similar (Fig. 2.6; 550 versus 520 °C in sample H33; 585 versus 535 °C in sample 87H-6D) and well within the uncertainty levels of the two thermometers. This could indicate that shearing occurred at close to peak metamorphic conditions at these structural levels. In contrast, at 2800 m above the MCT (sample 86H-4e) a deformation temperature of 570 °C is indicated by the Kruhl (1998) fabric opening angle thermometer, while garnet-biotite thermometry indicates a temperature of 720 °C (Fig. 2.6). This difference in estimated temperatures could indicate that penetrative shearing at higher structural level outlasted peak metamorphism and continued during the early stages of exhumation and cooling of rocks located in the sub-migmatitic core of the GHS. Alternatively, this difference in temperatures estimates could be due to the diffuse nature of the fabric for sample H7 (Fig. 2.6) and resultant inability to assign a meaningful opening angle.

2.6.2 Position of the Main Central Thrust

Detailed microstructural analysis of samples from the Dudh Kosi, Hinku, and Arun river valleys indicates that pervasive top-to-the-south shear sense occurred at temperatures above 500 °C. Searle et al. (2008) have argued that the MCT should be placed at the base of the zone of high strain ductile deformation commonly coinciding with the base of the zone of inverted metamorphism that places Tertiary metamorphic rocks of the GHS over unmetamorphosed or low grade rocks of the LHS. The position of the MCT (Fig. 2.3a) mapped by Streule (2009) is in broad agreement with this conceptual structural framework in that it is coincident with a broad zone of high penetrative strain. This mapped position of the MCT was used in calculating structural distance of our samples above/below the MCT (Figs. 2.6, 2.8 and 2.10).

However, in the Arun River Valley sample H58 located in the footwall to the footwall to the MCT (Fig. 2.3a) as mapped by Streule (2009) indicates a deformation temperature (640 °C; Fig. 10) that is usually characteristic of the MCT hanging wall. We therefore suggest that here the MCT should be placed at a lower structural level that could coincide with the mapped junction between the units of gt-bt schists (from which sample H58 was collected) and underlying chlorite grade metaquartzites and schists (Fig. 2.3a). This interpretation would be compatible with the deformation temperature of 490 °C (Fig. 2.10) obtained from the fabric opening angle in sample H54 located within a structural window in to these chlorite grade rocks in the Arun River Valley (Fig. 2.3a). Within this chlorite grade lithotectonic unit we note, however, that our structurally lowest sample (H31) yields an apparent deformation temperature of 540 °C based on fabric opening angle (Fig. 2.6). This estimated deformation temperature is clearly too high to be compatible with chlorite grade metamorphism, and could be interpreted as indicating the locally important role of hydrolytic weakening in controlling fabric development in these low-grade rocks.

A west-east trending antiform is present in the chlorite grade rocks located beneath all proposed positions of the MCT in the Dudh Kosi-Hinku region (Figs. 2.3b, c). The MCT is presumably folded over this footwall antiform, which must be taken in to account in estimating structural distances of samples beneath the MCT in this area. For example, sample H31 located many kilometers to the south of the mapped positions of the MCT on the south dipping limb of this antiform - with an estimated deformation temperature of 540 °C (Fig. 2.8) - may only be located a few hundreds of meters beneath the MCT when this fold structure is taken in to account (Fig. 2.3b). Once again, however, this inferred deformation temperature is too high for the sample's position within chlorite grade rocks. In contrast, sample H27 located on the north dipping limb of the antiform within the overlying garnet biotite schists (Fig. 2.3c) yields a deformation temperature of 590 °C (Fig. 2.8). This east-west trending antiform does not

correspond with the anticline indicated by Goscombe et al. (2006), as they mapped a north-south trending anticline through this area. How these two antiforms relate to each other structurally is undeterminable based on the current mapping.

Due to the presence of shear structures and high deformation temperatures, the Searle et al. (2008) definition of the MCT is appropriate for this study area, including all ductily deformed rocks in the MCTZ. We agree that the MCT should be placed at the base of this zone of ductile shearing, but the Streule (2009) mapped location of the MCT for the Dudh Kosi and Hinku rivers does not match our data. Instead, we suggest that the MCT south of Mt. Everest be placed in the chlorite grade schists previously marked as belonging to the LHS. Goscombe et al. (2006) suggest the MCT is exposed as a klippe in the Dudh Kusi-Hinku region, through mapping the MCT through the garnet-biotite grade schists and the chlorite schists, in what they call the Ulleri Formation. This mapping of the MCT is closer to what we propose, but does not account for our structurally lowest sample, H31 (Fig. 2.3a, c), which has a deformation temperature of 540 °C. However, with our current data set, we are not able to confidently predict the exact location of the MCT. We can only suggest that it be place at a lower structural level to fit the deformation features we see in our samples.

2.6.3 Comparison with quartz fabrics reported from along-strike studies across the MCT

The optically measured quartz c-axis fabrics reported in this study from hanging wall and footwall of the MCT in the Mount Everest area are very diffuse and weakly defined, relative to fabrics described from similar structural positions in other parts of the Himalaya. For example, Grujic et al. (1996) have described strongly developed and well-defined quartz fabrics measured by X-ray texture goniometry from the MCT hanging wall/footwall in the Bhutan Himalaya (Fig. 2.1). Similarly, Grasemann et al. (1999) have described well-defined quartz c-axis and a-axis fabrics from the hanging wall to the MCT in the Sutlej Valley of NW India (Fig. 2.1) measured by X-ray texture goniometry, and the strongly defined nature of the c-axis fabrics in these high strain rocks was subsequently confirmed optically by Law et al. (in press). Likewise, in the Annapurna Range of the central Himalaya, Bouchez and Pêcher (1981) have reported strongly developed quartz c-axis fabrics based on optical microscopy of relatively low grade quartzites within the lower part of the GHS.

The first question to be asked from this comparison is why are the fabrics from the Everest section across the MCT so diffuse in comparison with fabrics measured along strike in other parts of the Himalaya? Could it be due to a late static annealing that did not develop in these other areas? For example, Miocene age leucogranite generation within the overlying GHS is far more widespread in the Everest region (Searle et al., 1999, 2003, 2006) than in the

other areas. Could these leucogranites have provided an additional heat source that produced a static annealing of originally more strongly developed fabrics? Certainly we have recorded microstructural evidence for a locally limited late stage annealing in our samples from the Everest sections across the MCT. This suggestion is not compatible, however with the relatively strongly developed quartz c-axis fabrics reported by Law et al. (2004, 2011) from the immediate footwall to the STDS at the top of the GHS in the Everest region. If static annealing and reduction in fabric strength occurred at the base of the GHS in the Everest region, why did it not occur at the top of the section? Additionally, some experimental studies indicate that static annealing will strengthen rather than weaken a previously developed crystallographic fabric (Green et al., 1970), while other experimental studies shows no great change in crystallographic fabric when an entire sample is annealed (Heilbronner and Tullis, 2002).

Alternatively, could the difference in strength of fabric development be due to a difference in rock types analyzed in the different study areas, as the presence of second phase minerals may result in the development of more diffuse fabrics than would form in relatively pure quartzites (Starkey and Cutforth, 1978). This does provide a potential explanation for the diffuse fabrics recorded in the Hubbard (1989) samples from the Everest region that were primarily collected for metamorphic petrology, and are therefore rich in mica, garnet and alumino-silicate mineral phases. In comparison, the fabrics reported by Bouchez and Pecher (1981) and Grujic et al. (1996) from the MCT hanging wall / footwall in the central and eastern Himalaya were measured on relatively pure quartzites. However, the strongly defined fabrics measured by Grasemann et al. (1999) and Law et al. (in press) from the MCT hanging wall in the Sutlej valley of NW India (Fig. 2.1) NW India did include orthogneisses that were relatively rich in mica and feldspar. Similarly, the relatively strongly defined fabrics measured at the top of the GHS in the Everest region (Law et al. 2004, 2011) were dominantly from mica-rich gneisses and schists in which quartz was often a minor mineral phase. Additionally, some of the diffuse fabrics reported from the Streule (2009) collection of Everest samples were measured on pure quartzites (i.e. sample H7; Fig. 2.6) while some of the Streule (2009) pure quartzite samples in the Arun region gave strong fabrics (i.e. sample H54; Fig. 2.10). Therefore, rock type in itself cannot explain the relatively diffuse nature of the fabrics from the Everest section across the MCT.

The second question that arises from comparison with along-strike studies is how great a reliance should we place on deformation temperatures estimated from fabric opening angles in these relatively diffuse fabrics? Clearly given the diffuse nature of the c-axis fabrics it is difficult to assign opening angles - and hence inferred deformation temperatures - to these fabrics with any significant degree of certainty. As discussed above, this is demonstrably a problem with fabrics from the chlorite bearing rocks at the base of the Everest section where fabric opening

angles indicate deformation temperatures that are significantly higher than the stability field of chlorite. However, whether this is due to difficulty in meaningfully defining the opening angle in these diffuse fabrics, or is due to other factors such as hydrolytic weakening, remains to be determined. Here it would be instructive to both independently calculate deformation temperatures of the plastically deformed quartz grains using a method such as titanium in quartz thermometry (e.g. Thomas et al., 2010; Grujic et al., 2011) while simultaneously using infrared spectroscopy (e.g. Kronenberg and Wolf, 1990) to compare internal 'water' contents in quartz grains from the chlorite-rich rocks with those from the structurally higher structural units in which mineral assemblages indicate higher temperatures of metamorphism.

The nature of the quartz fabrics, together with the limited sampling coverage, makes it difficult to discuss the nature of the inverted deformation isograds above the MCT. The Hinku River transect (Fig. 2.3a, b) is the only transect that extends into the GHS, showing a significant increase in deformation temperature from 3000 - 7000 m away from the MCT. A higher density sampling coverage could help determine if deformation isotherms and/or metamorphic isograds are telescoped adjacent to the MCT, as seen along strike in other parts of the Himalaya.

2.7. Conclusions

1) Deformation temperatures associated with ductile shear in the hanging wall to the MCT range from ~500 °C to 650 °C in the study area located to the south of Mount Everest . Deformation temperatures of ~500 °C have been recorded in the immediate hanging wall to the MCT along the entire length of the Himalaya, indicating a surprising continuity of along-strike deformation conditions at the current level of exposure of the MCT.

2) At structural distances of up to 1000 m above the MCT, deformation temperature from opening angle and garnet-biotite thermometry yield temperatures within error of each other, suggesting that shearing occurred close to peak metamorphic conditions. Traced further upwards into the migmatitic core of the GHS, temperatures indicated by garnet-biotite and fabric opening angle thermometry do not match, suggesting that penetrative shearing outlasted peak metamorphism.

3. The position of the MCT in the Mount Everest region needs to be remapped, placing it at structurally lower than currently mapped, and at a structural level closer to where deformation thermometry indicates that penetrative shearing occurred at ~500 °C.

4. The diffuse nature of quartz c-axis fabrics in the Mount Everest region contrasts markedly with the well-defined quartz c-axis fabrics found along strike adjacent to the MCT in other parts of the Himalaya. Further sampling and laboratory analyses

(incorporating quartz fabric analyses, infrared spectroscopy measured of ‘internal water contents’ in quartz grains, complemented by independent methods of deformation thermometry such as the Ti-in-W method) are needed to better understand the deformation history of this section of the MCT.

References

Beaumont, C., Jamieson, R.A., Nguyen, M.H., Lee, B., 2001. Himalayan tectonics explained by extrusion of a low-viscosity crustal channel coupled to focused surface denudation. Nature 414, 738-742.

Beaumont, C., Jamieson, R.A., Nguyen, M.H., Medvedev, S., 2004. Crustal channel flows: 1 Numerical models with applications to the tectonics of the Himalayan-Tibetan orogen. Journal of Geophysical Research Solid Earth 109.

Bhattacharya, A.R., Weber, K., 2004. Fabric development during shear deformation in the Main Central Thrust Zone, NW-Himalaya, India. Tectonophysics 387, 23-46.

Bordet, P., 1961. Recherches geologiques dans l'Himalaya du Nepal, region du Makalu.

Bouchez, J.L., Pêcher, A., 1976. Microstructures and quartz preferred orientations in quartzites of the Annapurna area (central Nepal), in the proximity of the main central thrust. Himalayan Geology 6, 118-131.

Bouchez, J.L., Pêcher, A., 1981. The Himalayan Main Central Thrust pile and its quartz-rich tectonite in central Nepal. Tectonophysics 78.

Brunel, M., 1986. Ductile thrusting in the Himalayas; shear sense criteria and stretching lineations. Tectonics 5, 247-265.

Brunel, M., Kienast, J.-R., 1986. Etude petro-structurale des chevauchements ductiles himalayens sur la transversale de l'Everest-Makalu (Nepal oriental). Canadian Journal of Earth Sciences = Revue Canadienne des Sciences de la Terre 23, 1117-1137.

Burchfiel, B.C., Zhiliang, C., Hodges, K.V., Yuping, L., Royden, L.H., Changrong, D., Jiene, X., 1992. The South Tibetan detachment system, Himalayan orogen: Extension contemporaneous with and parallel to shortening in a collisional mountain belt. Geological Society of America Special Papers 269, 1-41.

Célérier, J., Harrison, T.M., Webb, A.A.G., Yin, A., 2009. The Kumaun and Garwhal Lesser Himalaya, India: Part 1. Structure and stratigraphy. Geological Society of America Bulletin 121, 1262-1280.

Colchen, M., Le Fort, P., Pecher, A., 1986. Carte Geologique Annapurna-Manaslu-Ganesh, Himalaya du Nepal.

Corrie, S.L., Kohn, M.J., Vervoort, J.D., 2010. Young eclogite from the Greater Himalayan Sequence, Arun Valley, eastern Nepal; P-T-t path and tectonic implications. Earth and Planetary Science Letters 289, 406-416.

Daniel, C.G., Hollister, L.S., Parrish, R.R., Grujic, D., 2003. Exhumation of the Main Central Thrust from lower crustal depths, eastern Bhutan Himalaya. Journal of Metamorphic Geology

21, 317-334.

DeCelles, P.G., Robinson, D.M., Quade, J., Ojha, T.P., Garzione, C.N., Copeland, P., Upreti, B.N., 2001. Stratigraphy, structure, and tectonic evolution of the Himalayan fold-thrust belt in western Nepal. Tectonics 20, 487-509.

DeCelles, P.G., Robinson, D.M., Zandt, G., 2002. Implications of shortening in the Himalayan fold-thrust belt for uplift of the Tibetan Plateau. Tectonics 21, 25-25.

England, P., Molnar, P., 1993. The interpretation of inverted metamorphic isograds using simple physical calculations. Tectonics 12, 145-158.

Gansser, A., 1964. The geology of the Himalayas.

Gansser, A., 1983. Geology of the Bhutan Himalaya. Denkschriften der Schweizerischen Naturforschenden Gesellschaft = Memoires de la Societe Helvetiques des Sciences Naturelles 96, 181-181.

Godin, L., Grujic, D., Law, R.D., Searle, M.P., Law, R.D., Searle, M.P., Godin, L., 2006. Channel flow, ductile extrusion and exhumation in continental collision zones; an introduction. Geological Society Special Publications 268, 1-23.

Goscombe, B., Gray, D., Hand, M., 2006. Crustal architecture of the Himalayan metamorphic front in eastern Nepal. Gondwana Research 10, 232-255.

Goscombe, B., Hand, M., Gray, D., 2003. Structural and metamorphic architecture of the east Nepal Himalayas. Geological Society of Australia, Specialist Group in Tectonics and Structural Geology, Conference Abstracts, Kalbarri, p. 135.

Grasemann, B., Fritz, H., Vannay, J.-C., 1999. Quantitative kinematic flow analysis from the Main Central Thrust Zone (NW-Himalaya, India); implications for a decelerating strain path and the extrusion of orogenic wedges. Journal of Structural Geology 21, 837-853.

Green II, H., Griggs, D., Christie, J., 1970. Syntectonic and annealing recrystallization of fine-grained quartz aggregates. Springer.

Grujic, D., Casey, M., Davidson, C., Hollister, L.S., Kundig, R., Pavlis, T., Schmid, S., 1996. Ductile extrusion of the Higher Himalayan Crystalline in Bhutan: evidence from quartz microfabrics. . Tectonophysics 260.

Grujic, D., Stipp, M., Wooden, J.L., 2011. Thermometry of quartz mylonites: Importance of dynamic recrystallization on Ti-in-quartz reequilibration. . Geochemistry, Geophysics, Geosystems (G3) 12.

Harrison, T.M., Ryerson, F.J., Le Fort, P., Yin, A., Lovera, O.M., Catlos, E.J., 1997. A late Miocene-Pliocene origin for the central Himalayan inverted metamorphism. Earth and Planetary Science Letters 146, E1-E7.

Heilbronner, R. and Tullis, J., 2002. The effect of static annealing on microstructures and crystallographic preferred orientaitions of quartites experimentally deforemd in axial compression and sherar. In: De Meer, S., Drury, M.D., de Bresser, J.H.P, Penncok, G.M., (eds) Deformation mechanisms, rheology and tectonics: current status and future perspectives Special Publication, 200, GSL, pp 191-218.

Heim, A., Gansser, A., 1939. Central Himalaya; geological observations of the Swiss expedition 1936, pp. 245-245.

Hirth, G., Tullis, J., 1992. Dislocation Creep Regimes in Quartz Aggregates. Journal of Structural Geology 14, 145-159.

Hodges, K.V., Hubbard, M.S., Silverberg, D.S., 1988. Metamorphic constrains on the thermal evolution of the central Himlayan orogen. Philosophical Transactions of the Royal Society a-Mathematical Physical and Engineering Sciences 326, 257-280.

Hodges, K.V., Parrish, R.R., Searle, M.P., 1996. Tectonic evolution of the central Annapurna Range, Nepalese Himalayas. Tectonics 15, 1264-1291.

Hubbard, M.S., 1988. Thermobarometry, 40Ar/39Ar Geochronology, and Structure of the Main Central Thrust Zone and Tibetan Slab, Eastern Nepal Himalaya [Ph.D. thesis]. Massachusetts Institute of Technology.

Hubbard, M.S., 1989. Thermobarometric constrains on the thermal history of the Main Central thrust zone and Tibetan slab, eastern Nepal Himalaya Journal of Metamorphic Geology 7, 19-30.

Hubbard, M.S., 1996. Ductile shear as a cause of inverted metamorphism: Example from the Nepal Himalaya. Journal of Geology 104, 493-499.

Hubbard, M.S., Harrison, T.M., 1989. (super 40) Ar/ (super 39) Ar age constraints on deformation and metamorphism in the Main Central Thrust zone and Tibetan Slab, eastern Nepal Himalaya. Tectonics 8, 865-880.

Jaupart, C., Provost, A., 1985. Heat focussing, granite genesis and inverted metamorphic gradients in continental collision zones. Earth and Planetary Science Letters 73, 385-397.

Jessup, M.J., Law, R.D., Searle, M.P., Hubbard, M.S., Law, R.D., Searle, M.P., Godin, L., 2006. Structural evolution and vorticity of flow during extrusion and exhumation of the Greater Himalayan Slab, Mount Everest Massif, Tibet/Nepal; implications for orogen-scale flow partitioning. Geological Society Special Publications 268, 379-413.

Johnson, M.R.W., Oliver, G.J.H., Parrish, R.R., Johnson, S.P., 2001. Synthrusting metamorphism, cooling, and erosion of the Himalayan Kathmandu Complex, Nepal. Tectonics 20, 394-415.

Kohn, M.J., Wieland, M.S., Parkinson, C.D., Upreti, B.N., 2004. Miocene faulting at plate tectonic velocity in the Himalaya of central Nepal. Earth and Planetary Science Letters 228, 299-

310.

Kohn, M.J., Wieland, M.S., Parkinson, C.D., Upreti, B.N., 2005. Five generations of monazite in Langtang gneisses; implications for chronology of the Himalayan metamorphic core. Journal of Metamorphic Geology 23, 399-406.

Kronenberg, A.K., Wolf, G.H., 1990. Fourier transform infrared spectroscopy determinations of intragranular water content in quartz-bearing rocks: implications for hydrolytic weakening in the laboratory and within the earth. Tectonophysics 172, 255-271.

Kruhl, J.H., 1998. Reply: Prism- and basal-plane parallel subgrain boundaries in quartz: a microstructural geothermobarometer. Journal of Metamorphic Geology 16, 142-146.

Larson, K.P., Godin, L., 2009. Kinematics of the Greater Himalayan sequence, Dhaulagiri Himal: implications for the structural framework of central Nepal. Journal of the Geological Society 166, 25-43.

Larson, K.P., Godin, L., Price, R.A., 2010. Relationships between displacement and distortion in orogens: Linking the Himalayan foreland and hinterland in central Nepal. Bulletin of the Geological Society of America 122, 1116-1134.

Law, R.D., Jessup, M.J., Searle, M.P., Francsis, M.K., Waters, D.J., Cottle, J.M., 2011. Telescoping of isotherms beneath the South Tibetan detachment system, Mount Everest Massif. Journal of Structural Geology 33, 1569-1594.

Law, R.D., Searle, M.P., Simpson, R.L., 2004. Strain, deformation temperatures and vorticity of flow at the top of the Greater Himalayan Slab, Everest Massif, Tibet. Journal of the Geological Society of London 161, 305-320.

Law, R.D., Stahr, D.W., Francsis, M.K., Ashley, K.T., Grasemann, B., Ahmad, T., in press. Deformation temperatrues and flow vorticities near the base of the Greater Himalayan Series, Sutlej Valley and Shimla Klippe, NW India. Journal of Structural Geology.

LeFort, P., 1975. HImalays, the collided range: present knowledge of the contiental arc. American Journal of Science 275, 1-44.

Lister, G.S., 1977. Crossed-girdle c-axis fabrics in quartzites plastically deformed by plane strain and progressive simple shear. Tectonophysics 39, 51-54.

Lister, G.S., Hobbs, B.E., 1980. The simulation of fabric development during plastic deformation and its application to quartzite; the influence of deformation history. Journal of Structural Geology 2, 355-370.

Long, S., McQuarrie, N., 2010. Placing limits on channel flow; insights from the Bhutan Himalaya. Earth and Planetary Science Letters 290, 375-390.

Long, S., McQuarrie, N., Tobgay, T., Hawthorne, J., 2011. Quantifying internal strain and

deformation temperature in the eastern Himalaya, Bhutan: Implications for the evolution of strain in thrust sheets. Journal of Structural Geology 33, 579-608.

Martin, A.J., DeCelles, P.G., Gehrels, G.E., Patchett, P.J., Isachsen, C., 2005. Isotopic and structural constraints on the location of the Main Central Thrust in the Annapurna Range, central Nepal Himalaya. Geological Society of America Bulletin 117, 926-944.

Molnar, P., England, P.C., 1990. Temperatures, heat flux, and frictional stress near major thrust faults. Journal of Geophysical Research 95, 4833-4856.

Morgan, S.S., Law, R.D., 2004. Unusual transition in quartzite dislocation creep regimes and crystal slip systems in the aureole of the EJB pluton, California: a case for anhydrous conditions creaed y decarbonation of adjacent marbles. . Tectonophysics 384, 209-231.

Parrish, R.R., Hodges, V., 1996. Isotopic constraints on the age and provenance of the Lesser and Greater Himalayan sequences, Nepalese Himalaya. Bulletin of the Geological Society of America 108, 904-911.

Robinson, D., DeCelles, P., Garzione, C., Pearson, O., Harrison, T., Catlos, E., 2003. Kinematic model for the Main Central thrust in Nepal. Geology 31, 359-362.

Robinson, D.M., DeCelles, P.G., Copeland, P., 2006. Tectonic evolution of the Himalayan thrust belt in western Nepal; implications for channel flow models. Geological Society of America Bulletin 118, 865-885, 861 sheet.

Robinson, D.M., DeCelles, P.G., Patchett, P.J., Garzione, C.N., 2001. The kinematic evolution of the Nepalese Himalaya interpreted from Nd isotopes. Earth and Planetary Science Letters 192, 507-521.

Schelling, D., 1992. The tectonostratigraphy and structure of the eastern Nepal Himalaya. Tectonics 11, 925-943.

Schmid, S., Casey, M., 1986. Complete fabric analysis of some commonly observed quartz c-axis patterns. Geophysical Monograph 36, 263-286.

Searle, M., Law, R., Jessup, M., 2006. Crustal structure, restoration and evolution of the Greater Himalaya in Nepal-South Tibet: implications for channel flow and ductile extrusion of the middle crust. Geological Society, London, Special Publications 268, 355-378.

Searle, M., Simpson, R., Law, R., Parrish, R., Waters, D., 2003. The structural geometry, metamorphic and magmatic evolution of the Everest massif, High Himalaya of Nepal–South Tibet. Journal of the Geological Society 160, 345-366.

Searle, M.P., Law, R.D., Godin, L., Larson, K.P., Streule, M.J., Cottle, J.M., Jessup, M.J., 2008. Defining the Himalayan Main Central Thrust in Nepal. Journal of the Geological Society 165, 523-534.

Searle, M.P., Rex, A.J., 1989. Thermal model for the Zanskar Himalaya. Journal of Metamorphic Geology 7, 127-134.

Searle, M.P., Stephenson, B., Walker, J., Walker, C., 2007. Restoration of the Western Himalaya: implications for metamorphic protoliths, thrust and normal faulting, and channel flow models. Episodes 30, 242.

Searle, M.P., Waters, D.J., Dransfield, M.W., Stephenson, B., Walker, C., Walker, J.D., Rex, D.C., 1999. Thermal and mechanical models for the structural evolution of Zanskar High Himalaya. Geological Society of London, Special Publication.

Srivastava, P., Mitra, G., 1996. Deformation mechanisms and inverted thermal profile in the North Almora Thrust mylonite zone, Kumaon Lesser Himalaya, India. Journal of Structural Geology 18, 27-39.

Starkey, J., Cutforth, C., 1978. A demonstration of the interdependence of the degree of quartz preferred orientation and the quartz content of deformed rocks. Canadian Journal of Earth Sciences 15, 841-847.

Stipp, M., Stunitz, H., Heilbronner, 2002. The Eastern Tonale Fault Zone: a 'natural labatory' for crystal plastic deformation of quartz over a temperature range from 250 to 700. Journal of Structural Geology 24.

Streule, M.J., 2009. The structural, metamorphic and magmatic evolution of the Greater Himalayan sequence and main central thrust, Eastern Nepal Himalaya [Ph.D. thesis]. Oxford University.

Thomas, J.B., Watson, E.B., Spear, F., Shemella, P.T., Nayak, S.K., Lanzirotti, A., 2010. TitaniQ under pressure: the effect of pressure and temperture on the solubility of Ti in quartz Contributions to Mineralogy and Petrology.

Tullis, J., Christie, J.M., Griggs, D.T., 1973. Microstructures and Preferred Orientations of Experimentally Deformed Quartzites. Geological Society of America Bulletin 84, 297-314.

Yakymchuk, C., Godin, L., Brown, M., 2012. Coupled role of deformation and metamorphism in the construction of inverted metamorphic sequences; an example from far-northwest Nepal. Journal of Metamorphic Geology 30, 513-535.

Chapter 3

Thermal Structure of the Moine and Sgurr Beag Thrust Sheets, NW Scotland

Sarah Elizabeth Mazza

3.1. Abstract

In the Caledonides of NW Scotland temperatures of metamorphism (*T*m) and deformation (*T*d) progressively increase up structural section in the Moine thrust sheet at the foreland edge of the Scandian (middle Silurian) orogenic wedge. However, the thermal history of the structurally overlying, more hinterland positioned, thrust sheets is less well constrained. This study focuses on determining *T*d and *T*m for both the Moine and overlying Sgurr Beag thrust sheets.

Preserved microstructures in the Moine and overlying Sgurr Beag thrust sheets imply a wide range of possible deformation temperatures that are quantified with the quartz c-axis fabric opening-angle thermometer developed by Kruhl (1998). *T*d from quartz opening-angle thermometry increases up section, ranging from 395 °C to 583 °C ± 50 °C. This study also presents new metamorphic *P-T* constraints for the Sgurr Beag thrust sheet, based on garnet-biotite thermometry and GASP barometry, indicating *T*m of ~ 620 °C at 5.8 - 7.4 kbar. Together, *T*d and *T*m indicate that penetrative deformation continued after peak metamorphic conditions recorded in the Sgurr Beag thrust sheet. The topology of measured quartz c-axis fabrics in the Moine and Sgurr Beag thrust sheets exposed to the north of Loch Fannich indicate constrictional strains associated with thrusting, while fabrics from these thrust sheets in the Ben Wyvis/Garve region indicate a phase of normal-sense shearing that post-dated thrusting.

3.2. Introduction

Within the eastward-dipping Moine and structurally overlying thrust sheets (or nappes) of northwest Scotland (Fig. 3.1) deformation fabrics in quartz- rich psammites and metamorphic indicator minerals in rare intercalated pelite horizons suggest that temperatures of deformation (*T*d) and metamorphism (*T*m) progressively increase up structural section from foreland to hinterland (Read, 1931; Soper and Brown, 1971; Winchester, 1974; Barr et al., 1986; see review by Johnson and Strachan, 2006). Historically this regional-scale foreland-hinterland increase in temperatures indicated by preserved fabrics and mineral assemblages has generally been interpreted in terms of west-directed thrusting of hotter over cooler rocks and/or late-stage penetrative retrograde shearing of originally higher temperature rocks (overprinting of higher temperature fabrics by lower temperature fabrics) during foreland-propagating thrusting (Peach et al. 1907; Read 1931; Butler 2010). However, even within individual thrust sheets - where

---

Figure 3.1
Next page. Regional scale geologic map of northwest Scotland, showing major lithologies and tectonic features. Location of study areas are highlighted. Cross-section from Braemore Junction to Rogie Falls (Fig. 3.3) is indicated by line A-A', crossing through the Moine and Sgurr Beag thrust sheets. Stars represent locations for new P-T constraints. Adapted from Thigpen et al., (2010).

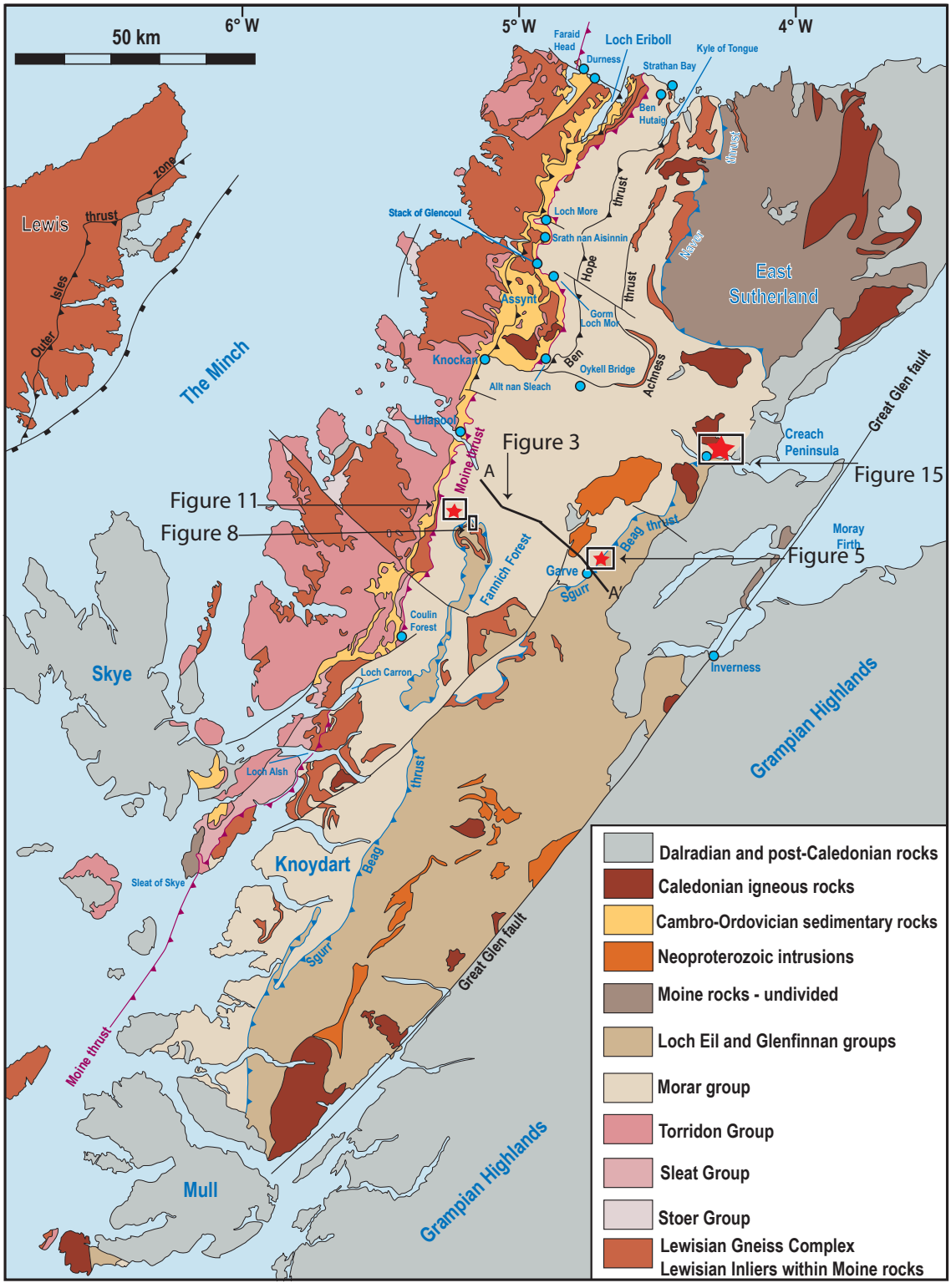
50 km
6° W
5° W
4° W
Faraid Head
Loch Eriboll
Durness
Kyle of Tongue
Strathan Bay
Ben Hutaig
thrust
Lewis
thrust
zone
Isles
Outer
Stack of Glencoul
Loch More
Srath nan Aisinnin
Hope
thrust
Morar
East Sutherland
Assynt
Gorm Loch Mor
Knockan
Ben Oykell Bridge
Achness
Allt nan Sleach
The Minch
Ullapool
Moine thrust
Figure 3
A
Figure 11
Figure 8
Creach Peninsula
Great Glen fault
Figure 15
Beag thrust
Moray Firth
Figure 5
Garve
Sgurr
A'
Fannich Forest
Coulin Forest
Skye
Loch Carron
Inverness
Grampian Highlands
Loch Alsh
thrust
Knoydart
Beag
Sleat of Skye
Sgurr
Great Glen fault
Moine thrust
Mull
Grampian Highlands
Dalradian and post-Caledonian rocks
Caledonian igneous rocks
Cambro-Ordovician sedimentary rocks
Neoproterozoic intrusions
Moine rocks - undivided
Loch Eil and Glenfinnan groups
Morar group
Torridon Group
Sleat Group
Stoer Group
Lewisian Gneiss Complex
Lewisian Inliers within Moine rocks

Figure 3.1

deformation fabrics appear to be broadly synchronous - it remains to be determined whether observed foreland to hinterland increases in temperature, usually traced over horizontal thrust transport-parallel distances of tens of kilometers, are associated with inverted thermal or right-way-up thermal structures. Only if isothermal surfaces and metamorphic isograds dip towards the hinterland in present-day coordinates (or dip to the foreland less steeply than the present day ground surface) will the thermal structure be inverted (Fig. 3.2). In contrast, if the isothermal surfaces and metamorphic isograds dip towards the foreland (more steeply than ground surface) than the thermal structure will be right-way-up even though deformation temperatures increase from foreland to hinterland.

Pressure and temperature (P-T) data are limited in the Scottish Caledonides on the north side of the Great Glen (Barr et al., 1986; Burns, 1994; Friend et al., 2000; Soper and Brown, 1971). This is partially due to the dominance of quartzo-feldspathic units in the Moine Supergroup from which the thrust sheets are formed, and partly due to the relative scarcity of pelite horizons containing appropriate assemblages of metamorphic indicator minerals. Thigpen et al. (in press) have recently quantified a foreland - hinterland increase in temperatures of deformation and metamorphism across the Moine, Ben Hope and Naver thrust sheets of northern Scotland, in an area extending from the north coast southwards towards the Assynt district (Fig. 3.1) using quartz c-axis fabric opening angles and garnet-biotite thermometry. They interpreted the foreland-hinterland increase in temperatures of deformation and metamorphism in the Moine and structurally higher thrust sheets as being associated with a right-way-up thermal structure, developed at the orogenic wedge scale, in which isotherms dip steeply towards the foreland.

In this thesis chapter estimates of deformation temperatures associated with penetrative shearing within the Moine and Sgurr Beag thrust sheets are reported for structural transects located to the south of the main area described by Thigpen et al. (in press). The positions of these transects are shown in Fig. 3.1 and from west to east include the: 1) Meall an t-Sìthe, 2) Alt Breabaig, 3) Ben Wyvis/Garve and 4) Creich Peninsula areas. A regional scale cross section drawn approximately parallel to thrust transport, and running between the first three of these transects, is shown in Fig. 3.3. Deformation temperatures for quartz-rich units are estimated using the quartz c-axis fabric opening angle thermometer developed by Kruhl (1998) and are compared with likely temperature ranges indicated by quartz recrystallization regimes associated

---

Figure 3.2
Next page. Schematic cross sections illustrating the possibilities for right way up and inverted thermal structures. Although thermometry data from a suite of samples collected along a foreland-hinterland transect may indicate that temperatures of deformation and/or metamorphism increase from foreland to hinterland, whether thermal structure is inverted or right way up depends on the dip of isothermal surfaces/isograds relative to topographic surface.

Flat-lying topographic surface

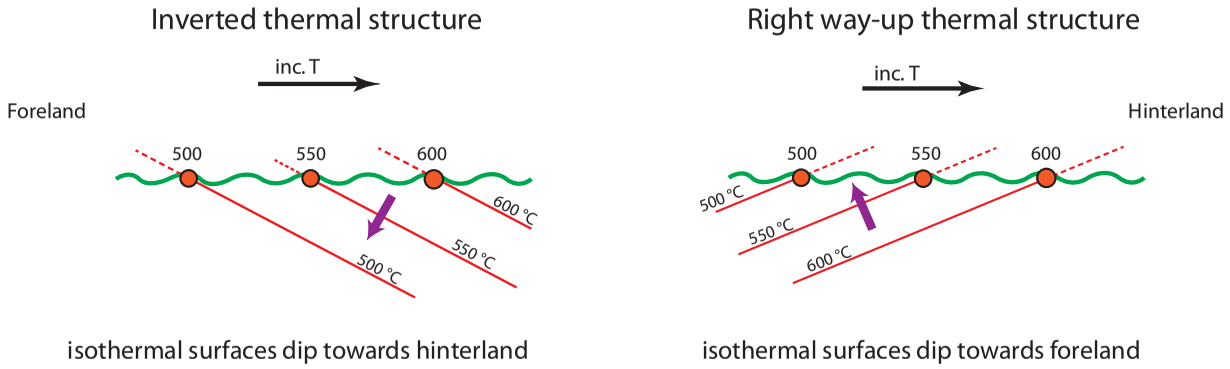

Steep topographic surface

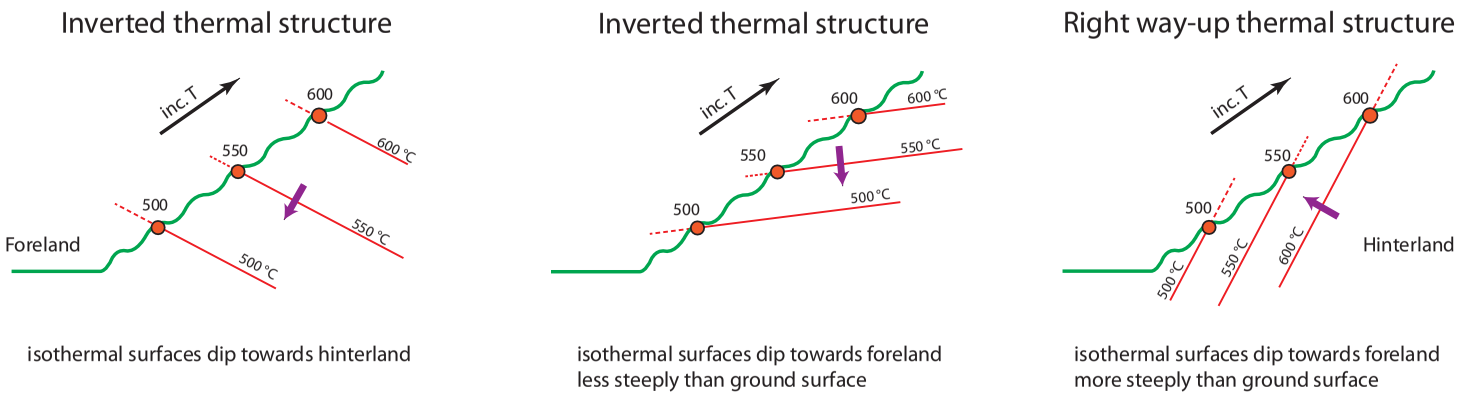

Figure 3.2

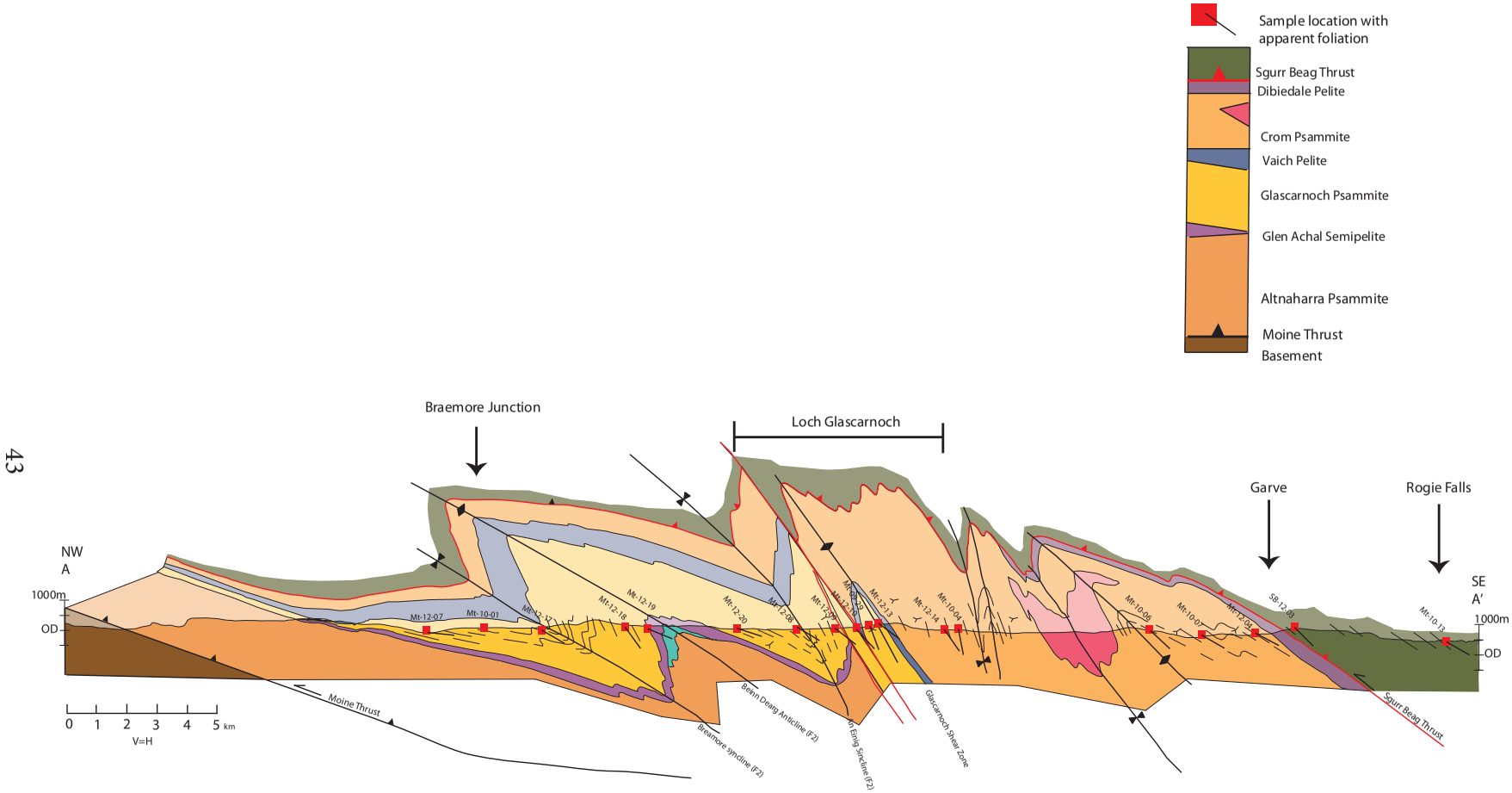
Sample location with apparent foliation
Sgurr Beag Thrust
Dibiedale Pelite
Crom Psammite
Vaich Pelite
Glascarnoch Psammite
Glen Achal Semipelite
Altnaharra Psammite
Moine Thrust
Basement
Braemore Junction
Loch Glascarnoch
Garve
Rogie Falls
NW
A
SE
A'
1000m
OD
Mt-12-07
Mt-10-01
Mt-12-18
Mt-12-19
Mt-12-20
Mt-12-08
Mt-12-13
Mt-12-14
Mt-10-04
Mt-10-05
Mt-10-07
Mt-12-04
58-12-08
Mt-10-13
Moine Thrust
Beinn Dearg Anticline (F2)
Braemore syncline (F2)
Glascarnoch Shear Zone
Sgurr Beag Thrust
0 1 2 3 4 5 km
V=H

Figure 3.3

with fabric development (Stipp et al. 2002). We also present temperature and pressure constraints for pelitic units from the Sgurr Beag thrust sheet, based on garnet-biotite thermometry, plagioclase-biotite-garnet-quartz thermobarometery, and pseudosection modeling.

3.3. Geological Background

The Caledonian mountain belt exposed in northwest Scotland has historically been one of the most intensely studied orogenic systems, with some of the earliest work being reported in the mid-late 1800s (see reviews by Butler 2010, Law and Johnson 2010). For example, the process of mylonitization was first described by Lapworth (1885) in the Loch Eriboll region of the Moine thrust zone (Fig. 3.1); the same area where Geike (1884) coined the term 'thrust'. The first systematic description of the entire Moine thrust zone, marking the foreland edge of the Caledonian orogenic wedge, was reported by Peach et al. (1907) together with a less detailed description of the multiphase deformation and metamorphism of the metasedimentary rocks (Moine Supergroup) that make up the overlying thrust sheets lying to the east.

The Moine Supergroup consists of a thick sequence of Neoproterozoic metasediments that are locally cut by pre-, syn-, and post orogenic igneous bodies (Harris and Johnson, 1991). The Moine Supergroup is subdivided from oldest to youngest into the Morar, Glenfinnan, and Loch Eil groups (see reviews by Holdsworth et al., 1994; Strachan et al., 2002, Strachan, 2010). The Morar group has been studied in great detail, and is a >5km thick sequence of psammites and pelites exposed along the western (foreland) edge of the Caledonian mountain belt. The Morar group is bound along its base by the Moine Thrust. In Sutherland, the Morar group is cut by the Ben Hope and Achness thrusts (Fig. 3.1). South of Assynt, the Moine thrust is succeeded by the Sgurr Beag thrust, which places Glenfinnan over Morar group rocks (Barr et al., 1986; Rathbone and Harris, 1979; Tanner, 1970). Further eastwards into the hinterland the Loch Eil group is preserved.

Three orogenic events have affected the Caledonian terrain in northwest Scotland: 1) the Knoydartian orogeny from 740-665 Ma based on Rb-Sr ages in pegmatites (Giletti et al., 1961); 2) the Grampian orogeny from 470-460 Ma based on U-Pb ages in zircons (Kinny et al., 1999) and, 3) the Scandian orogeny from 440-410 Ma based on a wide range of syn and post-thrusting igneous intrusions and the Glen Scaddle metagabbro (Kinny et al., 2003; Kocks et al., 2006;

Figure 3.3
Previous page. Regional cross section illustrating geologic structures in the Moine thrust sheet and overlying Sgurr Beag thrust sheet between Braemore junction and Rogie Falls. Line of section indicated in Fig. 3.1. Section drawn by Maarten Krabbendam, BGS Edinburgh, 2013. Location of samples collected in 2010 and 2012 adjacent to the A835 road in this area are projected on to cross section.

Strachan and Evans, 2008; Goodenough et al., 2011). These three orogenic events affect the various lithotectonic units to different extents, with the entire Moine Supergroup being deformed during the Scandian event (Kinny et al., 2003).

The Moine thrust separates Lewisian (Archean) basement rocks and unmetamorphosed Torridonian (Neoproterozoic) and Cambrian-Ordovician sedimentary successions from the Neoproterozoic age metasediments of the Moine Supergoup. The Moine thrust zone is a gently, eastward dipping series of thrust faults that mark the foreland edge of the Scandian orogenic wedge. The Moine thrust itself marks the structural top of the Moine thrust zone. Rocks of the Moine thrust zone were deformed under greenschist facies conditions, with deformation temperatures ranging between ~ 300 to 400°C (see reviews by Strachan et al. 2002; Butler 2010; Law and Johnson 2010). The age of thrusting within the Moine thrust zone is bracketed between 431and 429 Ma, based on U-Pb zircon dating from syntectonic igneous intrusions in the Assynt area (Goodenough et al., 2011).

Traced from foreland to hinterland in the Loch-Eriboll - Assynt area (Fig. 3.1), rocks of the Moine, Ben Hope and Achness thrust sheets have been subjected to relatively low grade (greenschist - lower amphibolite facies) metamorphism, while rocks of the overlying Naver, Swordly, and Skinsdale thrust sheets are associated with higher grade metamorphism (Barr et al., 1986; Kocks et al., 2006; Moorhouse and Moorhouse, 1988). South of Assynt and the Dornoch Firth the Sgurr Beag is the only mapped thrust sheet lying on top of the Moine thrust sheet. The Sgurr Beag thrust was originally thought to connect northwards with the Naver thrust (Strachan and Holdsworth, 1988). However, recent studies noting differences between migmatites in the Naver and Sgurr Beag thrust sheets, have led to the conclusion that the Sgurr Beag thrust is more likely to connect northwards with the Skinsdale thrust (Kocks et al., 2006; Mendum et al., 2009). Syntectonic igneous intrusions associated with the Naver and Skinsdale thrusts indicate that they are of Scandian age (Kinny et al., 2003; Kocks et al., 2006). In contrast, Tanner and Evans (2003) regarded metamorphism associated with motion on the Sgurr Beag thrust as being of Knoydartian age. If the Sgurr Beag thrust's northern counterpart is the Skinsdale, then one would assume that the age of thrusting would be synchronous, leading to less certainty about the linking of the hinterland thrusts. Though the age of movement on the Sgurr Beag thrust has yet to be determined, K-Ar cooling ages of 421 Ma from biotite closure temperatures suggest that thrusting on the Sgurr Beag had to be older (Kelley, 1988).

The Sgurr Beag thrust is an east-southeast dipping thrust associated with emplacement of Lewisian basement rock and Glenfinnan group metasedimentary rocks on top of Morar group rocks. The Glenfinnan group is cut by the Carn Gorm pegmatites, dated at 750 Ma (Rb-Sr; Long and Lambert, 1963) that were intruded prior to shearing (Wilson, 1975). Scandian age deformation associated with west-northwest transport is recorded in the footwall to the

Sgurr Beag thrust (Tanner and Evans, 2003). The age (or ages) of Sgurr Beag thrusting remains uncertain.

Metamorphism associated with thrusting in the Scandian orogenic wedge increases from upper greenschist in the foreland (Moine thrust zone) to mid and upper amphibolite facies in the hinterland (Soper and Brown, 1971; Powell and Phillips, 1985; Holdsworth, 1989). The Morar group reached peak temperatures in the mid- to lower amphibolite facies (Fettes et al., 1985; Thigpen et al., 2010), while the Naver nappe reached upper amphibolite facies (Soper and Brown, 1971). Constrains on P-T conditions are limited, with temperatures and pressures of 640-660 °C and 5kbar estimated from garnet-biotite thermometry for the Naver nappe (Burns, 1994; Friend et al., 2000). Above the Ben Hope thrust to the west, P-T conditions are estimated at 475 °C at 3-4 kbar (Burns, 1994). Due to a lack of appropriate mineral assemblages, there are no P-T constraints for the Skinsdale and Sgurr Beag thrust sheets (Kocks et al., 2006).

3.4. Microstructures and Quartz c-axis Fabrics

Thin sections for microstructural and fabric analyses were cut parallel to lineation and perpendicular to foliation, and examined using an optical petrographic microscope and Leitz universal stage. In all samples quartz has dynamically recrystallized, and in some samples exhibits microstructural evidence for static grain boundary adjustments, possibly associated with annealing. Quartz c-axis fabrics were measured optically on recrystallized grains, a minimum of 500 grains (and maximum - and mode - of 1000 grains) being measured in each sample using an Excel macro developed by S. Mulcahy at University of California, Davis. Fabrics were plotted and contoured on a lower hemisphere stereonet using the *Stereoplot* software package developed by N. Mancktelow at ETH, Zurich.

Quartz c-axis fabric opening angles were used to estimate deformation temperatures (Fig. 3.4a) using the opening angle thermometer of Kruhl (1998). Quartz c-axis fabrics were also used to estimate approximate 3D strain type (Fig. 3.4b) and shear sense (Fig. 3.4c) associated with crystal plastic deformation.

We classify quartz microfabrics associated with dynamic recrystallization using the terminology proposed by Stipp et al. (2002). Stipp et al. (2002) have also proposed that the three main types of recrystallization mechanism in quartz (grain boundary bulging, subgrain rotation and grain boundary migration) may be used to infer broad ranges of likely deformation temperature, assuming 'average' geologic strain rates. Here we use the term *bulging* (BLG) to describe recrystallized quartz grains that are small (~10μm), with all recrystallized grains located adjacent to parent grain boundaries, and indicating inferred deformation temperatures of ~280 °C to ~400 °C. Starting at approximately 400 °C subgrain rotation (SGR) becomes the dominant recrystallization mechanism, and is indicated by an increase in recrystallized grain

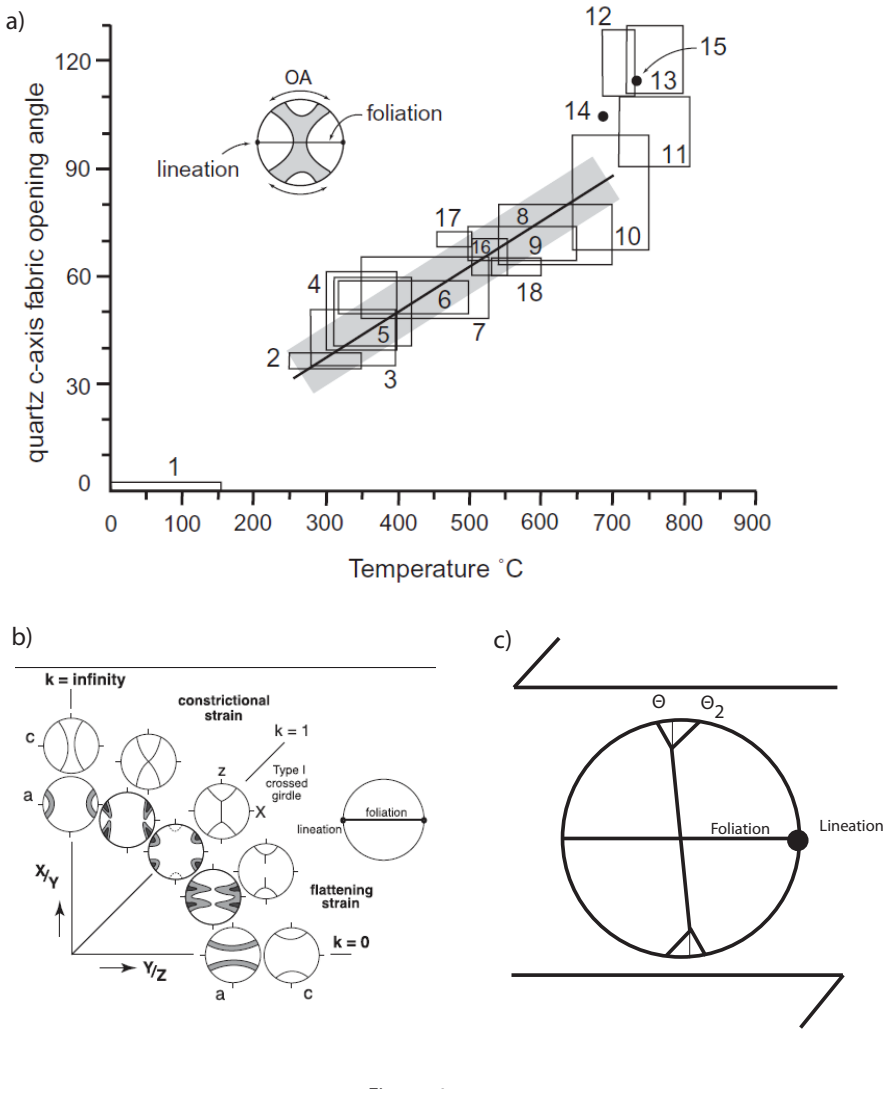

Figure 3.4
Quartz c-axis fabric applications. (a) Quartz c-axis fabric opening angle thermometer (Kruhl, 1998). Boxes indicate studies used to construct the best-fit linear relationship between opening angles and deformation temperatures up to 650 °C. (b) Range of quartz c-axis fabrics associated with flattening to constrictional strains; modified from Schmid and Casey (1986). (c) Explanation of shear sense indicated by quartz c-axis fabric asymmetry, where fabric opening angle is defined by $\theta + \theta 2$ and $\theta < \theta 2$ for sinistral shear sense shown.

size (15-30μm), a higher percentage of recrystallized grains and a *"core and mantle"* type microstructure. SGR is the dominant recrystallization mechanism up to deformation temperatures of ~500 °C, above which grain boundary migration (GBM) recrystallization becomes dominant. GBM is indicated by large recrystallized grains (>30μm) with lobate grain boundaries. BLG, SGR, and GBM correlate to the experimentally produced regime 1, regime 2, and regime 3 microstructures, respectively, described by Hirth and Tullis (1992).

Microstructural and quartz fabric analyses reported in this Chapter are concentrated on samples collected in the Moine and Sgurr Beag thrust sheets exposed from east to west in: 1) the Ben Wyvis/Garve, 2) Alt Breabaig and, 3) Meall an t-Sìthe areas. The positions of these sampling areas, relative to major structures, are shown in Figs. 3.1 and 3.3.

3.4.1 Ben Wyvis/Garve area - Moine thrust sheet

A detailed geologic map and cross section for the Ben Wyvis/Garve area, including sample locations for the Moine and Sgurr Beag thrust sheets, are shown in Figs. 3.5a and b. In the upper part of the Moine thrust sheet exposed in this area foliation dips to the SE, while associated mineral stretching lineations plunge to the S (Fig. 3.5a). Micrographs and quartz c-axis fabrics for samples collected from the Moine thrust sheet in the Ben Wyvis/Garve area are shown in Figs. 3.6 and 3.7 respectively. Lineations for the Moine thrust sheet are inferred from Grant and Harris (2000), as the samples collected for this study did not exhibit visible lineations.

The structurally lowest samples in the Ben Wyvis/Garve area (Fig. 3.5a) is sample MT-12-04, a biotite + muscovite + quartz + plagioclase + garnet pelite, collected 460 m below the Sgurr Beag thrust (Fig. 3.5b). Foliation is defined by a parallel alignment of biotite and muscovite grains that hinder grain boundary migration and growth of quartz (Fig. 3.6a). Subgrains are developed in quartz-rich domains and lobate quartz grain boundaries are also locally developed. Subgrain rotation appears to be the dominant recrystallization mechanism. A weak top-to-the-north shear sense is indicated by a positive phyllosilicate tilt to the north. Quartz c-axis preferred orientation in MT-12-04 defines a diffuse (maximum density of 3 times uniform)

Figure 3.5
Next page. Geologic map and cross section of the Sgurr Beag thrust zone, Ben Wyvis/ Garve. (a) Geologic map of the Sgurr Beag thrust zone between Garve and Ben Wyvis; modified from Grant and Harris (2000) and British Geological Survey (2004). Line A-A' indicates the line of section for Fig. 3.2b. Samples collected crossed the Crom psammite, Garve psammite, Ben Wyvis pelite and Ben Wyvis psammite, with a general south trending lineation. Lineations plotted are inferred, based on data from Grant and Harris (2000). Ordnance Survey grid coordinates (at 1 km spacing) indicated. (b) Geologic cross section line A-A' highlighting the Morar group in the footwall and the Glenfinnan group in the hanging wall to the Sgurr Beag thrust.

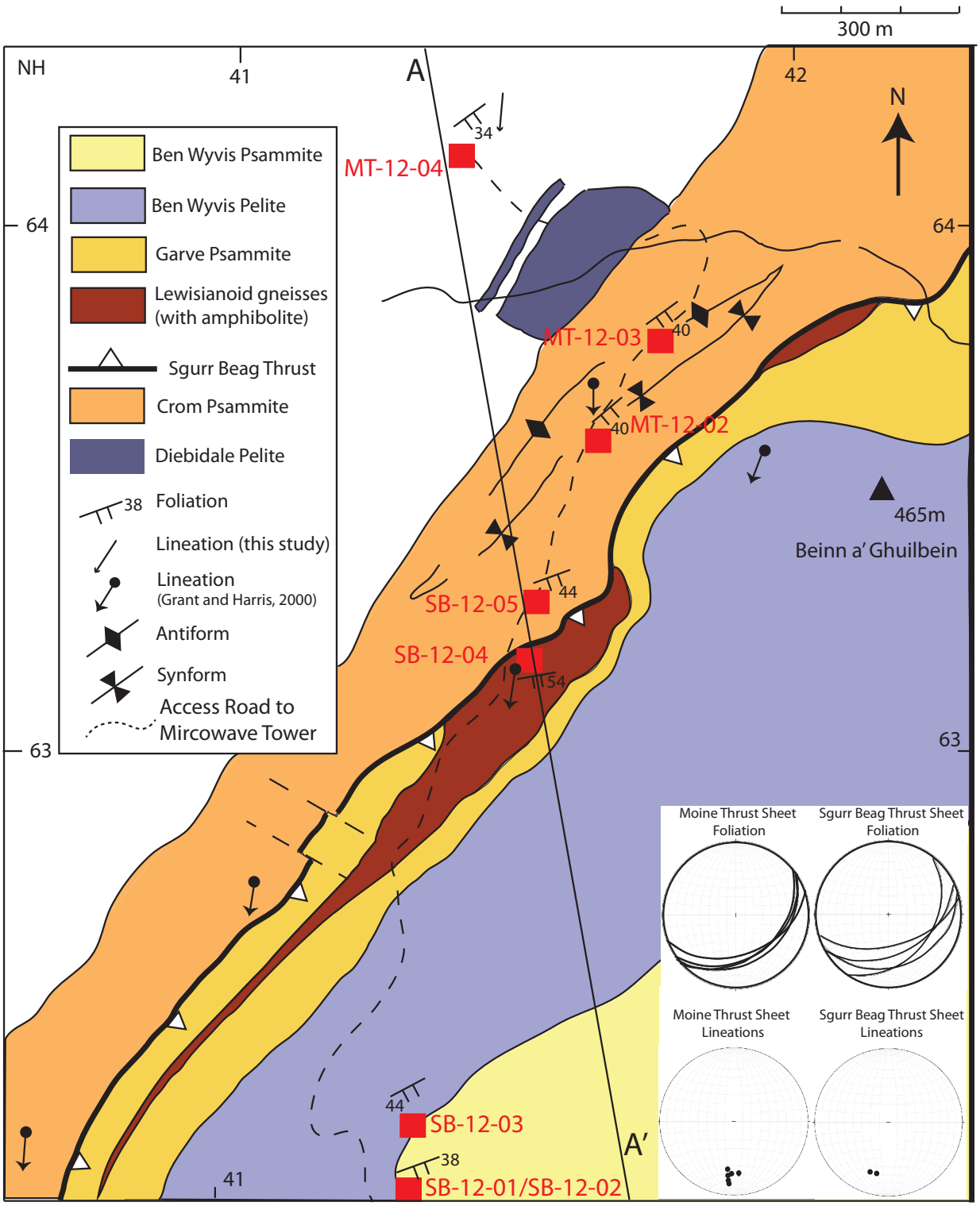
300 m
NH
41
42
A
A'
N
64
63
Ben Wyvis Psammite
Ben Wyvis Pelite
Garve Psammite
Lewisianoid gneisses
(with amphibolite)
Sgurr Beag Thrust
Crom Psammite
Diebidale Pelite
38 Foliation
Lineation (this study)
Lineation
(Grant and Harris, 2000)
Antiform
Synform
Access Road to
Mircowave Tower
MT-12-04
34
MT-12-03
40
MT-12-02
40
SB-12-05
44
SB-12-04
54
SB-12-03
44
SB-12-01/SB-12-02
38
465m
Beinn a' Ghuilbein
Moine Thrust Sheet
Foliation
Sgurr Beag Thrust Sheet
Foliation
Moine Thrust Sheet
Lineations
Sgurr Beag Thrust Sheet
Lineations

Figure 3.5a

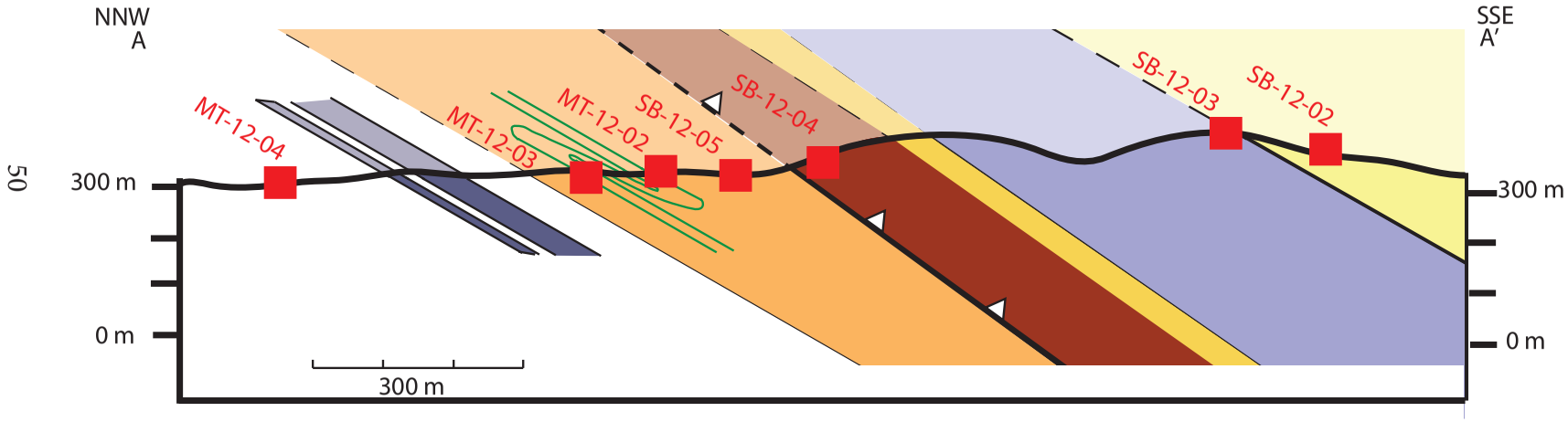
NNW
A
SSE
A'
MT-12-04
MT-12-03
MT-12-02
SB-12-05
SB-12-04
SB-12-03
SB-12-02
300 m
0 m
300 m
300 m
0 m
50

Figure 3.5b

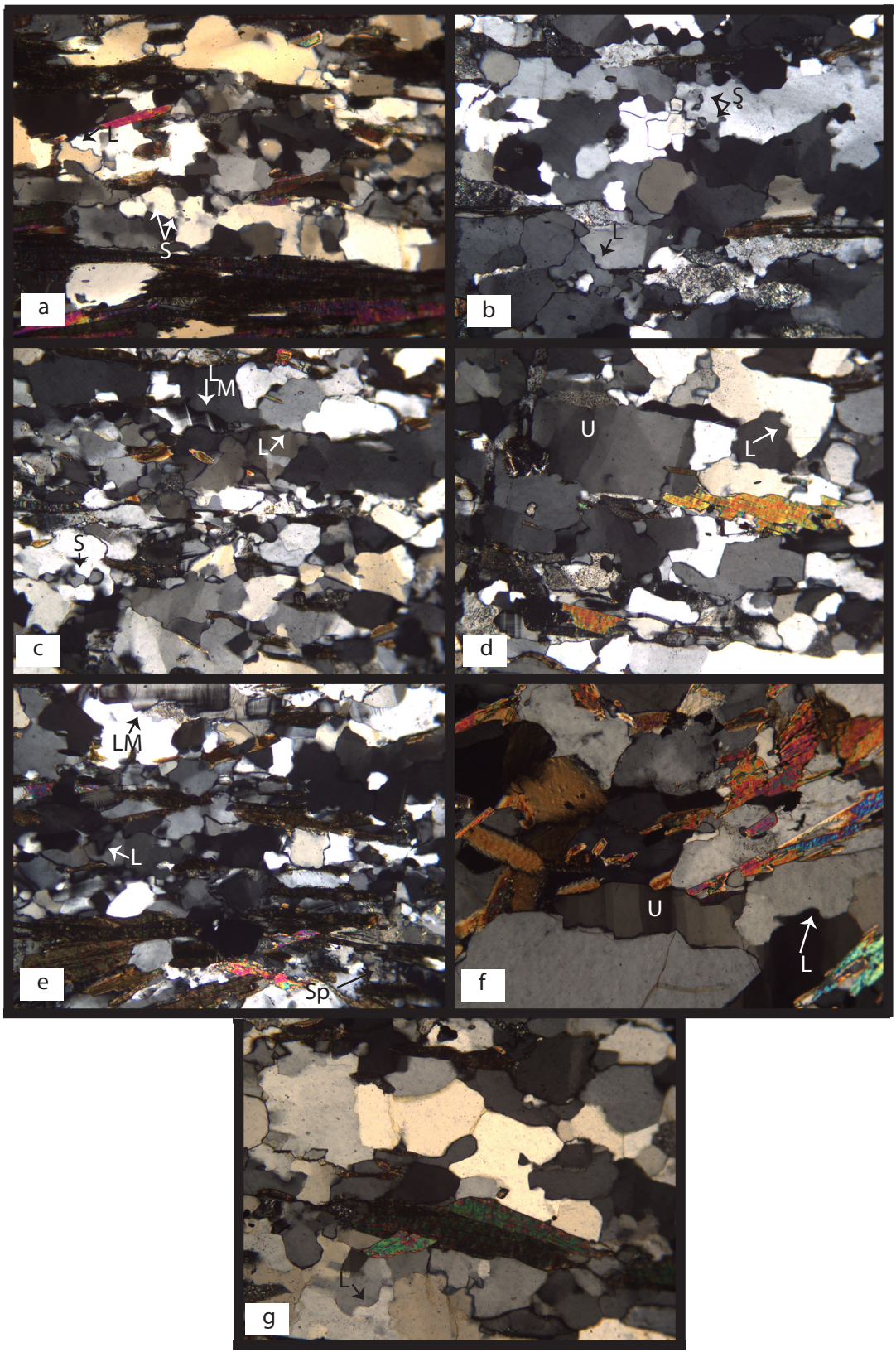

Figure 2.6

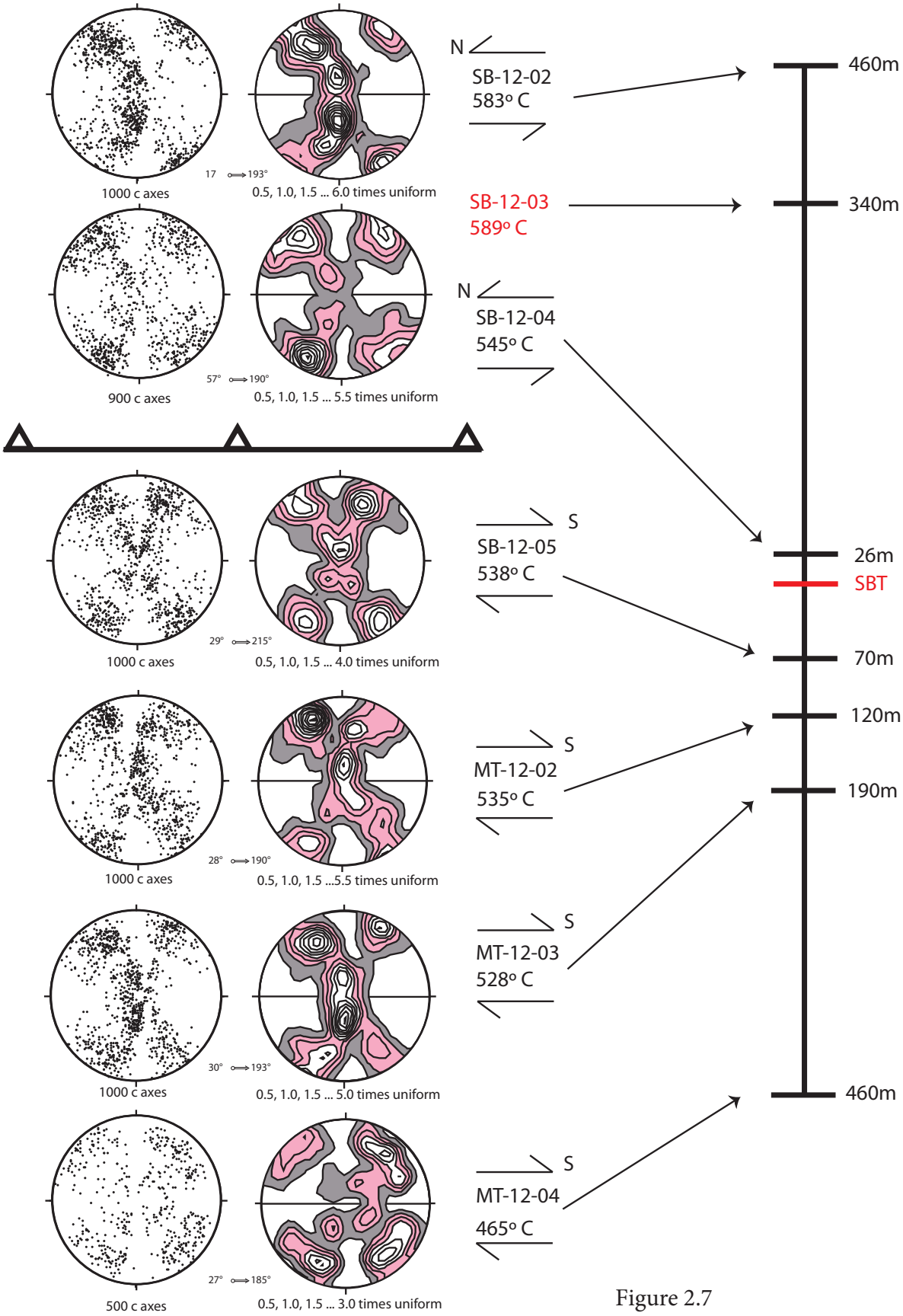
1000 c axes
17 ⟹ 193°
0.5, 1.0, 1.5 ... 6.0 times uniform
N
SB-12-02
583° C
460m
SB-12-03
589° C
340m
900 c axes
57° ⟹ 190°
0.5, 1.0, 1.5 ... 5.5 times uniform
N
SB-12-04
545° C
1000 c axes
29° ⟹ 215°
0.5, 1.0, 1.5 ... 4.0 times uniform
S
SB-12-05
538° C
26m
SBT
70m
1000 c axes
28° ⟹ 190°
0.5, 1.0, 1.5 ...5.5 times uniform
S
MT-12-02
535° C
120m
190m
1000 c axes
30° ⟹ 193°
0.5, 1.0, 1.5 ... 5.0 times uniform
S
MT-12-03
528° C
460m
500 c axes
27° ⟹ 185°
0.5, 1.0, 1.5 ... 3.0 times uniform
S
MT-12-04
465° C

Figure 2.7

asymmetric Type 1 (Lister, 1977) cross girdle fabric, indicating a top-to-the-south shear sense (Fig. 3.7). Opposite shear senses are therefore indicated by microstructures and crystal fabrics, potentially due to a second generation of movement in the shear zone, discussed later.

Sample MT-12-03 is a quartz + biotite + plagioclase + muscovite + epidote psammite (Fig. 3.6b) collected at 190 m below the Sgurr Beag thrust (Fig. 3.5b). Biotite, muscovite and epidote grains define a macroscopic foliation, and indicate a weak top-to-the-south shear sense. Lobate grain boundaries in plagioclase grains indicate the operation of limited crystal plastic deformation. Recrystallization in quartz is dominantly by GBM, with subgrains also being present. The quartz c-axis fabric is a well-defined (maximum density of 5 times uniform) asymmetric Type 1 cross girdle, with a top-to-the-south shear sense (Fig. 3.7).

MT-12-02 is a quartz + biotite + muscovite + microcline psammite (Fig. 3.6c) collected 120 m below the Sgurr Beag thrust (Fig. 3.5b). Foliation is defined by biotite and muscovite, with mica fish and mica grains tilted up from the macroscopic foliation, indicating a top-to-the-south shear sense. Recrystallization in quartz is mixed between GBM and SGR. Lobate grain boundaries are present in microcline indicating limited crystal plastic deformation in the feldspar grains. The quartz c-axis fabric in MT-12-02 is a well-defined (maximum density of 5.5 times uniform), asymmetric Type 1 cross girdle, with a top-to-the-south shear sense (Fig. 3.7).

70m below the Sgurr Beag thrust (Fig. 3.5b), SB-12-05 is a quartz + plagioclase + biotite + muscovite + microcline psammite (Fig. 3.6d). Foliation defined by phyllosilicates and quartz

---

Figure 3.6
Previous page. Microstructures associated with samples, Ben Wyvis/Garve. (See Figs. 3.5a, b for locations). (a) MT-12-04 with lobate quartz grain boundaries (L) and subgrain formation in quartz (S). (b) MT-12-03 with lobate quartz grain boundaries (L), and subgrains (S); (c) MT-12-02 with lobate grain boundaries in both quartz (L) and microcline (LM), as well as subgrains in quartz (S); (d) SB-12-05 with lobate quartz grain boundaries (L) and undulose extinction in quartz grains (U); (e) SB-12-04 with lobate grain boundaries in both quartz (L) and microcline (LM), as well as subgrains in quartz (S) and plagioclase (Sp); (f) SB-12-03 with lobate quartz grain boundaries (L) and undulose extinction in quartz grains (U); (g) SB-12-02 with lobate quartz grain boundaries (L).

Figure 3.7
Previous page. Optically measured quartz c-axis fabrics for psammites (MT-12-03, MT-12-02, SB-12-05, SB-12-04, SB-12-02) and pelities (MT-12-04), Ben Wyvis/Garve. (see Fig. 3.5a, b for locations). Asymmetric fabrics for MT-12-04, MT-12-03, MT-12-02, SB-12-05 indicate top-to-the-south transport. Fabrics for SB-12-04 and SB-12-02 indicate top-to-the-north transport. Deformation temperatures (Td) estimated from fabric opening angles and temperatures of metamorphism (Tm) estimated by garnet-biotite thermometry in individual samples are shown. All lower hemisphere equal area projection looking to the N-NE; foliation oriented 'left-right' and vertical, mineral stretching lineation trends 'right'.

grains indicate a weak top-to-the-south shear sense. GBM is the dominant quartz recrystallization mechanism, and larger quartz grains exhibit undulose extinction. The quartz c-axis fabric in SB-12-05 is a well-defined (maximum density of 5.5 times uniform) asymmetric Type 1 cross girdle, with a top-to-the-south shear sense (Fig. 3.7).

3.4.2 Ben Wyvis/Garve area - Sgurr Beag thrust sheet

In the lower part of the Sgurr Beag thrust sheet exposed in this area foliation dips to the SE, while associated mineral stretching lineations plunge to the SSW (Figs. 3.5a). Micrographs and quartz c-axis fabrics for samples collected from the Sgurr Beag thrust sheet in the Ben Wyvis/Garve area are shown in Figs. 3.6 and 3.7, respectively. Lineations for the Sgurr Beag thrust sheet are inferred from Grant and Harris (2000) because samples collected for this study lacked a visible lineation.

SB-12-04 is a biotite + quartz + plagioclase + microcline + muscovite + epidote psammite (Fig. 3.6e) collected 26 m above the Sgurr Beag thrust (Fig. 3.5b). Foliation defined by biotite and epidote grains indicates a top-to-the-north shear sense. Biotite grains shows evidence of retrogression, and muscovite grains typically cross cut the macroscopic foliation. A high microcline content in this sample suggests a Lewisian gneiss rather than Moine metasediment protolith. GBM appears to be the dominant quartz recrystallization mechanism, while subgrains are abundant. Subgrains are also present in plagioclase, and microcline grains have lobate boundaries indicating at least limited plastic deformation of feldspar. The quartz c-axis fabric in SB-12-04 is a well-defined (maximum density of 5.5 times uniform) asymmetric Type one cross girdle, with top-to-the-north shear sense (Fig. 3.7).

SB-12-03A is a biotite +quartz + plagioclase + muscovite + garnet pelite (Fig. 3.6f) collected 340 m above the Sgurr Beag thrust (Fig. 3.5b). Foliation is strongly defined by biotite and muscovite grains. Plagioclase shows signs of plastic deformation, such as lobate grain boundaries. Quartz grains commonly exhibit undulose extinction and deformation bands, with grain boundaries pinned by phyllosilicates. Lobate grain boundaries are occasionally preserved between adjacent quartz grains.

Sample SB-12-02 is a quartz + plagioclase + biotite + garnet psammite (Fig. 3.6g) collected 460 m above the Sgurr Beag thrust (Fig. 3.5b). Biotite grains define a weakly developed foliation and a potential top-to-the-north shear sense. Plagioclase grain boundaries are lobate (not pictured), and GBM is dominant in the quartz grains. Some quartz grain boundaries approach 120° equilibrium as seen with static annealing. The quartz c-axis fabric in SB-12-02 is a well-defined (maximum density of 6.0 times uniform) asymmetric Type 1 cross girdle, with a top-to-the-north shear sense (Fig. 3.7).

3.4.3 Alt Breabaig - Moine thrust sheet

A detailed geologic map for the Alt Breabaig river transect, including sample locations for the Moine and Sgurr Beag thrust sheet, is shown in Fig. 3.8. In the upper part of the Moine thrust sheet exposed in this area foliation dips gently to the SW, while associated mineral stretching lineations plunge to the SSE (Fig. 3.8). Micrographs and quartz c-axis fabrics for samples collected from the Moine thrust sheet on the Alt Breabaig river transect area are shown in Figs. 3.9 and 3.10, respectively.

Along the Alt Breabaig river transect sample MT-12-06, a quartz + biotite + muscovite + plagioclase psammite (Fig. 3.9a), was collected ~ 200 m below the Sgurr Beag thrust (Fig. 3.8). Foliation is preserved in biotite and muscovite, and shows a top-to-the-northwest shear sense. Quartz grains exhibit development of subgrains and lobate grain boundaries, with SGR being the slightly dominant recrystallization mechanism. The quartz c-axis fabric is a well-defined (maximum density of 6.0 times uniform) asymmetric Type 1 cross girdle, with a top-to-the-northwest shear sense (Fig. 3.10).

In the immediate footwall to the Sgurr Beag thrust sample MT-12-05, a flaggy quartz + plagioclase + biotite + muscovite psammite (Fig. 3.9b) was collected 35 m beneath the thrust (Fig. 3.8). Foliation defined by biotite and muscovite grains indicates a top-to-the-northwest shear sense. Quartz grain boundaries are generally lobate, while subgrains are also present, possibly indicating synchronous operation of subgrain rotation and grain boundary bulging. The quartz c-axis fabric is a well defined cross-girdle (maximum density of 5.5 times uniform) with a top-to-the-northwest shear sense (Fig. 3.10).

3.4.4 Alt Breabaig - Sgurr Beag thrust sheet

In the immediate hanging wall to the Sgurr Beag thrust mapped foliation patterns indicate the presence of a SE trending synform, with limbs gently dipping to the SW and NE, , while associated mineral stretching lineations plunge to the SSE (Fig. 3.8). Micrographs and quartz c-axis fabrics for samples collected from the Sgurr Beag thrust sheet on the Alt Breabaig river transect area are shown in Figs. 3.9 and 3.10 respectively.

Figure 3.8
Next page. Geologic map of the Sgurr Beag thrust zone along the Alt Breabaig river, north of Loch Fannich; adapted from Kelley (2010). Samples are from the Meall a Chrasgaidh psammite in the footwall to the Sgurr Beag thrust, and Meall an t-Sithe pelite and Lewisianoid gneiss in the hanging wall. Ordnance Survey grid coordinates (at 1 km spacing) indicated.

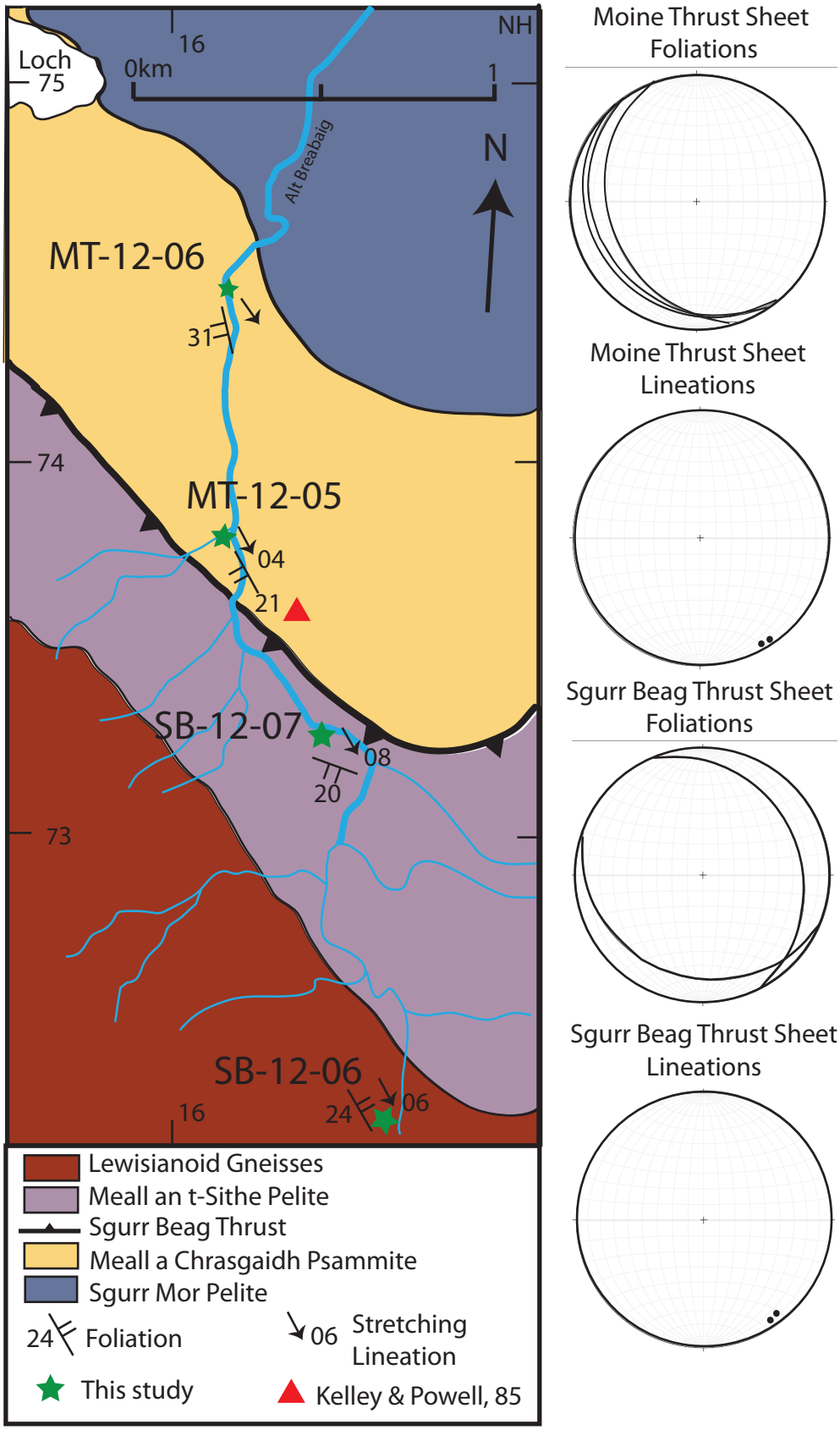
Loch
75
16
0km
1
NH
N
Alt Breabaig
MT-12-06
31
74
MT-12-05
04
21
SB-12-07
08
20
73
SB-12-06
16
24
06
Lewisianoid Gneisses
Meall an t-Sithe Pelite
Sgurr Beag Thrust
Meall a Chrasgaidh Psammite
Sgurr Mor Pelite
24 Foliation
06 Stretching Lineation
This study
Kelley & Powell, 85
Moine Thrust Sheet Foliations
Moine Thrust Sheet Lineations
Sgurr Beag Thrust Sheet Foliations
Sgurr Beag Thrust Sheet Lineations

Figure 3.8

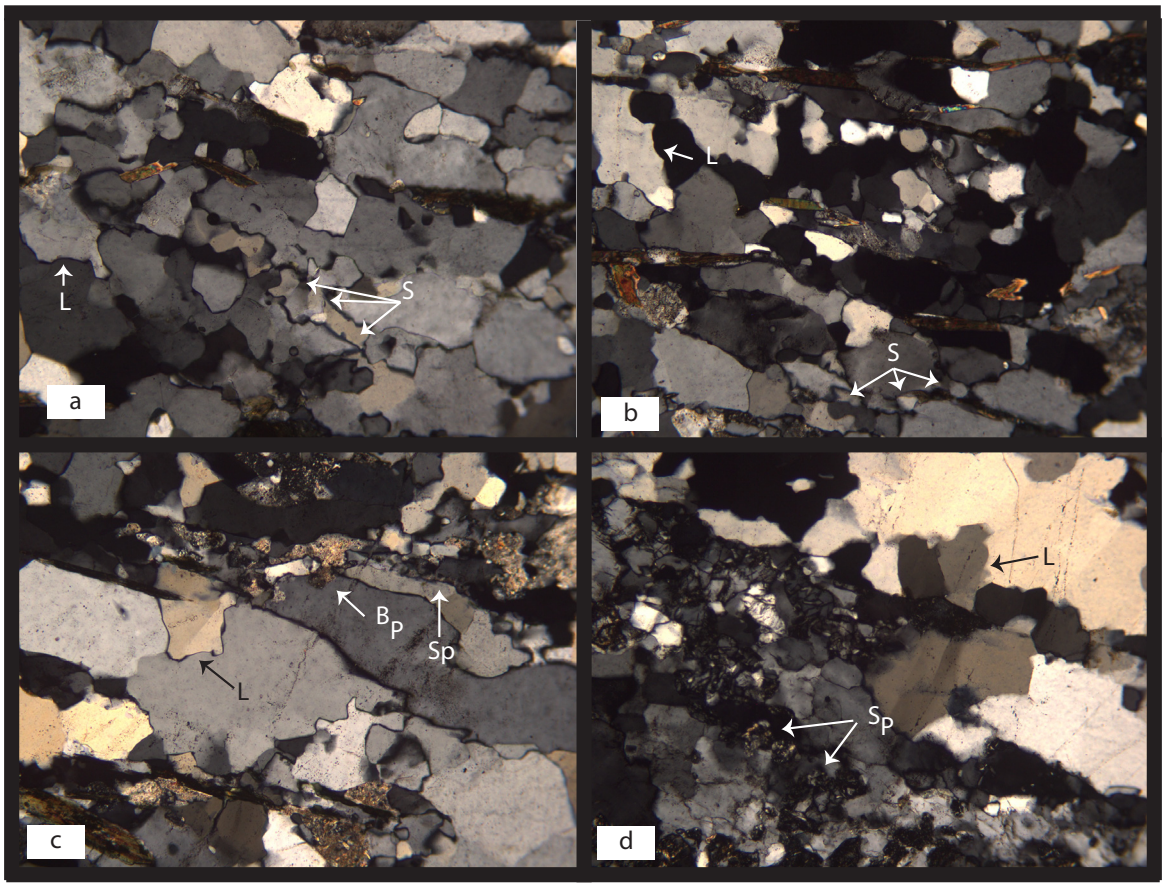

Figure 3.9
Next page. Microstructures associated with samples from the Alt Breabaig river transect (see Fig. 3.8 for locations). (a), (b) MT-12-06 and MT-12-05, respectively, with subgrains (S) and lobate (L) grain boundaries in quartz; (c) SB-12-07 with lobate (L) quartz grain boundaries, bulging plagioclase grain boundaries(BP), and subgrain development in plagiocase (SP); (d) SB-12-06 with lobate (L) quartz grain boundaries and subgrains in plagioclase (SP).

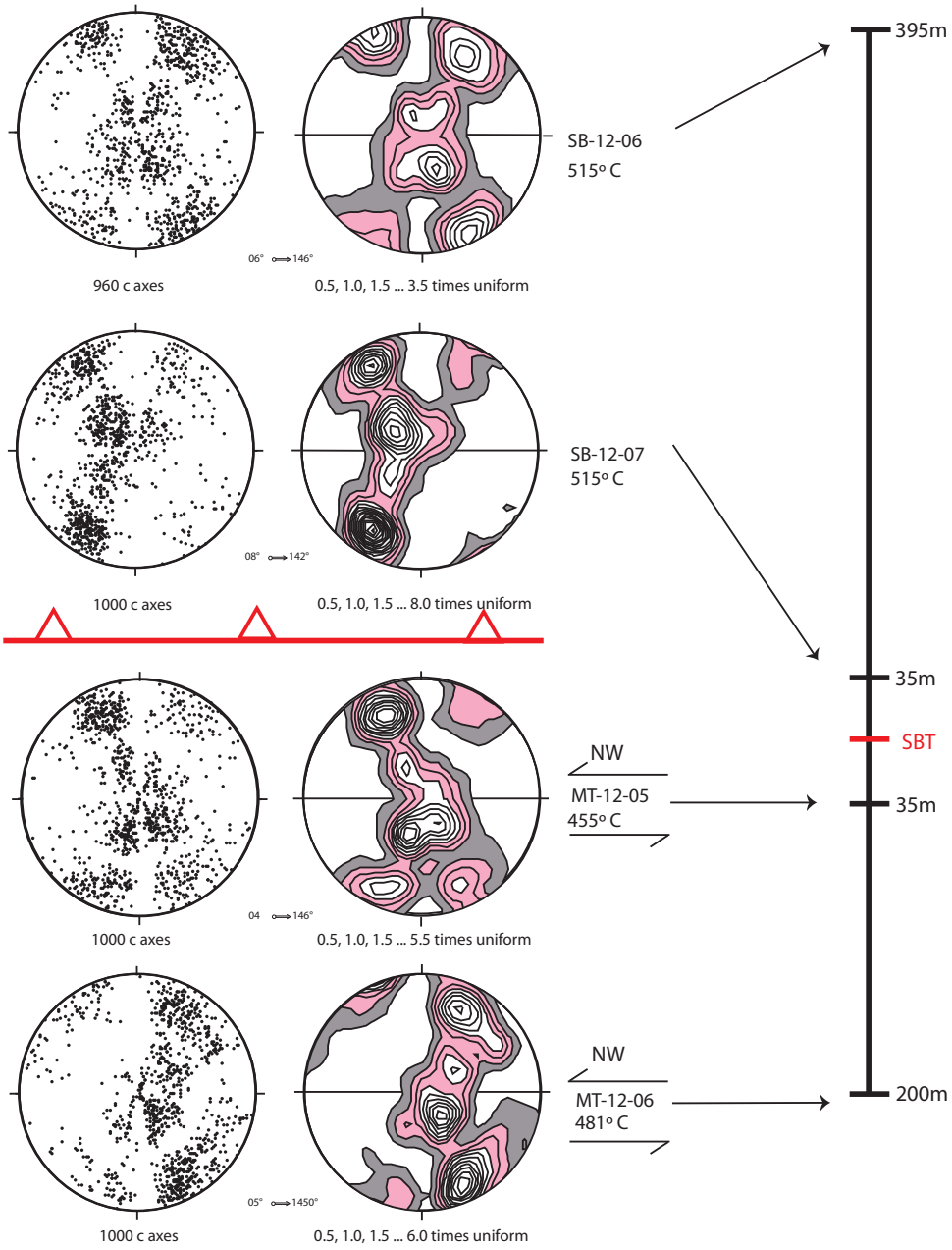

Figure 3.10
Optically measured quartz c-axis fabrics for psammites from the Alt Braebaig river (see Fig. 3.8 for locations). Asymmetric fabrics for MT-12-05 and MT-12-06 indicate top-to-the-north transport. Small circle girdle fabrics centered about the lineation in SB-12-07 and SB-12-06 indicates deformation within the constrictional strain field (Schmid and Casey, 1986; cf. Fig. 3.4b). Deformation temperatures (Td) estimated from fabric opening angles in individual samples are shown. All lower hemisphere equal area projection viewed to the NNW; foliation oriented 'left-right' and vertical, mineral stretching lineation trends 'right-left'.

Sample SB-12-07 is a quartz + muscovite + plagioclase + secondary chlorite psammite (Fig. 3.9c) collected 35 m above the Sgurr Beag thrust (Fig. 3.8). Muscovite and chlorite grains mark the foliation, and indicate a top-to-the-northwest shear sense. Quartz grains display a mixture of GBM, SGR and annealing microstructures, with GBM being the dominant recrystallization mechanism. Plagioclase grains with sericitic alteration have small bulges on their boundaries, and some plagioclase have subgrains, suggesting at least minor plastic deformation of these grains. The quartz c-axis fabric is a well-defined (maximum density of 8 times uniform), but incomplete, small-circle girdle centered about the lineation (Fig. 3.10) suggesting deformation within the constrictional field (Fig. 3.4b).

Sample SB-12-06 is a quartz + plagioclase + biotite + muscovite + garnet rock (Fig. 3.9d), collected 395 m above the Sgurr Beag thrust (Fig. 3.8), probably derived from Lewisian gneiss. Foliation is defined by biotite, muscovite and quartz grains, with a top-to-the-northwest shear sense. GBM is the dominant quartz recrystallization mechanism. Quartz grain boundaries approaching 120° equilibrium positions suggest either late static annealing or that recovery has outpaced work hardening during plastic deformation and dynamic recrystallization. Plagioclase grains display widespread mymerkitic alteration, as well as subgrains and lobate grain boundaries, indicating that plastic deformation occurred at relatively high temperatures (> 500-550 °C). Quartz c-axis preferred orientation in this sample defines a diffuse fabric (maximum density of 3.5 times uniform) that is intermediate between a cross-girdle and a small circle fabric centered about the lineation (Fig. 3.10), suggesting a strain state close to plane strain but slightly within the constrictional field (Fig. 3.4b).

3.4.5 Meall an t-Sìthe - Moine thrust sheet

A detailed geologic map and cross section for the Sgurr Beag klippe exposed on Meall an t-Sìthe are shown in Figs. 3.11a and 3.b, respectively. Micrographs and quartz c-axis fabrics for samples collected from the Moine and Sgurr Beag thrust sheets exposed on exposed on Meall an t-Sìthe are shown in Figs. 3.12 and 3.13, respectively.

Figure 3.11
Next page. Geologic map and cross section of the Sgurr Beag klippe, Meall an t'Sithe. (a) Geologic map of the Sgurr Beag klippe exposed on Meall An T-Sithe to the north of Loch Bhraoin; adapted from Kelley (2010) and British Geological Survey (2012). Location of samples used in this study indicated. (b) Cross section through the Sgurr Beag klippe exposed on Meall An T-Sithe, and illustrating structures in the underlying Moine thrust sheet. Section drawn by Maarten Krabbendam, BGS Edinburgh, 2013. Cross section line indicated in Fig. 3.11a. Location of samples used in this study also indicated.

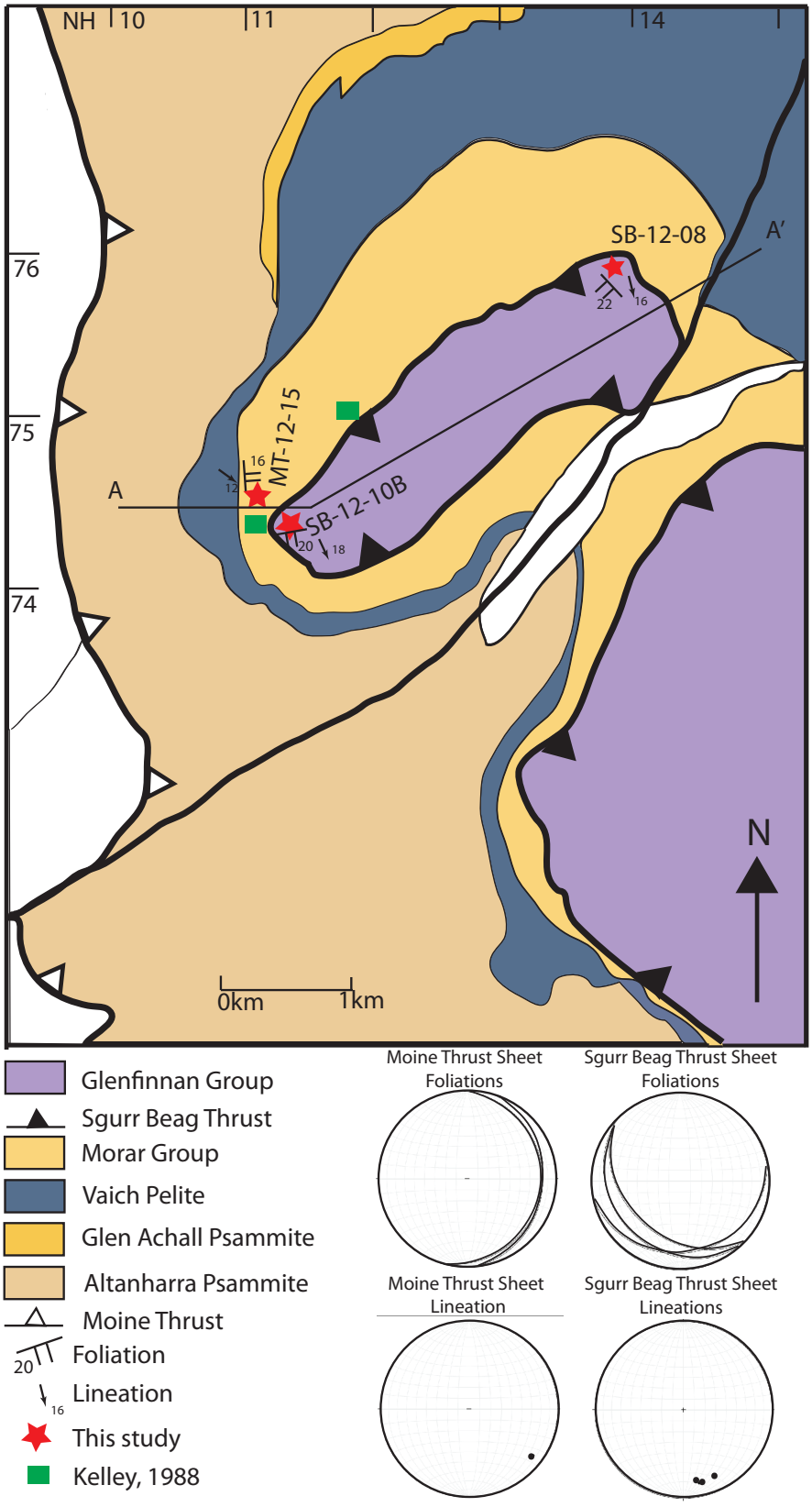
NH
10
11
14
76
75
74
SB-12-08
A'
22
16
MT-12-15
16
12
A
SB-12-10B
20
18
N
0km
1km
Glenfinnan Group
Sgurr Beag Thrust
Morar Group
Vaich Pelite
Glen Achall Psammite
Altanharra Psammite
Moine Thrust
20
Foliation
16
Lineation
This study
Kelley, 1988
Moine Thrust Sheet Foliations
Sgurr Beag Thrust Sheet Foliations
Moine Thrust Sheet Lineation
Sgurr Beag Thrust Sheet Lineations

Figure 3.11a

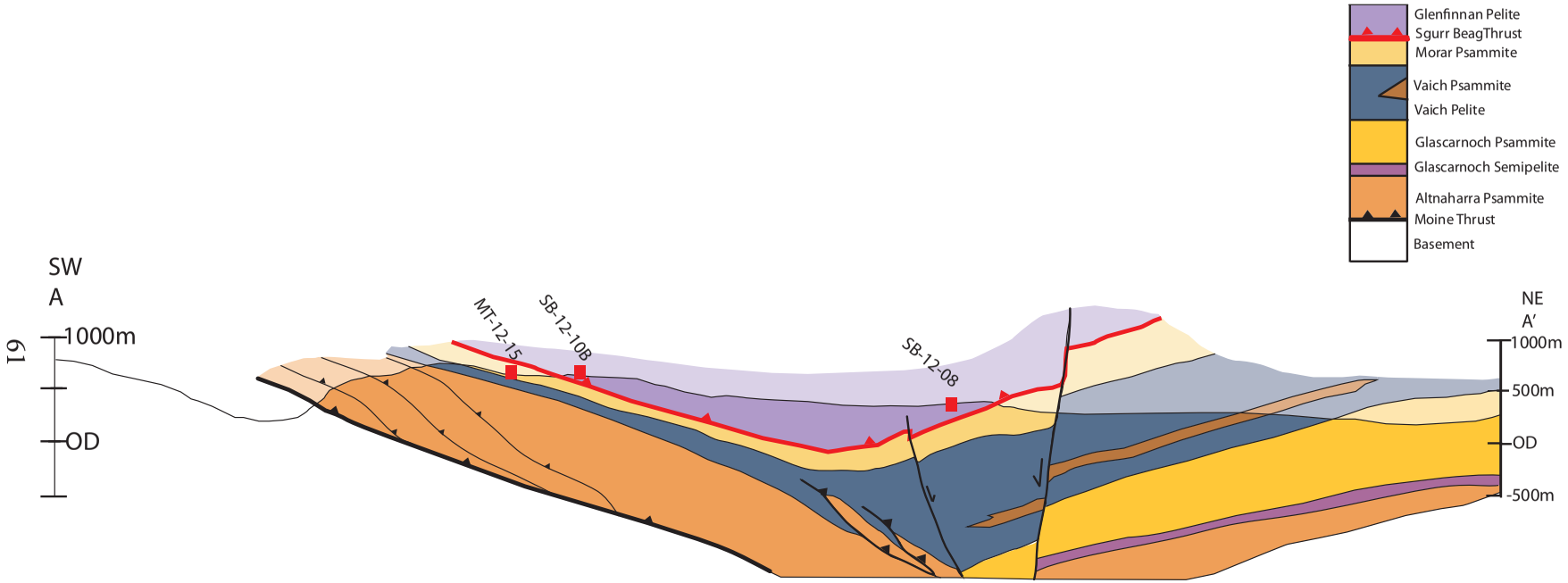
Glenfinnan Pelite
Sgurr BeagThrust
Morar Psammite
Vaich Psammite
Vaich Pelite
Glascarnoch Psammite
Glascarnoch Semipelite
Altnaharra Psammite
Moine Thrust
Basement
SW
A
1000m
OD
MT-12-15
SB-12-10B
SB-12-08
NE
A'
1000m
500m
OD
-500m
61

Figure 3.11b

Sample MT-12-15, a quartz + plagioclase + biotite + muscovite + garnet psammite (Fig. 3.12a) was collected to the southeast of Creag Rainich in the uppermost part of the Moine thrust sheet at ~145 m beneath the Sgurr Beag thrust (Figs. 3.11a and b). Muscovite grains define a weakly developed foliation. Many of the quartz grain boundaries are annealed. Relict recrystallized quartz grains are smaller (average 80µm) than those found in the immediate hanging wall to the Sgurr Beag thrust (discussed below), suggesting that SGR was dominant prior to static recovery. The quartz c-axis fabric is a well-developed (maximum density of 8 times uniform) asymmetric Type 1 cross girdle, with a top-to-the-north shear sense (Fig. 3.13).

3.4.6 Meall an t-Sìthe - Sgurr Beag klippe

Sample SB-12-10B is a garnet rich pelite (muscovite + biotite + quartz + plagioclase + garnet + sulfides) (Fig. 3.12b) collected from the summit peak of Creag Rainich (Fig. 3.11a) 50 m above the Sgurr Beag thrust. Garnet and phyllosilicates are coarse grained. Recrystallized quartz grains are larger than those in MT-12-15 (average 145µm) and dominated by GBM. Plagioclase has lobate grain boundaries suggesting at least limited plasticity of feldspar at this structural position. The quartz c-axis fabric is a diffuse (maximum density of 3.0 times uniform) Type 1 cross girdle (Fig. 3.13).

SB-12-08 is a quartz + muscovite + plagioclase + biotite + garnet pelite (Fig. 3.12c) collected from the summit peak of Meall an t-Sìthe at 120 m above the Sgurr Beag thrust (Figs. 3.11a and b). A top-to-the-north shear sense is indicated by the muscovite microstructure. Recrystallized quartz is coarse grained (average 225µm), often with undulose extinction and deformation bands preserved, and recrystallization is dominantly by GBM. Plagioclase grains have lobate grain boundaries. The quartz c-axis fabric is a poorly defined small-circle girdle with a maximum density of 4.5 times uniform, centered about the lineation (Fig. 3.13), and potentially indicating deformation within the constrictional field.

Figure 3.12
Next page. Microstructures from samples in Moine thrust sheet (MT-12-15) and overlying Sgurr Beag klippe (SB-12-10B and SB-12-08) exposed on Meall an t-Sithe to the north of Loch Bhrao-in. (a) MT-12-15 showing annealing in quartz grains (A); (b) SB-12-10B showing lobate quartz grain boundaries (L) and undulose extinction in quartz (U); (c) SB-12-08 showing lobate quart grain boundaries (L). Scale bars 500µm in length.

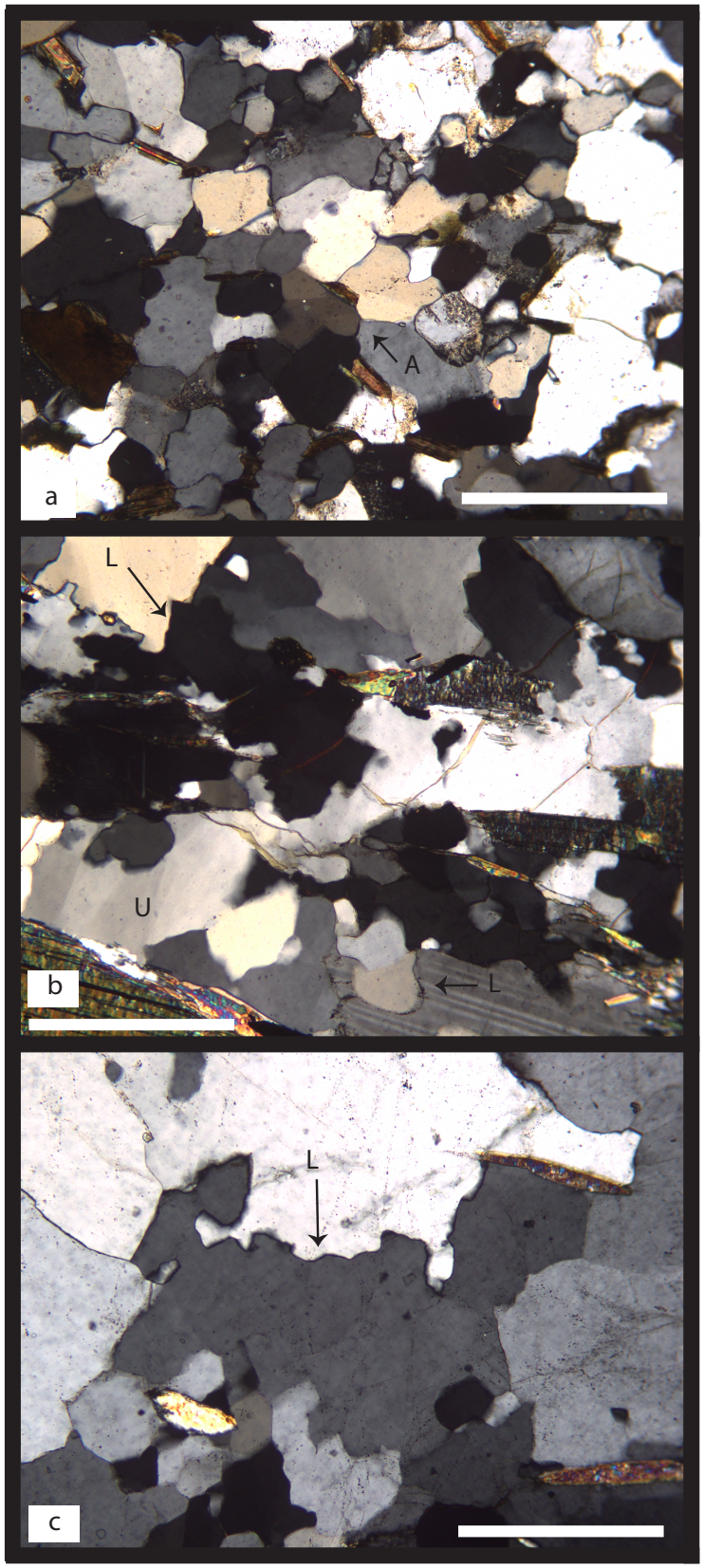

Figure 3.12

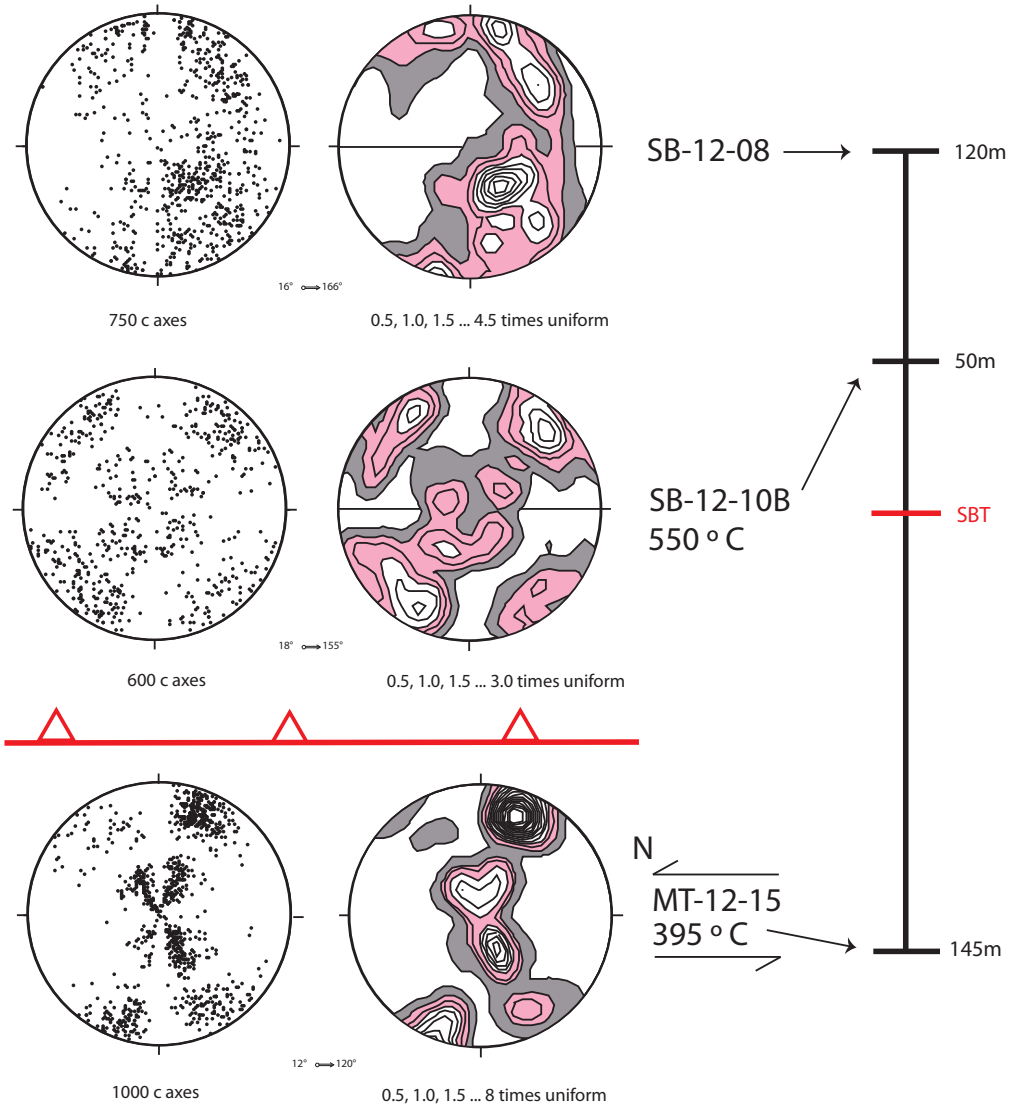

Figure 3.13
Optically measured quartz c-axis fabrics for psammite (MT-12-15) in Moine thrust sheet and pelites (SB-12-10B, SB-12-08) from the Sgurr Beag klippe, exposed on Meall an t-Sithe to the north of Loch Bhroin. Asymmetric fabric for MT-12-15 indicates a top-to-the-north shear sense. The asymmetric fabric for SB-12-10B is too diffuse to determine shear sense. The small circle girdle fabric for SB-12-08 indicates deformation in the constrictional strain field (cf. Fig. 3.4b). Deformation temperatures (Td) estimated from fabric opening angles and temperatures of metamorphism (Tm) estimated by garnet-biotite thermometry in individual samples are shown. All lower hemisphere equal area projection viewed to the NNW; foliation oriented 'left-right' and vertical, mineral stretching lineation trends 'right-left'.

3.4.7 Braemore Junction to Loch Glascarnoch - Moine thrust sheet

Samples were collected along an 18 km traverse across the Moine thrust sheet from Braemore Junction in the west to the eastern edge of Loch Glascarnoch (Figs. 3.1 & 3.3; Table 3.1). These samples complete a sampling traverse begun in 2010 between Braemore Junction at the leading edge of the Moine thrust sheet and Rogie Falls within the overlying Sgurr Beag thrust sheet (MT-10-01, MT-10-04,MT-10-06, MT-10-07, MT-10-13 sample locations indicated on Fig. 3.3). The samples range from psammite to pelite, with varying degrees of foliation and lineation development. In two cases, MT-12-18 and MT-12-11, multiple generations of foliations were preserved (Fig. 3.14a and b). Plagioclase grains behave rigidly in this suite of samples, with sericitic alteration common. SGR is the dominant recrystallization mechanism in quartz, with gradually increasing importance of GBM approaching the hinterland edge of the Moine thrust sheet. More pelitic samples show an increase in the abundance of small subgrains and possible bulging on grain boundaries (Fig. 3.14a, b, and d). While the psammite units show a higher percentage of straight edge grain boundaries, suggesting static grain boundary recovery (Fig. 3.14c). The percentage of recrystallized quartz grains is relatively constant between Braemore Junction and Loch Glascarnoch, with approximately 50% recrystallization of the quartz However, more pelitic samples show an increase in the percentage of quartz recrystallized Quartz c-axis fabrics from these samples have not yet been measured.

3.5. Deformation Temperatures

Deformation temperatures associated with penetrative shearing in our samples may be estimated using the quartz c-axis fabric opening angle thermometer described by Kruhl (1998) who compiled results from multiple experimental and field-based studies correlating fabric opening angles with temperatures of deformation and/or metamorphism (Fig. 3.4a). The approximate inferred relationship between opening angle and deformation temperature is linear through greenschist to mid-upper amphibolite facies conditions (Kruhl, 1998; see discussion by Morgan and Law, 2004) and is limited to deformation temperatures less than ~650-700 °C. Temperature estimates based on the Kruhl (1998) opening angle thermometer are usually quoted with an uncertainty of ± 50 °C and are dependent on critical resolved shear stresses for operative crystal glide systems being controlled by deformation temperature, rather than hydrolytic weakening or strain rate (cf. (Law et al., 2004; Lister and Hobbs, 1980; Morgan and Law, 2004; Tullis et al., 1973).

In the Garve/Ben Wyvis area fabric opening angles (Fig. 3.7) indicate that deformation temperatures increase up section from 465 °C in the footwall to the Sgurr Beag thrust to 583 °C in the hanging wall. Between 190 m below the thrust and 26 m above the thrust, estimated deformation temperature only vary between 528 and 545 °C.

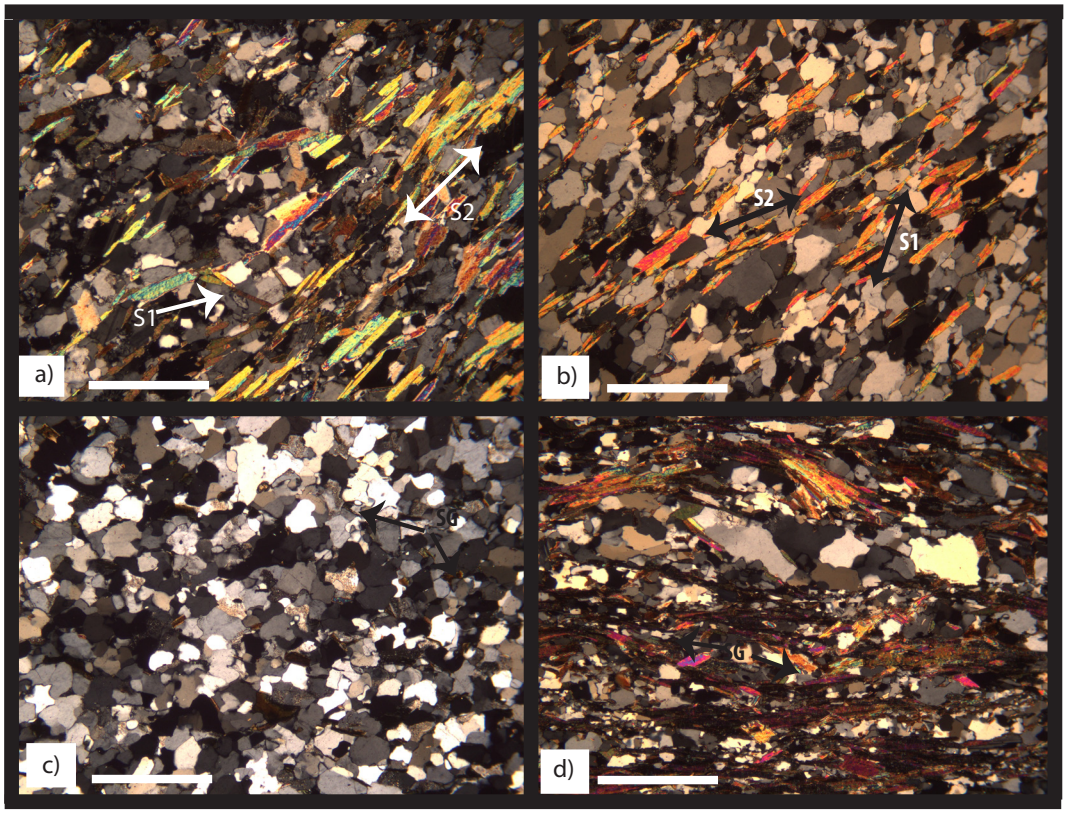

Figure 3.14
Examples of microstructures from the Moine thrust sheet, from Braemore Junction to Rogie Falls. (Figs. 3.1 and 3.3). (a) MT-12-18 and (b) MT-12-11 shows two generations of foliation, with S1 being the weaker, potentially earlier foliation, and S2 being the dominant foliation. (c) MT-12-08 shows subgrain rotation (SG) as a recrystallization regime and (d) MT-12-20 shows a higher percentage of subgrain rotation occurring around phyllosilicates. Scale bar is 1mm in length.

Table 3.1:
Dynamic recrystallization regimes and sampling information for samples collected from Braemore Junction to Rogie Falls.

Sample	Lithology	Dynamic Recrystallization	Other Recrystallization Present	Stretching Lineation			
MT-12-07	psammite	SGR		05 → 146	19745	78807	NH
MT-12-17	psammite	SGR		28 → 140	22799	76805	NH
MT-12-18	psammite	SGR		34 → 152	24266	75006	NH
MT-12-19	psammite	SGR		18 → 180	25456	74828	NH
MT-12-20	pelite	SGR		05→ 186	27936	74201	NH
MT-12-08	feldspathic psammite	SGR		06 → 162	29689	74511	NH
MT-12-09	psammite	SGR	GBM	27 → 148	30809	737412	NH
MT-12-10	pelite	SGR		-	31583	72997	NH

Approximately 20 km to the west of the Garve/Ben Wyvis area, along the Alt Breabaig stream section transect (Fig. 3.8), Morar rocks below the Sgurr Beag thrust were deformed at 455- 481 °C. In the overlying Sgurr Beag thrust sheet, deformation temperatures are estimated at 515 °C. However, these estimated hanging wall temperatures may be minima due to the potentially constrictional strains indicated by the fabric patterns (cf. Figs. 3.4b and 3.10 - sample SB-12-07 and SB-12-06).

To the NW of the Alt Breabaig stream section deformation temperatures of ~ 395 °C (sample MT-12-15) are indicated in the footwall to the Sgurr Beag thrust (SW corner of the Meall an t-Sìthe klippe; Fig. 3.13), while in the immediately overlying hanging wall deformation temperatures of 550 °C are indicated by the fabric opening angle in Glenfinnan Groups sample SB-12-10B. In the NE corner of the Meall an t-Sìthe klippe the c-axis fabric for sample SB-12-08 (collected at a similar structural distance to SB-12-10B above the Sgurr Beag thrust) indicates deformation within the constrictional strain field (Fig. 3.4b), and no temperature estimate is derived from the fabric.

Kelley and Powell (1985) have suggest that movement on the Sgurr Beag thrust in the Fannich Forest area (which includes the Alt Breabaig and Meall an t-Sìthe sampling locations) was synchronous with metamorphism, based on recrystallization of biotite in shear bands associated with thrusting. K-Ar data from biotites near Meall an t-Sìthe consistently indicate cooling ages of 421 ±3 Ma (Kelley, 1988). Microstructures and deformation temperatures observed in our samples support these conclusions. Shearing clearly occurred during metamorphic mineral growth and the ~ 420 Ma cooling ages indicate a minimum age for Scandian thrust-related shearing.

Following the general correlation between quartz recrystallization regimes and deformation temperature proposed by Stipp et al. (2002), the rocks within the Moine thrust sheet between Braemore Junction and Loch Glascarnoch (Fig. 3.3) were deformed at between 400 and 500 °C, with deformation temperatures in samples located further to the east (more hinterland positions) approaching the lower 500 °C range.

3.6. Mineral Chemistry and Metamorphic Pressure-Temperature Estimates

Metamorphic mineral assemblages in metasedimentary rocks of the Morar and Glenfinnan groups generally do not facilitate robust P-T analysis. However, samples from three localities within the Sgurr Beag thrust sheet contained biotite + garnet + plagioclase + muscovite assemblages, making them suitable for quantitative thermobarometry. These locations include from west to east (Fig. 3.1): a) the Meall an t-Sìthe /Sgurr Beag klippe (sample SB-12-10B, Fig. 3.11); b) the Ben Wyvis/Garve area (SB-12-03A, Fig. 3.5) and, c) the Creich Peninsula (SB-12-14, Fig. 3.15).

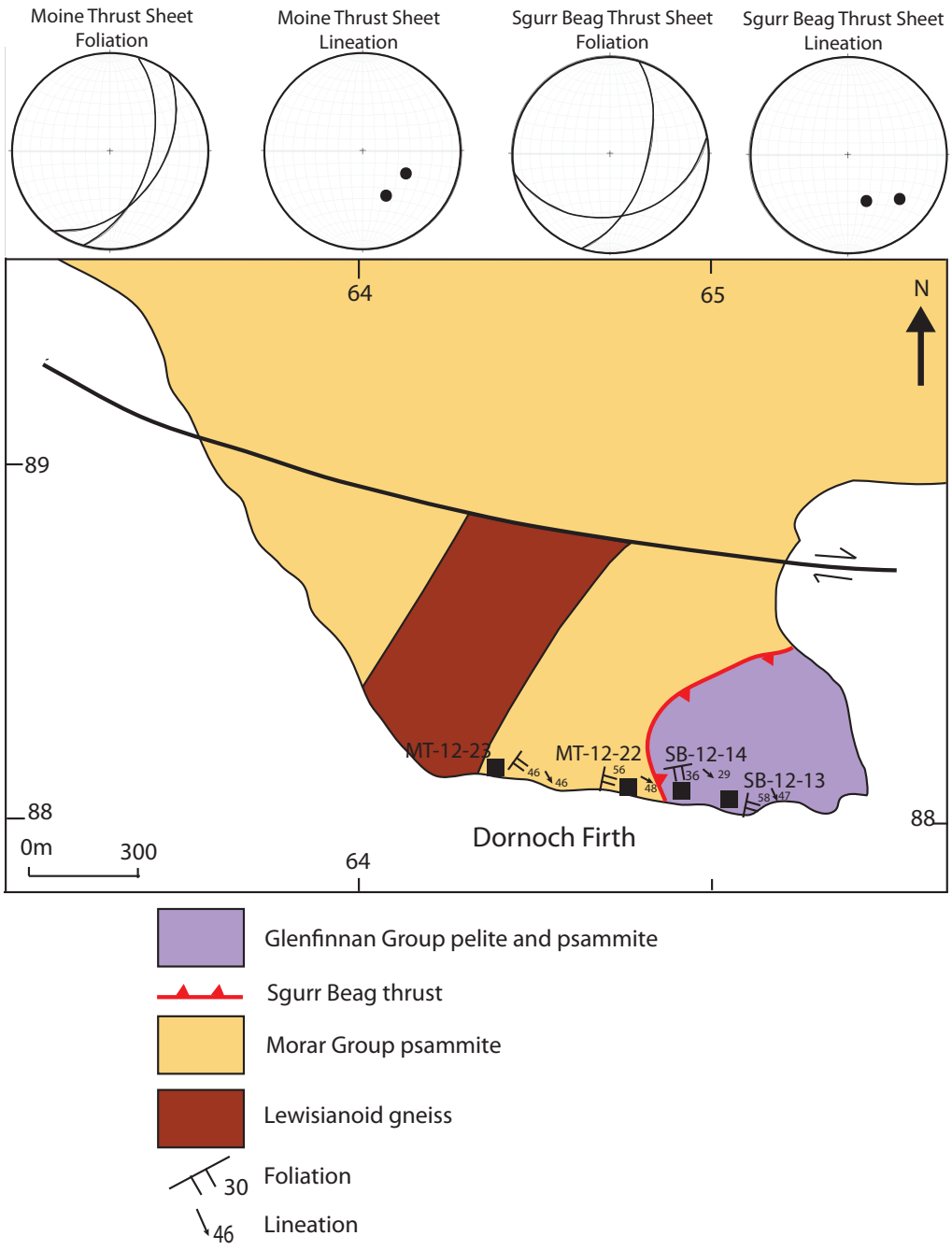

Figure 3.15

Geologic map of the Sgurr Beag and Moine thrust sheets exposed on the Creich Peninsula; adapted from Strachan et al. (2010) and Grant and Harris (2000). Location of sample SB-12-14 in the Glenfinnan group is indicated. Ordnance Survey grid coordinates (at 1 km spacing) indicated.

Garnets are commonly zoned in these samples, with the cores potentially recording pre-Scandian metamorphic events (Vance et al., 1998; Bird et al., in press). Mineral chemical analyses were completed in the Electron Microprobe Lab, Department of Geosciences, Virginia Tech, using a Cameca SX 50 microprobe with a beam current of 20nA and an acceleration voltage of 15 kV. Bulk rock compositions for SB-12-10B and SB-12-14 (Table 3.2) were obtained for representative 5 gram samples, with all weathered edges removed. The samples were powdered in an aluminum ball mill and passed through 80μm mesh sieve. The powders were analyzed at the Franklin and Marshal X-ray laboratory using a PANalytical 2404 XRF, measuring major element chemistry with titration (for ferric iron estimation) and loss on ignition.

Table 3.2: Bulk rock composition for SB-12-10B and SB-12-14.

Wt%	SB-12-10B	SB-12-14
SiO2	59.03	51.43
TiO2	1.13	1.3
Al2O3	19.51	23.8
Fe2O3T	9.9	10.84
MnO	0.15	0.24
MgO	2.65	2.71
CaO	1.57	2.37
Na2O	1.72	2.84
K2O	4	4.14
P2O5	0.27	0.45
SO3	0.06	0.05
Total	99.99	100.17
LOI	3.71	3.06
FeO	5.9	8.2
Fe2O3	3.34	1.73
ppm		
Sr	184	274
Zr	224	247
V	150	157
Cr	128	123

Rim-core zoning of garnet grains was quantified in terms of variation in almandine, spessartine, pyrope, and grossular garnet components (Fig. 3.16). Point analyses were conducted on biotite, muscovite, and plagioclase grains. For all samples little compositional variability was noted; thus an average composition was calculated for thermobarometric calculations (Table 3.3) using THERMOCALC ver. 3.33 " average PT" mode (Powell and Holland, 1994). Bulk rock compositions for SB-12-10B and SB-12-14 were used for PT pseudosection modeling based on the Holland and Powell (1998 - with 2004 update) data set. Free energy minimizations were made with the program Perplex (Connolly, 1990, 2005). Mineral solution models were biotite (Powell and Holland, 1999), garnet (White et al., 2005), feldspar (Fuhrman and Lindsley, 1988), muscovite (Coggon & Holland, 2002), chlorite, (Holland et al., 1998), staurolite, chloritoid, cordierite (all based on Mahar et al., 1997), and an ideal ilmenite-geikielite-pyrophanite solution. Quartz, Al_2SiO_5 polymorphs and rutile were treated as end-member compositions, and fluid was pure water. SB-12-03A only represents garnet-biotite thermometry, as we did not analyze it's bulk rock composition.

3.6.1 P-T Conditions from Mineral Chemistry

P-T conditions were first constrained in THERMOCALC using garnet, biotite, plagioclase and white mica mineral chemistry (Table 3.3), yielding pressures ranging from 6.4 ± 1.4 kbar (SB-12-10B, plotted on Fig. 15 and 16) to 5.1 ± 1.5 kbar (SB-12-14, plotted on Fig. 3.17 and 3.18). These pressures correspond to temperatures of 564 and 609 °C, respectively. Garnet-biotite thermometry uses the exchange of $(X^{Mg}/X^{Fe})_{garnet}$ with $(X^{Mg}/X^{Fe})_{biotite}$, with the ratio preserved at the rim of the grain representing peak growth conditions. Based on the zoning of the garnets used (Fig. 3.16), we infer that the garnet rims most likely preserve the metamorphic peak conditions these rocks had experienced, with minimal subsequent diffusion across the grains. Thus, using the garnet rim composition and the average biotite composition (Table 3.3), the Ferry and Spear (1978) thermometer yields temperatures of 611 ± 50 °C, 662 ± 50 °C, and 589 ± 50 °C (SB-12-10B, SB-12-14, and SB-12-03A respectively).

Figure 3.16
Next page. Scanning electron microscope images of garnet grains from the Sgurr Beag thrust sheet, mapped for chemical zoning (a) SB-12-10B, (c) SB-12-14, (e) SB-12-03A. Corresponding microprobe chemical traverse for end members almandine (Alm), spessartine (Sps), pyrope (Pyp), and grossular (Grs) for (b) SB-12-10B, (d) SB-12-14, (f) SB-12-03A.

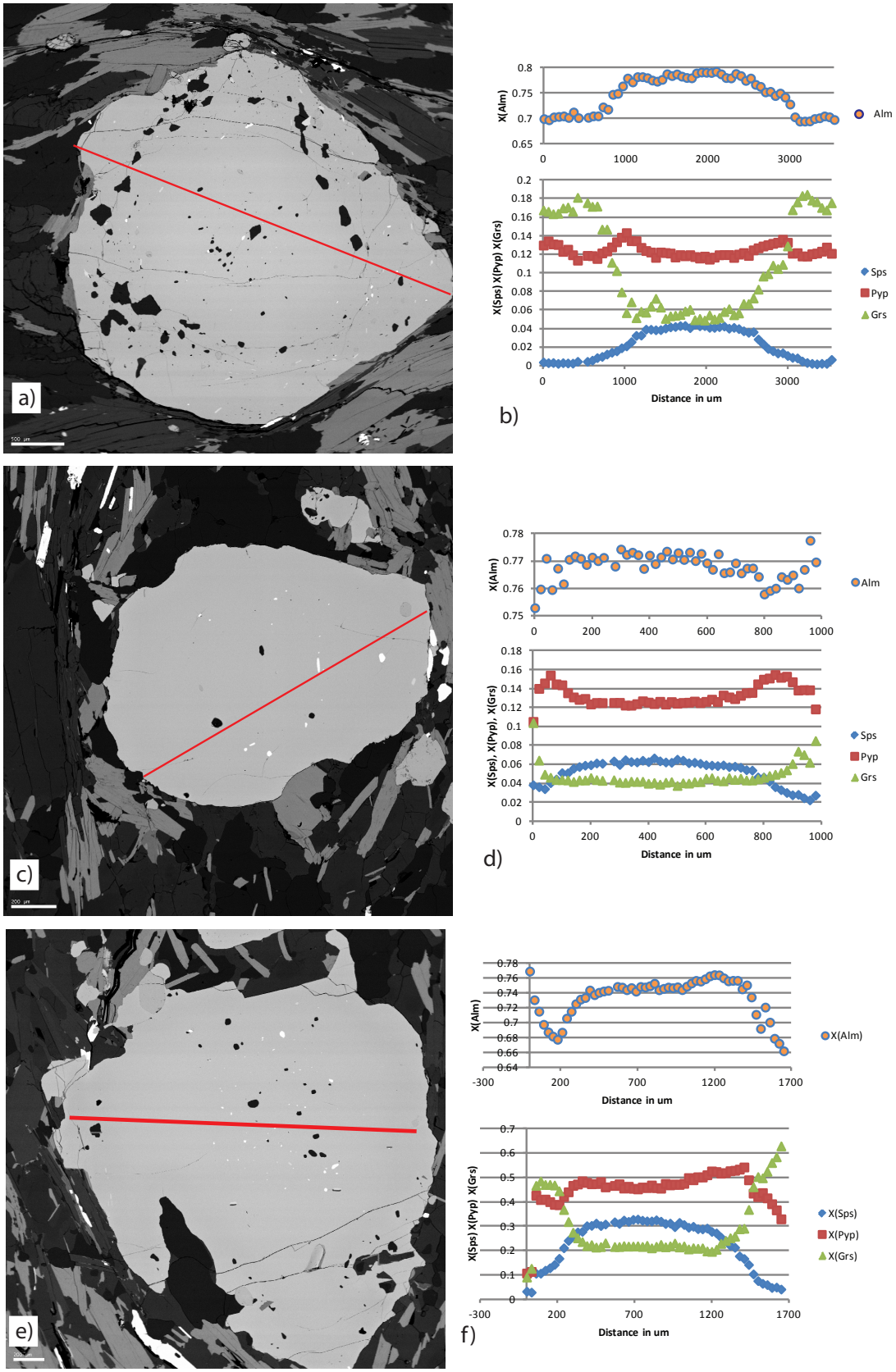
a)
X(Alm)
0.8
0.75
0.7
0.65
0
1000
2000
3000
Alm
X(Sps) X(Pyp) X(Grs)
0.2
0.18
0.16
0.14
0.12
0.1
0.08
0.06
0.04
0.02
0
Sps
Pyp
Grs
Distance in um
b)
c)
X(Alm)
0.78
0.77
0.76
0.75
0
200
400
600
800
1000
Alm
X(Sps), X(Pyp), X(Grs)
0.18
0.16
0.14
0.12
0.1
0.08
0.06
0.04
0.02
0
Sps
Pyp
Grs
Distance in um
d)
e)
X(Alm)
0.78
0.76
0.74
0.72
0.7
0.68
0.66
0.64
-300
200
700
1200
1700
Distance in um
X(Alm)
X(Sps) X(Pyp) X(Grs)
0.7
0.6
0.5
0.4
0.3
0.2
0.1
0
-300
200
700
1200
1700
Distance in um
X(Sps)
X(Pyp)
X(Grs)
f)

Figure 3.16

Table 3.3: Mineral compositions for SB-12-10B, SB-12-14, and SB-12-03A**.**

	Garnet(Rim)			Biotite			Muscovite			Plagioclase		
	SB-12-10B	SB-12-14	SB-12-03A	SB-12-10B	SB-12-14	SB-12-03A	SB-12-10B	SB-12-14	SB-12-03A	SB-12-10B	SB-12-14	SB-12-03A
wt%												
SiO2	37.58	37.41	37.41	36.38	36.31	35.42	46.30	45.03	45.55	63.57	60.97	62.78
TiO2	0.04	0.02	0.05	1.94	1.49	1.77	0.94	0.87	0.84	0.00	0.00	0.00
Al2O3	21.89	21.82	22.03	18.78	19.86	18.99	33.02	35.20	35.64	23.47	25.02	24.11
Cr2O3	0.02	0.02	0.04	0.03	0.04	0.05	0.01	0.02	0.04	0.00	0.00	0.00
MgO	3.29	3.30	3.05	9.96	8.68	9.93	1.45	0.75	0.79	0.00	0.00	0.00
CaO	6.20	3.17	6.77	0.01	0.29	0.00	0.00	0.02	0.00	4.45	6.32	5.48

3.6.2 P-T Conditions from Pseudosections

Pseudosections calculated from bulk rock chemistry for SB-12-10B (Figs. 3.17 and 3.18) and SB-12-14 (Figs. 3.19 and 3.20) from the Meall an t-Sìthe klippe and Creich Peninsula, respectively, are helpful with further quantifying the possible P-T range associated with metamorphism in the Sgurr Beag thrust sheet. The mineral assemblage found in the thin section for SB-12-10B extends across a wide P-T space in its pseudosection (Fig. 3.17), following both the Plag-Mus-Par-Ilm-Bio-Gt-q and Plag-Mus-Ilm-Bio-Gt-q fields. Estimated temperatures thus range from 500-700 °C, with pressures ranging from 2.6 to 8 kbar. Because this P-T space is so large, it is important to model mineral abundance (Fig. 3.18) in order to help narrow the range of P-T conditions. A narrower range of 5.3-5.6 kbar and 586-604 °C is consistent with both modeled and observed abundance of plagioclase, white mica, biotite, quartz and garnet. This is the best fit for a P-T space for SB-12-10B, as it falls within error of the temperature predicted by garnet-biotite thermometry, and within the pressure window predicted by THERMOCALC's average P-T mode (Fig. 3.17).

The pseudosection calculated for SB-12-14 from the Creich Peninsula shows a narrow range of P-T space (Fig. 3.19) that fits the observed mineral assemblage, 540-635 °C and 2.6-6.0 kbar, following the field for St-Plag-Mus-Ilm-Bio-Gt-q. This temperature range is significantly lower than the temperature predicted by garnet-biotite thermometry (662 ± 50 °C). Again, modeling the mineral abundance (Fig. 3.20) can help narrow the range of possible P-T conditions.

Figure 3.17
Next page. NaCaMnKFMASHTO pseudosection for sample SB-12-10B. Mineral abbreviations: Gt (garnet), Mus (white mica), Bio (biotite), q (quartz), Plag (plagioclase), St (staurolite), Ilm (ilmenite), sill (sillimanite), Chl (chlorite), Ctd (chloritoid) and zo (zoiesite). Pink bar represents pressure +/- 1.4 kbar calculated determined under peak conditions via THERMOCALC. Pink star represents Ferry and Spear (1978) garnet-biotite temperature for pressure of 6.4 kbar, with purple bars corresponding to error in temperature and pressure used to calculate temperature. Yellow elipsoid marks error in P-T conditions from THERMOCALC.

Figure 3.18
Next page. Modeled mineral volume of sample SB-12-10B for (a) plagioclase, (b) white mica, (c) biotite, (d) quartz, (e) garnet. Colored lines represent different phase volumes at respective P and T conditions. Grey shaded region represents the approximate phase volume found in thin section. Black box represents P-T space that where all modeled phase volumes match what is observed in thin section. Red star within red box represents temperature with degree of uncertainty calculated from the Ferry and Spear (1978) garnet-biotite thermometer. Black bar represents pressure calculated by THERMOCALC with degree of uncertainty.

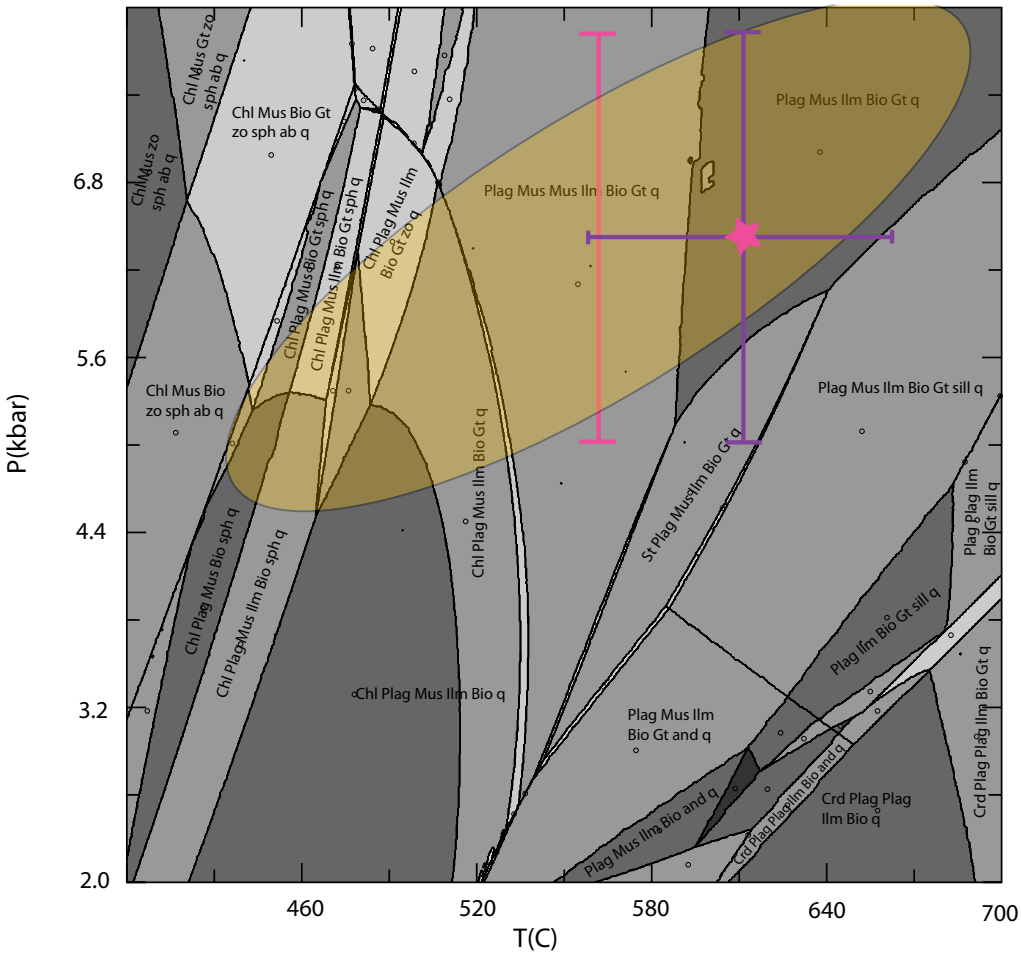
P(kbar)
6.8
5.6
4.4
3.2
2.0
460
520
580
640
700
T(C)
Chl Mus Gt zo sph ab q
Chl Mus Bio Gt zo sph ab q
Chl Mus zo sph ab q
Plag Mus Ilm Bio Gt q
Plag Mus Mus Ilm Bio Gt q
Chl Plag Mus Bio Gt sph q
Chl Plag Mus Ilm Bio Gt sph q
Chl Plag Mus Ilm Bio Gt zo q
Chl Mus Bio zo sph ab q
Plag Mus Ilm Bio Gt sill q
Chl Plag Mus Ilm Bio Gt q
St Plag Mus Ilm Bio Gt q
Plag Plag Ilm Bio Gt sill q
Chl Plag Mus Bio sph q
Chl Plag Mus Ilm Bio sph q
Plag Ilm Bio Gt sill q
Chl Plag Mus Ilm Bio q
Plag Mus Ilm Bio Gt and q
Crd Plag Plag Ilm Bio Gt q
Plag Mus Ilm Bio and q
Crd Plag Plag Ilm Bio and q
Crd Plag Plag Ilm Bio q

Figure 3.17

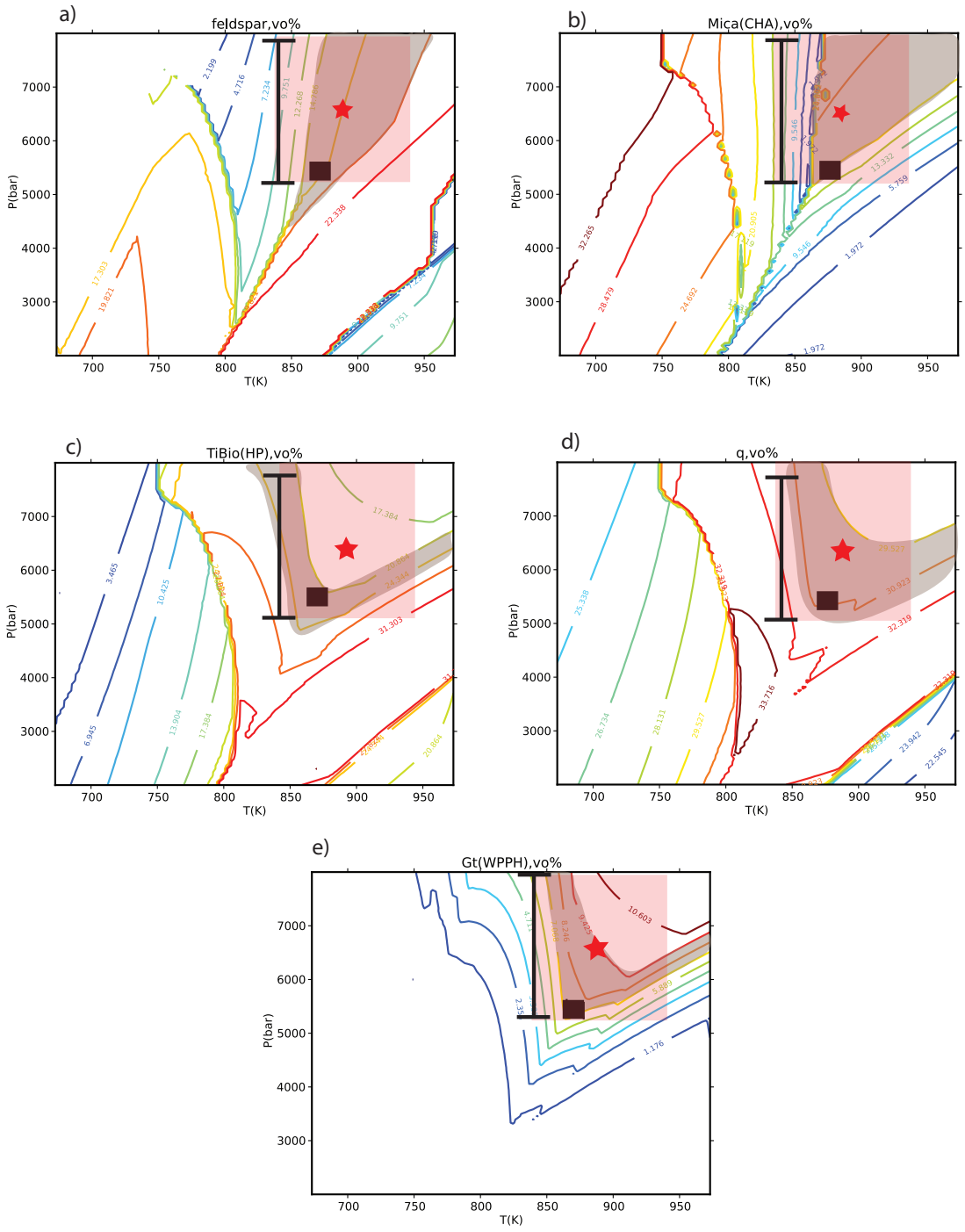
a)
feldspar,vo%
b)
Mica(CHA),vo%
c)
TiBio(HP),vo%
d)
q,vo%
e)
Gt(WPPH),vo%
P(bar)
T(K)

Figure 3.18

Staurolite (Fig. 3.20d) is one of the most useful constraints for P and T, because it occupies a unique field in P-T space, which overlaps between 600 and 625 °C with the uncertainty bound from garnet-biotite thermometry, as well as within the pressure range predicted by THERMOCALC (4.8-5.8 kbar). Mineral abundance observed in thin section verses the modeled abundance for white mica, biotite, and garnet also fit with estimated P-T conditions of 600-625 °C and 4.8-5.8 kbar. Quartz and feldspar do not fall within this P-T space, as the observed volume requires lower temperatures and higher pressures. The observed verse modeled quartz and feldspar abundance difference could be due to uncertainties in point counting, sample heterogeneity and bulk rock composition uncertainties.

3.7. Discussion

3.7.1 Multiple movement on the Sgurr Beag thrust

Grant and Harris (2000) have conducted a petrofabrics-based, kinematic study over the same traverse in the Ben Wyvis/Garve region as reported in this Chapter, highlighting senses of movement along the Sgurr Beag thrust. Several of the observations noted by Grant and Harris (2000), such as an increase in foliation intensity towards the thrust, south plunging lineations, and two preserved shear senses, were also observed in this study. Based on these observations, Grant and Harris (2000) suggested that movement along the Sgurr Beag thrust was accompanied by penetrative shearing extending in to the footwall and hanging wall over a total distance of ~ 200 m. Our petrofabric data suggests that penetrative shearing associated with motion on the

---

Figure 3.19
Next page. NaCaMnKFMASHTO pseudosection for SB-12-14. Mineral abbreviations: Gt (garnet), Mus (white mica), Bio (biotite), q (quartz), Plag (plagioclase), St (staurolite), Ilm (ilmenite), sill (sillimanite), Chl (chlorite), Ctd (chloritoid) and zo (zoiesite). Pink bar represents pressure +/- 1.5 kbar determined under peak conditions via THERMOCALC. Orange star represents Ferry and Spear (1978) garnet-biotite temperature for pressure of 5.1 kbar , with purple bars representing error in temperature and pressure used to calculate temperature. Green ellipsoid represent error for P-T calculated in THERMOCALC.

Figure 3.20
Next page. Modeled mineral volume of SB-12-14 for (a) plagioclase, (b) quartz, (c) white mica, (d) staurolite, (e) biotite, (f) garnet. Colored lines represent different phase volumes at respective P and T conditions. Grey shaded region represents the approximate phase volume found in thin section. Red star within red box represents temperature with degree of uncertainty calculated from the Ferry and Spear (1978) garnet-biotite thermometer. Black bar indicates pressure calculated by THERMOCALC with degree of uncertainty.

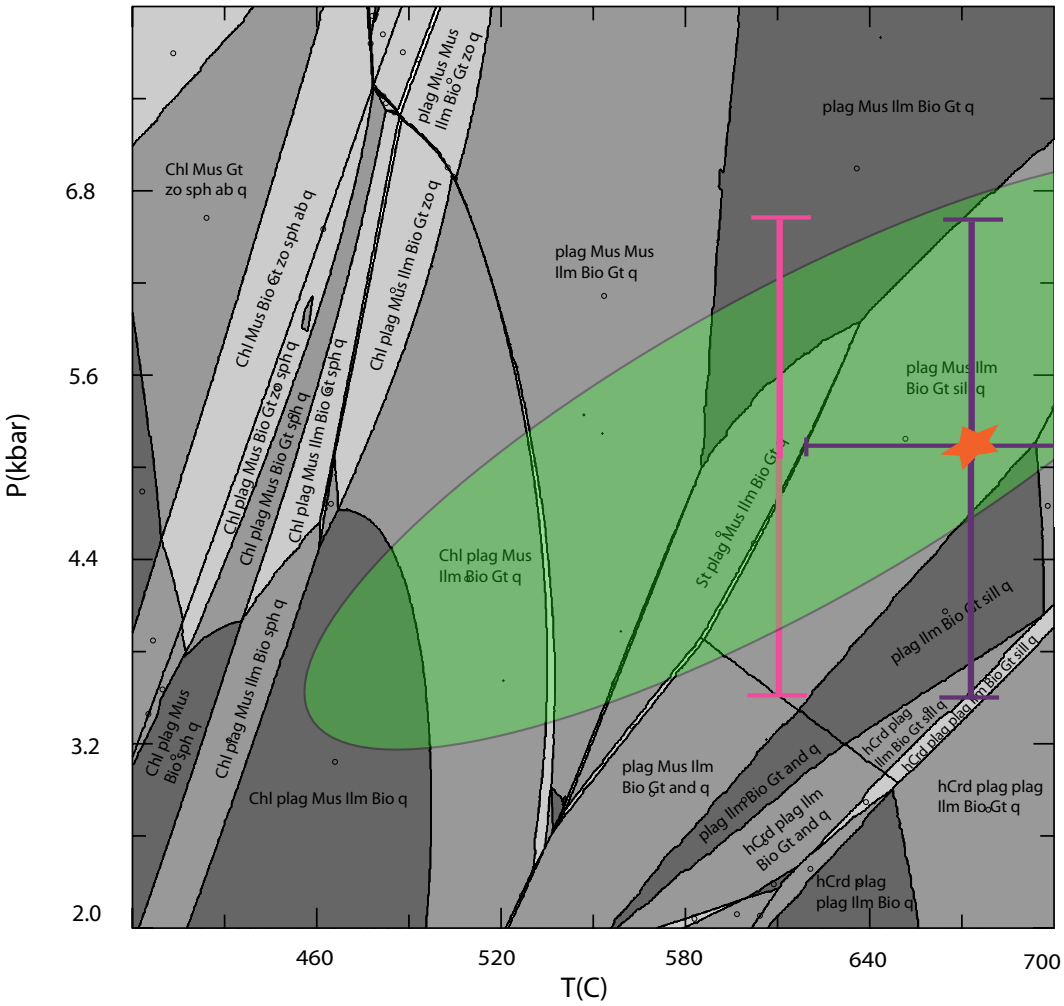
P(kbar)
6.8
5.6
4.4
3.2
2.0
460
520
580
640
700
T(C)
Chl Mus Gt
zo sph ab q
Chl Mus Bio Gt zo sph ab q
Chl plag Mus Bio Gt zo sph q
Chl plag Mus Ilm Bio Gt sph q
Chl plag Mus Ilm Bio Gt zo q
plag Mus Mus
Ilm Bio Gt zo q
plag Mus Mus
Ilm Bio Gt q
plag Mus Ilm Bio Gt q
plag Mus Ilm
Bio Gt sill q
St plag Mus Ilm Bio Gt q
Chl plag Mus
Ilm Bio Gt q
plag Ilm Bio Gt sill q
hCrd plag
Ilm Bio Gt sill q
hCrd plag plag
Ilm Bio Gt sill q
Chl plag Mus
Bio sph q
Chl plag Mus Ilm Bio sph q
Chl plag Mus Ilm Bio q
plag Mus Ilm
Bio Gt and q
plag Ilm Bio Gt and q
hCrd plag Ilm
Bio Gt and q
hCrd plag plag
Ilm Bio Gt q
hCrd plag
plag Ilm Bio q

Figure 3.19

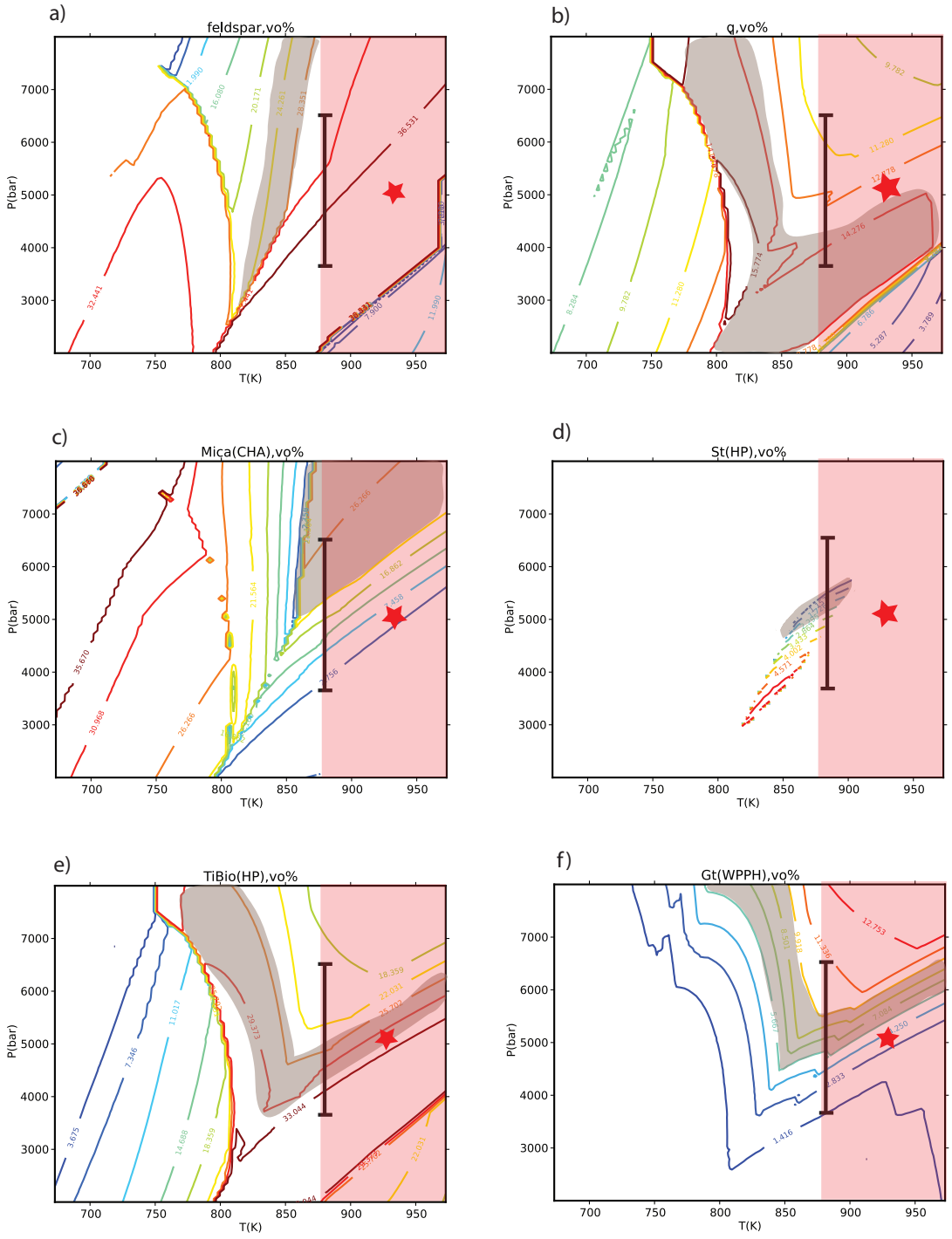
a)
feldspar,vo%
b)
q,vo%
c)
Mica(CHA),vo%
d)
St(HP),vo%
e)
TiBio(HP),vo%
f)
Gt(WPPH),vo%
P(bar)
T(K)

Figure 3.20

thrust may extend further in to both the footwall and hanging wall than suggested by Grant and Harris (2000). For example, the high density quartz c-axis fabrics (4 - 6 times uniform maximum density distribution) suggests that this zone of penetrative shearing may extend at least 400 m in to the hanging wall.

Grant and Harris (2000) also noted a second generation of movement along the Sgurr Beag thrust in the Ben Wyvis/Garve area, based on top-to-the-south shear sense indicators from quartz fabrics in both the footwall and hanging wall. They associate this top-to-the-south shear sense with normal dip-slip movement that occurred during retrogression and exhumation/ cooling. Our study yields similar results, although petrofabric evidence for normal sense shearing is confined to samples from the hanging wall. Additionally, quartz recrystallization microstructures and fabric opening angles are very similar in samples with reverse- and normal-sense shear indicators, suggesting that both phases of motion occurred under similar deformation temperatures (535-545°C).

3.7.2 Constrictional strains in Sgurr Beag thrust sheet north of Loch Fannich

The Sgurr Beag thrust sheet crops out as two klippen in the Loch Fannich region (Fig. 3.1). In both klippen, small-circle girdle fabrics centered about the principal stretching direction (Figs. 3.10 and 3.13) suggest that penetrative shearing occurred within the general constrictional field (Fig. 3.4b), rather than under the approximate plane strain conditions indicated by cross girdle fabrics at other structural locations both in the hanging wall and footwall to the thrust. The tectonic cause of these apparent constrictional strains is unknown. Local constrictional strain regimes in thrust terrains have previously been explained by a range of variously plausible mechanisms including: a) motion over an irregular fault surfaces (e.g. Bygdin conglomerate of Norwegian Caledonides; Hossack, 1968) and, b) along-strike overlapping of domains of flattening strain compensated for by intervening zones of thrust transport-parallel constrictional strain (e.g. Norwegian Caledonides; Sylvester and Janecky, 1988; see review by Law, 2010). With the limited data currently available we are unable to speculate any further on the likely origin of these local constrictional strains within the Sgurr Beag thrust sheet. From a historical perspective we note, however, that what would now be called *'constrictional strains with a principal stretch direction oriented parallel to tectonic transport'* were first recognized by C.T. Clough in the early 20th century for mylonitic rocks in both the Ben Wyvis (Peach et al., 1912, p. 49) and Fannich Mountains (Peach et al. 1913, p. 20), based on macroscopic grain shape fabrics.

Though our fabrics hint that constrictional strain affected the Sgurr Beag north of Loch Fannich, quartz c-axis fabrics described by Kelley and Powell (1985) suggest that the region was primarily affected by plane strain deformation, probably close to simple shear. From approximately the same location as MT-12-05 on the Alt Breabaig river transect (Fig. 3.8),

Kelley and Powell (1985) report a weak single girdle fabric (their figure 14b), indicating top-to-the-north shear. The shear sense they report agrees with our regional shear sense for samples from the Alt Breabaig transect (Fig. 3.10), but our samples are characterized by cross girdle rather than single girdle fabrics. Similarly, in the footwall to the Sgurr Beag klippe on Meall an t-Sìthe (Fig. 3.11a) Kelley and Powell (1985) report a strongly developed single girdle fabric (their figure 4c) that contrasts with the cross girdle fabric measured in our sample MT-12-15 (Fig. 3.13).

3.7.3 Relative ages of thrusting, folding, penetrative shearing / fabric formation

Based on the regional scale cross-section shown in Fig. 3.3 it is clear that the now eroded westward continuation of the Sgurr Beag thrust (locally preserved in the Fannich klippen) is folded around a series WNW-vergent antiforms and synforms defined by lithotectonic units (Krabbendam et al., 2011) in the underlying Moine thrust sheet. The structural relationship between these km-scale ESE dipping folds and the underlying Moine thrust is unknown, although it seems at least structurally plausible that they be at least broadly synchronous with top to the WNW motion on the Moine thrust, and therefore would be expected to detach on to the underlying Moine thrust.

Relative age relationships between these WNW-vergent folds and the tectonic grain shape fabrics (foliation and lineation) and associated quartz c-axis fabrics in our individual samples are less clear. Krabbendam et al. (2011) and Krabbendam (personal communication, 2013) have argued that the grain shape fabrics observed at outcrop to hand sample scale developed essentially synchronously with formation of the km-scale WNW-vergent folds in the Moine thrust sheet, rather than being pre-folding fabrics that have been passively rotated around these folds. If this interpretation is correct, then opposite shear sense might be expected to be indicated by microstructures and crystal fabrics on adjacent fold limbs. Additionally, foliation might be expected to either be axial planar to these folds or at least display a fanning pattern in fold profile planes - with opposite senses of obliquity of foliation to lithotectonic units on adjacent fold limbs, and foliation at a high angle to lithotectonic units in fold cores. Although very limited in quantity, our foliation data from samples collected along the Braemore Junction - Garve/Ben Wyvis - Rogie Falls transect (Fig. 3.3) appears to tentatively support this suggestion that observed grain shape fabrics in the Moine thrust sheet developed during WNW-vergent folding. For example, in the core of the Beinn Dearg Anticline grain shape foliation is at a high angle to the mapped boundaries between lithotectonic units.

This does not, however, preclude the possibility that continued WNW-directed overthrusting and penetrative shearing along the base of the Moine thrust sheet may have outlasted folding in the overlying metasedimentary rocks. Thus, although formed during the

same overall deformation event, the observed gently dipping grain shape foliations (with ESE trending stretching lineations) in the immediate hanging wall to the Moine thrust at the western (foreland) end of the Braemore Junction - Garve/Ben Wyvis - Rogie Falls transect (Fig. 3.3) may have developed later than the steeply dipping grain shape foliation (with ~ N-S trending stretching lineations) recorded further to the east at higher structural levels. This interpretation is in close accord with the conclusions by Kelley and Powell (1985) and Kelley (1988), based on microstructural and K-Ar cooling age data from the Fannich Mountains area immediately to the south of this transect, that penetrative shearing along the base of the Moine thrust sheet is younger than or outlasted penetrative shearing at higher structural levels further to the east (see also reviews by Butler, 2010; Law and Johnson, 2010). Kelley and Powell (1985) also note that D2 foliations in the Loch Fannich region increase in intensity towards the Sgurr Beag thrust, a potential indicator that folding occurred during thruting.

3.7.4 P-T correlation between study areas

Between the north coast and Assynt (Fig. 3.1) Thigpen et al. (in press) have demonstrated that temperatures associated with Scandian (435-425 Ma) thrust-related shearing increase traced from the Moine thrust eastwards through the Moine and Ben Hope thrust sheets in to the Naver thrust sheet. In the immediate hanging wall of the Naver thrust sheet deformation temperatures indicated by quartz fabric opening angles (655 °C) were very similar to temperatures of metamorphism indicated by garnet-biotite thermometry (645 °C; Barr et al., 1986) in samples collected from adjacent outcrops.

Within analytical uncertainty, these estimated temperatures are very similar to those we have calculated further to the south for the immediate hanging wall to the Sgurr Beag thrust in the Meall an t-Sìthe klippe (Figs. 3.11a and b) of the Fannich Mountains, based on both microprobe-based pseudosection analyses (586-604 °C at 5.3-5.6 kbar) and fabric opening angles (550 °C; Fig. 3.13). Temperature and pressure estimates from this most foreland-positioned exposure of the Sgurr Beag thrust sheet (Fig. 3.1) in the Fannich Mountains are also very similar to those we have estimated in the immediate hanging wall to the Sgurr Beag thrust exposed on the Creich Peninsula (600-625 °C at 4.8-5.8 kbar) located some 60 km to the east of the Fannichs, measured parallel to an assumed WNW transport direction (Fig. 3.1). These reconnaissance data indicate that penetrative shearing in the more hinterland thrust sheets exposed both towards the north coast and to the south in the Fannich Mountains - Ben Wyvis - Creich Peninsula area occurred at broadly similar crustal depths and temperatures. Kelley and Powell (1985) noted that thrust-related shearing in the Fannichs occurred during metamorphism, and at minimum temperatures consistent with biotite recrystallization. Our P-T conditions across the Sgurr Beag thrust sheet support the conclusion that thrusting was synchronous with

metamorphism. Perhaps more surprising is the similarity in estimated PT conditions for the immediate hanging wall to the Sgurr Beag thrust exposed in extreme foreland (Meall an t-Sìthe klippe) and hinterland (Creich Peninsula) positions, where intuitively it might be expected that peak PT conditions in the foreland would be significantly lower than those in the hinterland.

3.8. Conclusions

Microstructural, quartz petrofabric, and microprobe-based petrology data from four transects across the immediate hanging wall of the Sgurr Beag thrust and into the underlying Moine thrust sheet indicate that:

1) Penetrative shearing associated with top to the west and north reverse sense movement along the Sgurr Beag thrust occurred under amphibolite facies conditions, with deformation temperatures increasing from footwall to hanging wall. The Ben Wyvis/Garve region saw an increase in deformation temperature from 465 °C to 583 °C, corresponding to fabrics that ranged from a maximum density of 3.0 to 6.0 times uniform. The Alt Breabaig traverse showed footwall deformation temperatures of 455 °C - 481 °C to temperatures greater than 515 °C in the hanging wall, corresponding to fabrics that ranged from a maximum density of 3.5 to 8.0 times uniform. Meall an t'Sithe exposure of the Sgurr Beag klippe deformed at 395 °C in the footwall and 550 °C in the hanging wall, corresponding to fabrics that ranged from a maximum density of 3.0 to 8.0 times uniform.
2) A regional top-to-the-north/northwest shear sense was preserved both in microstructures and quartz c-axis fabrics for the Alt Braebaig traverse, Meall an t'Sithe klippe, and the hanging wall to the Sgurr Beag at Ben Wyvis/Garve.

3a) A later phase of normal-sense dip-slip movement is locally (Ben Wyvis/Garve only) indicated by quartz c-axis fabrics.

3b) Quartz microstructures and fabrics indicate that normal sense shearing occurred under similar temperatures to the earlier reverse sense shearing.

4) Although penetrative shearing dominantly occurred under approximate plane strain conditions, constrictional strains locally developed in the hanging wall to the Sgurr Beag exposed in klippen to the north of Loch Fannich.
5) Peak metamorphism in the immediate hanging wall to the Sgurr Beag thrust occurred at temperatures of 586-625 °C and pressures ranging from 4.8-5.8 kbar. No significant change in peak conditions was found between more foreland and more hinterland exposures of the Sgurr Beag thrust sheet.
6) Km-scale NW-vergent folds in the Moine thrust sheet between Braemore Junction and Garve are demonstrably younger than the overlying Sgurr Beag thrust, but are probably broadly synchronous with, and detach on to, the underlying Moine thrust. Grain shape and

crystallographic fabrics in the interior of the Moine thrust sheet probably developed during formation of these NW-vergent folds. However, top-to-the WNW shearing along the base of the Moine thrust sheet may be younger than, or have outlasted, penetrative shearing and NW-vergent folding at higher structural levels.

References

Barr, D., Holdsworth, R.E., Roberts, A.M., 1986. Caledonian ductile thrusting in a Precambrian metamorphic complex: The Moine of northwestern Scotland. Geological Society of America Bulletin 97, 754-764.

Bird, A.F., Thirlwall, M.F., Strachan, R.A., in press. Lu-Hf and Sm-Nd dating on metamorphic garnet: evidence for multiple arrection events during the Caledonian orogeny in Scotland. Journal of the Geological Society.

British Geological Survey, 2004. Ben Wyvis. Scotland Sheet 93W. Bedrock and Superficial Deposits. , 1:50 000 Geology Series. Keyworth, Nottingham, British Geological Survey.

British Geological Survey, 2011. Loch Fannich. Scotland Sheet 92E. Bedrock. 1:50 000 Geology Series. Keyworth, Nottingham: British Geological Survey.

Burns, I.M., 1994. Tectonothermal evolution and petrogensis of the Naver and Kirtomy nappes, north Sutherland, Scotland. Oxford Brookes University.

Butler, R.W.H. 2010. The role of thrust tectonic models in understanding structural evolution in NW Scotland. *In*: Law, R.D., Butler, R.W.H., Holdsworth, R., Krabbendam, M. & Strachan, R. (eds) *Continental Tectonics and Mountain Building - The Legacy of Peach and Horne*. Geological Society, London, Special Publications 335, 293-320.

Coggon, R., Holland, T., 2002. Mixing properties of phengitic micas and revised garnet-phengite thermobarometers. Journal of Metamorphic Geology 20, 683-696.

Connolly, J.A.D., 1990. Multivariable phase diagrams; an algorithm based on generalized thermodynamics. American Journal of Science 290, 666-718.

Connolly, J.A.D., 2005. Computation of phase equilibria by linear programming: A tool for geodynamic modeling and its application to subduction zone decarbonation. Earth and Planetary Science Letters 236, 524-541.

Ferry, J.t., Spear, F., 1978. Experimental calibration of the partitioning of Fe and Mg between biotite and garnet. Contributions to Mineralogy and Petrology 66, 113-117.

Fettes, D., Long, C., Bevins, R., Max, M., Oliver, G., Primmer, T., Thomas, L., Yardley, B., 1985. Grade and time of metamorphism in the Caledonide Orogen of Britain and Ireland, in: Harris, A.L. (Ed.), The Nature, London and timing of orogenic activityin the Caledonian rocks of the British Isles. Memoirs of the Geological Society. Geological Society of London, London, pp. 41-53.

Friend, C., Jones, K., Burns, I., 2000. New high-pressure granulite event in the Moine Supergroup, northern Scotland: Implications for Taconic (early Caledonian) crustal evolution. Geology 28, 543-546.

Furman, M., Lindsley, D., 1988. Ternary feldspar modeling and thermometry. Am Mineral 73, 201-215.

Geikie, A., 1884. The crystalline rocks of the Scottish Highlands. Nature 30, 29-31.

Giletti, B.J., Moorbath, S., Lambert, R.S.J., 1961. A geochronological study of the metamorphic complexes of the Scottish Highlands. Quarterly Journal of the Geological Society 117, 233-264.

Goodenough, K.M., Millar, I., Strachan, R.A., Krabbendam, M., Evans, J.A., 2011. Timing of regional deformation and development of the Moine Thrust Zone in the Scottish Caledonides: constraints from the U-Pb geochronology of alkaline intrusions. Journal of the Geological Society 168, 99-113.

Grant, C.J., Harris, A.L., 2000. The kinematic and metamorphic history of the Sgurr Beag Thrust, Ross-shire, NW Scotland. Journal of Structural Geology 22, 191-205.

Harris, A., Johnson, M., 1991. Moine, Geology of Scotland. Geological Society of London, pp. 87-123.

Hirth, G., Tullis, J., 1992. Dislocation Creep Regimes in Quartz Aggregates. Journal of Structural Geology 14, 145-159.

Holdsworth, R.E., 1989. The geology and structurl evolution of a Caledonian fold and ductile thrust zone, Kyle of Tongue region, Sutherland, Northern Scotland. Journal of the Geological Society 146, 809-823.

Holdsworth, R.E., Strachan, R.A., Harris, A.L., 1994. The Moine Supergroup, in: Gibbons, W., Harris, A.L. (Eds.), A Revised Correlation of Precambrian rocks in the British Isles. Geological Society of London Special Reports, pp. 23-32.

Holland, T., Baker, J., Powell, R., 1998. Mixing properties and activity-composition and relationships of chlorites in the system MgO-FeO-Al 2 O 3-SiO 2-H 2 O. European Journal of Mineralogy 10, 395-406.

Holland, T., Powell, R., 1998. An internally consistent thermodynamic data set for phases of petrological interest. Journal of Metamorphic Geology 16, 309-343.

Hossack, J.R., 1968. Pebble deformation and thrusting in the Bygdin area (southern Norway). Tectonophysics 5, 315-339.

Johnson, M., Strachan, R., 2006. A discussion of possible heat sources during nappe stacking: the origin of Barrovian metamorphism within the Caledonian thrust sheets of NW Scotland. Journal of the Geological Society 163, 579-582.

Kelley, S.P. 1988. The relationship between K-Ar mineral ages, mica grain sizes and movement on the Moine thrust zone, NW Highlands, Scotland. *Journal of*

the Geological Society, London, **145**, 1-10.

Kelley, S. & Powell, D. 1985. Relationships between marginal thrusting and movement on major internal shear zones in the northern Highland Caledonides, Scotland. *Journal of Structural Geology*, **7**, 161-174.

Kelley, S. 2010. Excursion 9: Loch a' Bhraoin, Braemore and Loch Broom, p. 166. In: Strachan, R.A., Alsop, I., Friend, C.R.L., Miller, S., 2010. An excursion guide to the Moine geology of the Northern Highlands of Scotland. Edinburgh Geological Society & Geological Society of Glasgow, Edinburgh, Scotland.

Kinny, P.D., Friend, C.R.L., Strachan, R.A., Watt, G.R., Burns, I.M., 1999. U-Pb geochronology of regional migmatites in East Sutherland, Scotland: evidence for crustal melting during the Caledonian orogeny. Journal of the Geological Society 156, 1143-1152.

Kinny, P.D., Strachan, R.A., Friend, C.R.L., Kocks, H., Rogers, G., Paterson, B.A., 2003. U-Pb geochronology of deformed metagranites in central Sutherland, Scotland: evidence for widespread late Silurian metamorphism and ductile deformation of the Moine Supergroup during the Caledonian orogeny. Journal of the Geological Society 160, 259- 269.

Kocks, H., Strachan, R.A., Evans, J.A., 2006. Heterogeneous reworking of Grampian metamorphic complexes during Scandian thrusting in the Scottish Caledonides: insights from the structural setting and U-Pb geochronology of the Strath Halladale Granite. Journal of the Geological Society 163, 525-538.

Krabbendam, M., Prave, T., Cheer, D., 2008. A fluvial origin for the Neoproterozoic Morar Group, NW Scotland; implications for Torridon–Morar Group correlation and the Grenville Orogen foreland basin. Journal of the Geological Society 165, 379-394.

Krabbendam, M., Strachan, R.A., Leslie, A.G., Goodenough, K.M., Bonsor, H.C., 2011. The internal structure of the Moine Nappe Complex and the stratigraphy of the Morar Group in the Fannichs-Beinn Dearg area, NW Highlands. Scottish Journal of Geology 47, 1-20.

Kruhl, J.H., 1998. Reply: Prism- and basal-plane parallel subgrain boundaries in quartz: a microstructural geothermobarometer. Journal of Metamorphic Geology 16, 142-146.

Lapworth, C., 1885. The Highland Controversy in British Geology. Nature 32, 558-559.

Law, R., Johnson, M., 2010. Microstructures and crystal fabrics of the Moine thrust zone and Moine nappe: history of research and changing tectonic interpretations. Geological Society, London, Special Publications 335, 443-503.

Law, R.D., Searle, M.P., Simpson, R.L., 2004. Strain, deformation temperatures and vorticity of flow at the top of the Greater Himalayan Slab, Everest Massif, Tibet. Journal of the Geological Society of London 161, 305-320.

LeFort, P., 1975. HImalays, the collided range: present knowledge of the contiental arc. American Journal of Science 275, 1-44.

Lister, G.S., 1977. Crossed-girdle c-axis fabrics in quartzites plastically deformed by plane strain and progressive simple shear. Tectonophysics 39, 51-54.

Lister, G.S., Hobbs, B.E., 1980. The simulation of fabric development during plastic deformation and its application to quartzite; the influence of deformation history. Journal of Structural Geology 2, 355-370.

Long, L.E., Lambert, R.S.J., 1963. Rb-Sr isotopic ages from the Moine Series, in: Johnson, M.R.W., Stewart, F.H. (Eds.), The British Caledonides, pp. 217-247.

Mahar, E.M., Baker, J., Powell, R., Holland, T., Howell, N., 1997. The effect of Mn on mineral stability in metapelites. Journal of Metamorphic Geology 15, 223-238.

Mendum, J., Barber, A., Butler, R., Flinn, D., Goodenough, K.M., Krabbendam, M., Park, R., Stewart, A., 2009. Lewisian, Torridonian and Moine Rocks of Scotland. Joint Nature Conservation Committee.

Moorhouse, S.J., Moorhouse, V.E., 1988. The Moine assemblage in Sutherland, in: Winchester, J.A. (Ed.), Later Proterozoic Stratigraphy of the Northern Atlantic Regions. Blackie and Sons, Glasgow, pp. 54-73.

Morgan, S.S., Law, R.D., 2004. Unusual transition in quartzite dislocation creep regimes and crystal slip systems in the aureole of the EJB pluton, California: a case for anhydrous conditions creaed y decarbonation of adjacent marbles. . Tectonophysics 384, 209-231.

Peach, B.N., Horne, J., Gunn, W., Clough, C.T., Hinxman, L.W., Teall, J.J.H., 1907. The geological structure of the North-West Highlands of Scotland. British Geological Survey Memoir.

Peach, B.N., Gunn, W., Clough, C.T., Hinxman, L.W., Crampton, C.B. & Anderson, E.M. 1912. *The Geology of Ben Wyvis, Carn Chuinneag, Inchbae and the Surrounding Country (Sheet 93).* British Geological Survey Memoir, 189 pp.

Peach, B.N., Horne, J., Gunn, W., Clough, C.T. & Greenly, E. 1913. *The Geology of the Fannich Mountains and the Country Around Upper Loch Maree and Strath Broom (Sheet 92).* British Geological Survey Memoir, 127 pp.

Powell, D., Holland, T., 1994. Optimal geothermometry and geobarometry. Am Mineral 79, 120-133.

Powell, R., Holland, T., 1999. Relating formulations of the thermodynamics of mineral solid solutions: activity modeling of pyroxenes, amphiboles, and micas. Am Mineral 84, 1-14.

Powell, D., Phillips, W., 1985. Time of deformation in the Caledonide Orogen of Britain and Ireland. Geological Society, London, Memoirs 9, 17-39.

Rathbone, P.A., Harris, A.L., 1979. Basement-cover relationships at Lewisian inliers in the Moine rocks. Geological Society, London, Special Publications 8, 101-107.

Read, H., 1931. The geology of central Sutherland (Sheets 108 and 109). British Geological Survey Memoir, 238.

Schmid, S., Casey, M., 1986. Complete fabric analysis of some commonly observed quartz c-axis patterns. Geophysical Monograph 36, 263-286.

Soper, N., Brown, P., 1971. Relationship between metamorphism and migmatization in the northern part of the Moine Nappe. Scottish Journal of Geology 7, 305-325.

Stipp, M., Stunitz, H., Heilbronner, 2002. The Eastern Tonale Fault Zone: a 'natural labatory' for crystal plastic deformation of quartz over a temperature range from 250 to 700. Journal of Structural Geology 24.

Strachan, R., Evans, J., 2008. Structural setting and U-Pb zircon geochronology of the Glen Scaddle Metagabbro: evidence for polyphase Scandian ductile deformation in the Caledonides of northern Scotland. Geological Magazine 145, 361.

Strachan, R.A., Holdsworth, R.E., 1988. Basement cover relationships and structure within the Moine rocks of central and southeast Sutherland. Journal of the Geological Society 145, 23-36.

Strachan, R.A., Holdsworth, B., Krabbendam, M., Leslie, G., Soper, J. 2010. Excursion 10: South and Central Sutherland, pp-184. In: Strachan, R.A., Alsop, I., Friend, C.R.L., Miller, S., 2010. An excursion guide to the Moine geology of the Northern Highlands of Scotland. Edinburgh Geological Society & Geological Society of Glasgow, Edinburgh, Scotland.

Sylvester, A. G. & Janecky, D. R. 1988. Structure and petrofabrics of quartzite and elongate pebbles at Sandviksfjell, Bergen, Norway. *Norsk Geologisk Tidsskrift*, **68**, 31-50.

Tanner, P.W.G., 1970. The Sgurr Beag Slide–a major tectonic break within the Moinian of the Western Highlands of Scotland. Quarterly Journal of the Geological Society 126, 435- 463.

Tanner, P.W.G., Evans, J.A., 2003. Late Precambrian U-Pb titanite age for peak regional metamorphism and deformation (Knoydartian orogeny) in the western Moine, Scotland. Journal of the Geological Society 160, 555-564.

Thigpen, J.R., Law, R.D., Lloyd, G.E., Brown, S.J., Cook, B., 2010. Deformation temperatures, vorticity of flow and strain symmetry in the Loch Eriboll mylonites, NW Scotland: implications for the kinematic and structural evolution of the northernmost Moine Thrust zone. Geological Society, London, Special Publications 335, 623-662.

Thigpen, J.R., Law, R.D., Loehn, C., Strachan, R.A., Tracy, R., Lloyd, G., Roth, B., Brown, S., in press. Thermal structure and tectonic evolution of the Scandian orogenic wedge, Scottish Caledonides: Integrating geothermometry, deforamtion temperatures, and kinematic-thermal modeling. Journal of Metamorphic Geology.

Tullis, J., Christie, J.M., Griggs, D.T., 1973. Microstructures and Preferred Orientations of Experimentally Deformed Quartzites. Geological Society of America Bulletin 84, 297-314.

Vance, D., Strachan, R., Jones, K., 1998. Extensional versus compressional settings for metamorphism: Garnet chronometry and pressure-temperature-time histories in the Moine Supergroup, northwest Scotland. Geology 26, 927-930.

Wilson, D., 1975. Structure and metamorphism of the Ben Wyvis District, Ross-shire. University of Edinburgh.

Winchester, J.A., 1974. The zonal pattern of regional metamorphism in the Scottish Caledonides. Journal of the Geological Society 130, 509-524.

White, R., Pomroy, N., Powell, R., 2005. An in situ metatexite–diatexite transition in upper amphibolite facies rocks from Broken Hill, Australia. Journal of Metamorphic Geology 23, 579-602.